PNL-6500 Pt. 3
UC-402

/7

Pacific Northwest Laboratory Annual Report for 1987 to the DOE Office of Energy Research

Part 3 Atmospheric Sciences
August 1988

Prepared for the U.S. Department of Energy
under Contract DE-AC06-76RLO 1830

Pacific Northwest Laboratory
Operated for the U.S. Department of Energy
by Battelle Memorial Institute

Battelle

DISCLAIMER

This report was prepared as an account of work sponsored by an agency of the United States Government. Neither the United States Government nor any agency thereof, nor Battelle Memorial Institute, nor any or their employees, makes any warranty, expressed or implied, or assumes any legal liability or responsibility for the accuracy, completeness, or usefulness of any information, apparatus, product, or process disclosed, or represents that its use would not infringe privately owned rights. Reference herein to any specific commercial product, process, or service by trade name, trademark, manufacturer, or otherwise does not necessarily constitute or imply its endorsement, recommendation, or favoring by the United States Government or any agency thereof, or Battelle Memorial Institute. The views and opinions of authors expressed herein do not necessarily state or reflect those of the United States Government or any agency thereof, or Battelle Memorial Institute.

PACIFIC NORTHWEST LABORATORY
operated by
BATTELLE MEMORIAL INSTITUTE
for the
UNITED STATES DEPARTMENT OF ENERGY
under Contract DE-AC06-76RLO 1830

Printed in the United States of America
Available from
National Technical Information Service
United States Department of Commerce
5285 Port Royal Road
Springfield, Virginia 22161

NTIS Price Codes
Microfiche A01

Printed Copy

Pages	Price Codes
001-025	A02
026-050	A03
051-075	A04
076-100	A05
101-125	A06
126-150	A07
151-175	A08
176-200	A09
201-225	A010
226-250	A011
251-275	A012
276-300	A013

3 3679 00057 6126

PNL-6500 Pt.3
UC-402

Pacific Northwest Laboratory Annual Report for 1987 to the DOE Office of Energy Research

Part 3: Atmospheric Sciences

C. E. Elderkin and Staff

August 1988

Prepared for the U.S. Department of Energy
under Contract DE-AC06-76RLO 1830

Pacific Northwest Laboratory
Richland, Washington 99352

PREFACE

This 1987 Annual Report from Pacific Northwest Laboratory (PNL) to the U.S. Department of Energy (DOE) describes research in environment, safety and health conducted during fiscal year 1987. The report again consists of five parts, each in a separate volume.

The five parts of the report are oriented to particular segments of the PNL program. Parts 1 to 4 report on research performed for the DOE Office of Health and Environmental Research in the Office of Energy Research. Part 5 reports progress on all research performed for the Assistant Secretary for Environment, Safety and Health. In some instances, the volumes report on research funded by other DOE components or by other governmental entities under interagency agreements. Each part consists of project reports authored by scientists from several PNL research departments, reflecting the multidisciplinary nature of the research effort.

The parts of the 1987 Annual Report are:

Part 1:	Biomedical Sciences Program Manager:	J.F. Park	D.L. Felton, Report Coordinator and Editor
Part 2:	Environmental Sciences Program Manager:	R.E. Wildung	S.G. Weiss, Report Coordinator G.P. O'Connor, Editor
Part 3:	Atmospheric Sciences Program Manager:	C.E. Elderkin	C.E. Elderkin, Report Coordinator E.L. Owczarski, Editor
Part 4:	Physical Sciences Program Manager:	L.H. Toburen	L.H. Toburen, Report Coordinator P.L. Gurwell, Editor
Part 5:	Environment, Safety, Health, and Quality Assurance Program Managers:	L.G. Faust B.L. Steelman J.M. Selby	L.G. Faust and B.L. Steelman, Report Coordinators S.K. Ennor, M.T. Upton, and J.M. Gephart, Editors

Activities of the scientists whose work is described in this annual report are broader in scope than the articles indicate. PNL staff have responded to numerous requests from DOE during the year for planning, for service on various task groups, and for special assistance.

Credit for this Annual Report goes to the many scientists who performed the research and wrote the individual project reports, to the progam managers who directed the research and coordinated the technical progress reports, to the editors who edited the individual project reports and assembled the five parts, and to Ray Baalman, editor in chief, who directed the total effort.

Members of the Scientific Advisory Committee, established in 1985, are:

Dr. Franklin I. Badgley	University of Washington
Dr. Leo K. Bustad	Washington State University
Dr. Franklin Hutchinson	Yale University
Dr. Albert W. Johnson	San Diego State University
Dr. J. Newell Stannard	University of Rochester; University of California, San Diego

W.J. Bair, Manager
Environment, Health and Safety
Research Program

Previous reports in this series:

Annual Report for	
1951	HW-25021, HW-25709
1952	HW-27814, HW-28636
1953	HW-30437, HW-30464
1954	HW-30306, HW-33128, HW-35905, HW-35917
1955	HW-39558, HW-41315, HW-41500
1956	HW-47500
1957	HW-53500
1958	HW-59500
1959	HW-63824, HW-65500
1960	HW-69500, HW-70050
1961	HW-72500, HW-73337
1962	HW-76000, HW-77609
1963	HW-80500, HW-81746
1964	BNWL-122
1965	BNWL-280, BNWL-235, Vol. 1-4; BNWL-361
1966	BNWL-480, Vol. 1; BNWL-481, Vol. 2, Pt. 1-4
1967	BNWL-714, Vol. 1; BNWL-715, Vol. 2, Pt. 1-4
1968	BNWL-1050, Vol. 1;, Pt. 1-2; BNWL-1051, Vol. 2, Pt. 1-3
1969	BNWL-1306, Vol. 1;, Pt. 1-2; BNWL-1307, Vol. 2, Pt. 1-3
1970	BNWL-1550, Vol. 1;, Pt. 1-2; BNWL-1551, Vol. 2, Pt. 1-2
1971	BNWL-1650, Vol. 1;, Pt. 1-2; BNWL-1651, Vol. 2, Pt. 1-2
1972	BNWL-1750, Vol. 1;, Pt. 1-2; BNWL-1751, Vol. 2, Pt. 1-2
1973	BNWL-1850, Pt. 1-4
1974	BNWL-1950, Pt. 1-4
1975	BNWL-2000, Pt. 1-4
1976	BNWL-2100, Pt. 1-5
1977	PNL-2500, Pt. 1-5
1978	PNL-2850, Pt. 1-5
1979	PNL-3300, Pt. 1-5
1980	PNL-3700, Pt. 1-5
1981	PNL-4100, Pt. 1-5
1982	PNL-4600, Pt. 1-5
1983	PNL-5000, Pt. 1-5
1984	PNL-5500, Pt. 1-5
1985	PNL-5750, Pt. 1-5
1986	PNL-6100, Pt. 1-5

FOREWORD

The Atmospheric Sciences Program at the Pacific Northwest Laboratory (PNL) centered its initial emphasis on short-range diffusion and worldwide fallout studies for the Atomic Energy Commission (AEC). Early tracer developments were used in dispersion experiments to produce an extensive data base defining instantaneous and continuous plumes diffusing over a limited, relatively flat portion of the Hanford Site. Plume characteristics for a uniform surface in steady-state conditions were evaluated as a function of meteorological parameters. In fallout studies, very sensitive radiological detection methods permitted detailed characterization of seasonal and year-to-year variations in air concentrations of radionuclides over western North America.

As the program evolved, early research also dealt with wet and dry scavenging of nuclear contaminants. Much of the field experimentation on scavenging processes involved simulation of nuclear particulates with tracers. Releases of tracers at the surface investigated dry removal and below-cloud wet removal processes and, later in our initial research aircraft operations, tracers were released into clouds to study in-cloud scavenging processes. As energy development was undertaken more broadly, our research extended beyond nuclear concerns to include the transport, transformation, and wet removal of fossil energy contaminants on a local to multi-state basis, preceding by several years the recognition of acid rain as a national problem.

Currently, the broad goals of atmospheric research at PNL are to describe and predict the nature and fate of atmospheric contaminants and to develop an understanding of the atmospheric processes contributing to their distribution on local, regional, and continental scales in the air, in clouds, and on the surface. For several years, studies of transport and diffusion have been extended to mesoscale areas of complex terrain. Atmospheric cleansing research has expanded to a regional scale, multilaboratory investigation of precipitation scavenging processes involving the transformation and wet deposition of chemicals composing "acid rain." In addition, the redistribution and long-range transport of transformed contaminants passing through clouds is recognized as a necessary extension of our research to even larger scales in the future. A few long-range tracer experiments conducted in recent years and the special opportunity for measuring the transport and removal of radioactivity following the Chernobyl reactor accident of April 1986 offer important initial data bases for studying atmospheric processes at these super-regional scales.

The description of ongoing atmospheric research at PNL is organized in terms of the following study areas:

- **Atmospheric Studies in Complex Terrain**
- **Large-Scale Atmospheric Transport and Processing of Emissions**
- **Measurement and Analysis Developments**
- **Atmosphere-Surface Interactions.**

Atmospheric Studies in Complex Terrain

Air pollution in regions of nonuniform terrain is a particularly difficult problem because of the complexity of meteorological conditions over spatial scales ranging from individual valley slopes to systems of many valleys and ridges of a region, and the diurnal coupling/decoupling phenomena between air in individual valleys and the regional convective boundary layer. This research has coordinated activities in the areas of boundary layer meteorology, development of valley circulations and their interactions with synoptic flow, and the transport and dispersion of contaminated air parcels in mountainous terrain settings. The coordinated program attempts to integrate theoretical analysis, model development, and results from field experiments. Improved understanding of transport and diffusion in complex terrain gained through this interactive approach will allow the development of assessment models that can be applied with improved reliability to the siting and emergency response concerns of many energy facilities of DOE and U.S. industry.

Large-Scale Atmospheric Transport and Processing of Emissions

Understanding the large-scale transport of contaminants in the atmosphere and their movement and chemical behavior within cloud systems is important in developing methods to predict the deposition of such contaminants. A current major effort is our participation in the Processing of Emissions by Clouds and Precipitation (PRECP) program.

PRECP is a multilaboratory effort to improve understanding of the phenomena that are important in acid rain. Ultimately, understanding of these processes will contribute to the implementation of effective control strategies. Personnel at PNL are primarily responsible for advances in understanding precipitation scavenging; major activities involve the conduct of large-scale field studies. Data obtained from these experiments are being analyzed and used to develop and improve cloud chemistry and precipitation scavenging numerical models. These, in turn, are combined with other elements of regional-scale acid rain models as part of the larger National Acid Precipitation Assessment Program.

Measurement and Analysis Techniques

Since the early developments in tracer technologies and methods for detecting fallout materials, the importance of continually advancing capabilities for measuring and analyzing atmospheric constituents and properties has been recognized by PNL. The long-standing operation of a precipitation chemistry network and the evolution of its measurement and analysis technology has steadily pushed forward the state-of-the-art in this area. The early establishment of a research aircraft capability was followed by an annual re-evaluation of

sensors and data systems for meteorological, cloud physics, atmospheric chemistry, aerosol, and other air pollution measurements. To obtain the levels of sensitivity and accuracy needed in experiments, improvements have been continually made, including, by necessity, many instrumentation developments. PNL, in its internal exploratory research, looks even further to the future for new concepts in measurement and analysis to maintain a position in the forefront of this important aspect of research.

Atmosphere-Surface Interaction

Research on air-to-surface exchange processes had its beginnings in the nuclear area where deposition and resuspension of radionuclide particulates were investigated. Transfers of energy-related contaminants between the atmosphere and surfaces of various physical, chemical, and biotic composition remain a serious concern. It is recognized that future research must deal in an integrated manner with transfer processes for energy, moisture, and nutrients involved in the maintenance of biological systems at the earth's surface together with the contaminants introduced by humans that may impact these systems. Indeed, international attention is currently being focussed on the functioning of the earth's environment as an integrated system and the changes that we can anticipate, even on a global basis, due to human activities. The International Geosphere-Biosphere Program (IGBP) will promote a broad, interdisciplinary research effort, including as a high priority the study of interactions between the atmosphere and the earth's biological and geological systems. PNL is examining expanded research in this area for DOE, which would draw on our experience to complement these international efforts.

This report describes the progress in FY 1987 in each of these areas. A divider page summarizes the goals of each area and lists project titles that support research activities.

CONTENTS

Atmospheric Studies in Complex Terrain

ATMOSPHERIC STUDIES IN COMPLEX TERRAIN

The ASCOT program investigates atmospheric boundary layer circulations and contaminant transport and dispersion in areas where surface features strongly influence or control these processes. Three projects at PNL investigate related aspects of the ASCOT research and are closely coordinated with ASCOT projects at other DOE laboratories.

The primary transfers of energy and momentum that drive and retard all atmospheric circulations take place at the earth's surface and in the adjacent atmospheric boundary layer. In areas of complex terrain these transfers can first be reflected in local and mesoscale circulations before being passed on to the general atmosphere. Relatively isolated circulations can develop within the constraints of significant terrain features during strong diurnal energy loss from the near-surface air; these are later reversed and coupled once again to the general atmospheric gradient flow as diurnal gains in energy reconfigure airflow over slopes and within valleys. Contaminants released within these boundary-layer circulations can be trapped in valleys aod basins, "fumigated"and impinged on valley floor and wall surfaces, and eventually vented from valleys as energy exchanges evolve. Even in rather idealized complex terrain these flows and the associated contaminant transport and dispersion are not easily described or predicted. Consequently, ASCOT research is aimed at understanding the role of energy exchange, terrain configuration, and scale interactions for coupled flows (e.g., slope, valley, and gradient) in developing and destroying boundary-layer circulations and in dispersing contained contaminants. Experiments are conducted at mountainous sites where prominent terrain features are thoroughly characterized and the strong diurnal variations in energy fluxes are well documented. Resultant temperature, wind, and turbulence fields in the thermally generated mesoscale circulations are measured with in situ and remote sensing instrumentation. The general flow features over the region to which the terrain-induced circulations and contaminant plumes are periodically linked are characterized with soundings and tracers.

Closely coordinated investigations in the three ASCOT projects are systematically developing a generalized understanding of the relevant processes, expressed in increasingly reliable theoretical/analytical descriptions and models. Such models hold the promise of translating descriptive and forecasting capabilities to the large number of other locations where boundary layer flow and contaminant dispersion and transport are influenced by terrain features and surface energy exchange processes but to a lesser extent than for the highly organized, decoupled mesoscale flows studied in ASCOT.

The three projects that compose the ASCOT research program at PNL are:

- **Atmospheric Boundary Layer Studies**
- **Atmospheric Diffusion in Complex Terrain**
- **Coupling/Decoupling of Synoptic and Valley Circulations.**

APPLICATION OF REMOTELY SENSED RADIATIVE DATA TO COMPLEX TERRAIN METEOROLOGICAL RESEARCH

J. M. Hubbe, C. D. Whiteman, H. P. Foote and L. G. McWethy

Digital elevation models (DEM) and Landsat 5 Thematic Mapper (TM) scenes are available in image resolution over typical domains of interest in complex terrain meteorology. Techniques for applying these data to research problems are being developed.

Airflow in deep valleys is influenced by the presence of the valley sidewalls and is constrained within them. When these valleys are sunlit, there is usually a difference in surface heating from one side to the other, often causing a secondary circulation toward the warmer sidewall at the valley floor. On clear nights, the ground surfaces cool more quickly by radiation than the air, and the air near the surface, cooled conductively, flows down in the valley as far as the density stratification will allow. The airflow is often decoupled from the larger scale air motions outside or above the valley.

One such valley domain that has been intensively studied is the Brush Creek valley in western Colorado. During a major field experiment conducted during September and October of 1984, arrays of rawinsondes, tethersondes, meteorological towers, surface energy-budget stations, sodars, tracer equipment, and lidars were deployed to measure the nighttime flows and the morning transition from well-developed nocturnal drainage flow to daytime convective flow (Whiteman and Barr 1986; Horst, Allwine and Whiteman 1987).

Part of the Brush Creek data analysis is the atmospheric energy budget; a very important contribution to this is the valley surface energy budget (Whiteman et al. 1987). Specifically, data from five surface energy-budget measurement stations are being interpolated/extrapolated to a rectangular grid using a surface energy simulation based on both analytical relations and parameterizations tuned to the data (Whiteman et al. 1987). Support of this energy budget study motivated our involvement in remotely sensed radiative data.

A preliminary DEM was created for Brush Creek from a 7.5-minute quadrangle topographic map. Direct beam solar shading was performed on slope elements using the Minnaert model of reflectance (Justice, Wharton and Holben 1981). In several cases oblique views were generated for viewpoints from which photographs had been taken during the experiment. Figure 1 compares the simulated shading (1a) with a photograph (1b) taken near the mouth of the valley. These shaded topographies are directly applicable, both qualitatively and quantitatively, to the study of energy input.

FIGURE 1a. Simulated Shadows from Same Place and Time as Photograph in Figure 1b.

FIGURE 1b. 35-mm Photograph Taken from the Mesa Rim Near the Mouth of the Valley at 0830 LDT on September 20, 1984.

Thematic Mapper Day Scene

For the purpose of developing tools to apply remotely sensed radiative data to the ongoing energy-budget work, we searched for a daytime scene acquired by the Landsat 5 TM. A date during summer of 1986 (July 28) was identified on which a cloud-free daytime scene including Brush Creek had been acquired and archived. This quarter scene was purchased from Earth Observations Satellite Company (EOSat). Nine 7.5-minute DEM quadrangles encompassing Brush Creek were purchased from the U.S. Geological Survey and were combined to produce a base topography file. The daytime scene was registered and resampled to this topographic grid.

Decorrelation of Direct Beam Shading

The calculation of an albedo field from these data is ongoing. The portion of this task discussed here is the extraction of surface reflectance through the modeling of topographically caused variations in radiance. Based on previous experience, we chose to use the nonlambertian Minnaert reflectance model (Justice, Wharton and Holben 1981; Horn 1981)

$$L = Ln[\cos(i)^K \cos(e)^{K-1}] \qquad (1)$$

where L = radiance, Ln = radiance for i = e = 0, i = incidence angle, e = exitance angle, and K = Minnaert constant. K is found from the slope of the linear regression of log[L cos(e)] on log[cos(i) cos(e)].

Bands 1 Through 5. For a given TM band, a series of test regions was defined for making estimates of K. Correlation coefficients (r) on the order of 0.75 were achieved in the most successful regions. A conelike test region on the east side of the mouth of Brush Creek gives K = 0.63 for TM Band 5. This feature can be seen in Figure 2a, which is a gray-scale representation of the July 28, 1986, TM Band 5 scene. Brush Creek runs diagonally from upper left to lower right of the frame (north is at the top). The elevation angle and azimuth angle at the time of this acquisition were 54° and 107°, respectively. This test region is illuminated intensely on the southeast side and dimly on the northwest side. Figure 2b is the residual after decorrelation using the K = 0.63 model. The removal of topographic shading appears successful in the test region and in similar box-canyon/flat-iron features. The extent to which the shadow-like features on the mesas between major valleys result from topographic shading or from variation in ground cover remains uncertain. The same test region produced r = 0.80 and K = 0.43 for Band 1.

FIGURE 2a. A Gray-Scale Representation of the July 28, 1986, TM Band 5 Scene.

FIGURE 2b. Residual of Band 5 After Decorrelation Using the K = 0.63 Model.

Other test regions, particularly those on the mesas, produced lower values of both r and K.

Band 6. Band 6 is a special case, measuring emittance rather than reflectance. Note that Band 6 has one-fourth the spatial resolution of the other bands. The calibration of the band 6 digital number (DN) to surface temperature, without correction for atmospheric absorption, is as follows:

$$T_u = K_2/(K_1/R_u + 1) \qquad (2)$$

where

$K_1 = 60.776$ (mw cm^{-2} sr^{-1} μm^{-1})
$K_2 = 1260.56$ (K)
$R_u = 0.123 + 0.005632 * DN$
(mw cm^{-2} sr^{-1} μm^{-1}).

Figure 3a is a gray-scale representation of the July 28, 1986, TM Band 6 scene. Uncorrected temperatures range from 290 to 319 K. The accuracy of TM Band 6 uncorrected temperatures is expected to be on the order of ±1.5°C. The surface temperature is expected to be correlated with the irradiance of the surface elements, with other influences including surface reflectivity and surface heat conductivity. In subsequent work, estimates of these quantities will be made; here they are considered unknowns. Figure 3b represents a decorrelation using a lambertian model.

FIGURE 3b. Residual of Band 6 After Decorrelation Using a Lambertian Model.

Thematic Mapper Night Scene

Under clear night skies, the temperature structure of the valley atmosphere is stably stratified, and the flow is decoupled from the large-scale flow. The valley atmosphere is more bounded by the topography than during the day; that is, the surface accounts for a larger fraction of the boundary of the valley flow. This suggests the importance of ground surface temperature to nighttime flows.

Calibration

No Landsat 5 nighttime overflights were available from the 1984 experiment and none on archive included Brush Creek, so two special acquisitions were ordered for fall of 1986. November 25 was cloudless and snow-free. Figure 4 is a gray-scale representation of the TM Band 6. Surface temperatures, uncorrected for atmospheric transmittance, ranged from 256 to 270 K. The important features of the image are the colder temperatures on the mesa, the warmer temperatures on the valley sidewall, and a band of cooler temperatures along the valley bottom.

FIGURE 3a. Gray-Scale Representation of the July 28, 1986, TM Band 6 Scene.

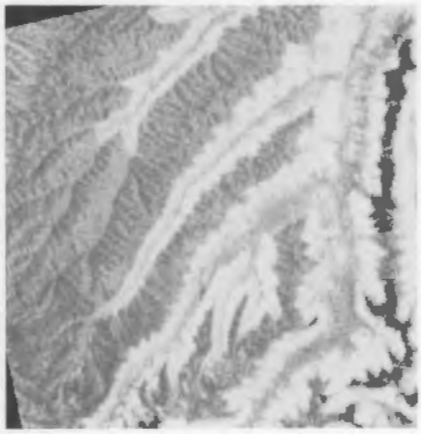

FIGURE 4. Gray-Scale Representation of the November 25, 1986, TM Band 6 Scene.

Correlation of Surface Temperature with Surface Height

Figure 5 is a scattergram of ground surface height above sea level (DEM) on surface temperature (T_u). The discrete values indicate the narrow range of temperatures from the standpoint of the DN resolution. The scattergram is analogous to a vertical sounding of surface temperature in the Brush Creek watershed. Superimposed is an approximation of a typical vertical sounding of atmospheric temperature near midnight in the center of the valley. It has been left-shifted so the lowest altitude temperature matches the ground surface temperature. This crude but reasonable approximation is performed here to compensate for the different dates and the lack of atmospheric corrections. The intent is to make a rough estimate of the horizontal temperature difference between the ground surface at the mesa rim and the atmosphere over the valley axis. This temperature difference represents the driving force for the nocturnal drainage flow.

Summary

We have shown a sample of intermediate digital image products that have been useful in our ongoing studies of the energetics of atmospheric flows in a deep valley. The techniques used to produce these images as well as the techniques by which they will be applied to the understanding and simulation of valley flows are still under development. The progress to this point in achieving quantitative tools is very encouraging. Future work includes making atmospheric corrections to the remotely sensed radiances: combining the flattened reflectances to estimate a bulk albedo field, and investigating surface heat conductivity using simulated irradiance, the albedo, and surface temperature fields.

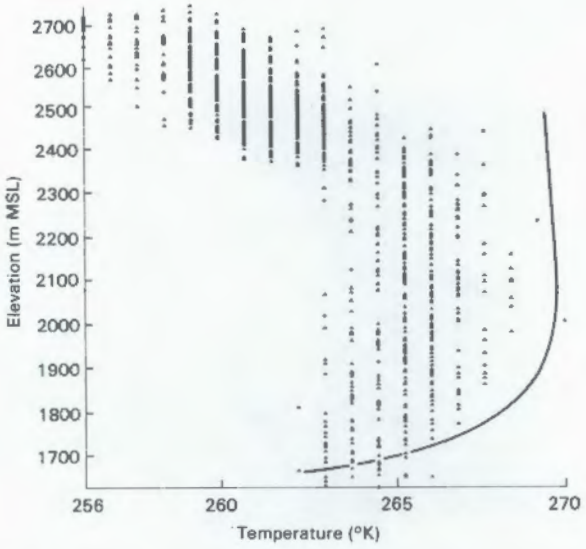

FIGURE 5. Scatter Gram of Ground Surface Height Above Sea Level (DEM) on Surface Temperature (T_u). The solid curve represents a typical nighttime atmospheric temperature profile, as obtained from September 1984 experiments in the Brush Creek valley.

References

Horn, B. K. P. 1981. "Hill Shading and the Reflectance Map." In Proceedings of the IEEE 69(1):14-47.

Horst, T. W., K. J. Allwine and C. D. Whiteman. 1987. "A Thermal Energy Budget for Nocturnal Drainage Flow in a Simple Valley." In Proceedings of the Fourth Conference on Mountain Meteorology, American Meteorological Society, Boston, Massachusetts.

Justice, C. O., S. W. Wharton and B. N. Holben. 1981. "Application of Digital Terrain Data to Quantify and Reduce the Topographic Effect on Landsat Data." Int. J. Remote Sensing 2(3).

Whiteman, C. D., K. J. Allwine, J. M. Hubbe, H. P. Foote, M. M. Orgill and L. J. Fritschen. 1987. "Radiation and Surface Energy Budgets for a Colorado Valley." In Proceedings of the Fourth Conference on Mountain Meteorology, American Meteorological Society, Boston, Massachusetts.

Whiteman, C. D., and S. Barr. 1986. "Atmospheric Mass Transport by Along-Valley Wind Systems in a Deep Colorado Valley." J. of Climate Appl. Meteor. 25(9).

BOWEN RATIO SURFACE ENERGY BUDGET MEASUREMENTS IN A COLORADO VALLEY

C. D. Whiteman, K. J. Allwine, M. M. Orgill, and L. J. Fritschen[a]

Five surface energy budget stations were installed and operated in Colorado's Brush Creek Valley in September and October 1984 as part of the ASCOT program. The five stations used the well-known Bowen ratio technique to measure the components of the surface energy budget (Miller 1981, Oke 1978). The Bowen ratio stations, as described by Fritschen et al. (1985), were located at sites that were chosen to be representative of the main

(a) University of Washington, Seattle, Washington.

topographic regimes of the Brush Creek valley. Figure 1 shows these site locations. Two stations were situated on the east (E) and west (W) sidewalls of the valley. Two other stations, operated by the Wave Propagation Laboratory (WPL) and PNL, were located on the valley floor at different distances from the valley mouth. (The WPL site was situated in a meadow on the valley floor and will hereafter be called the meadow site.) The final station was situated east of the valley on Skinner Ridge and will hereafter be referred to as the ridge-top (RDG) site. This ridge is actually a broad plateau area.

This article describes the surface energy balance in the valley at the five stations on September 25, 1984--a nearly clear day in which a layer of cirrostratus clouds made several advances into the valley from the south in the mid- to late afternoon.

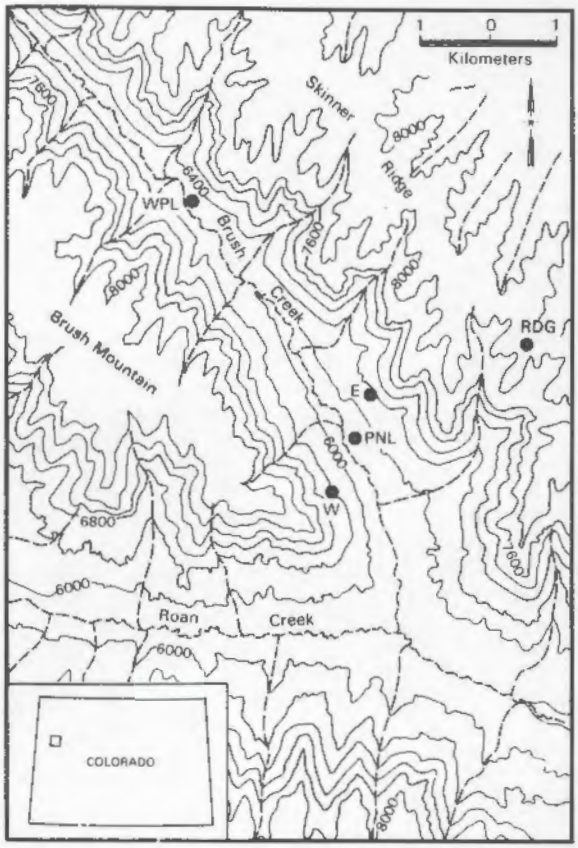

FIGURE 1. Locations of Energy Budget Measurement Sites (dots) in the Brush Creek Valley Area (elevations in feet).

Surface Energy Balance

Daily Course of Energy Budget Parameters

Figure 2 shows the diurnal variation of net radiation, ground heat flux, latent heat flux, and sensible heat flux at the five sites on September 25, 1984. Figures are plotted from 30-min averages.

Net radiative loss at night was 40 to 70 W/m^2, with the largest losses from the ridge-top site. A comparison of the nighttime Bowen ratio-derived flux values with values obtained by other investigators at adjacent sites using the eddy-correlation method has been recently described by Doran and Hubbe (1987). At the PNL, ridge-top, and meadow sites, located on level ground, net radiation was symmetric about solar noon, with highest net radiative gains at the ridge-top site. Strong asymmetries occurred on the sloping surfaces. The effect on the curves of the varying times of local sunrise and sunset is seen even in these 30-min averages.

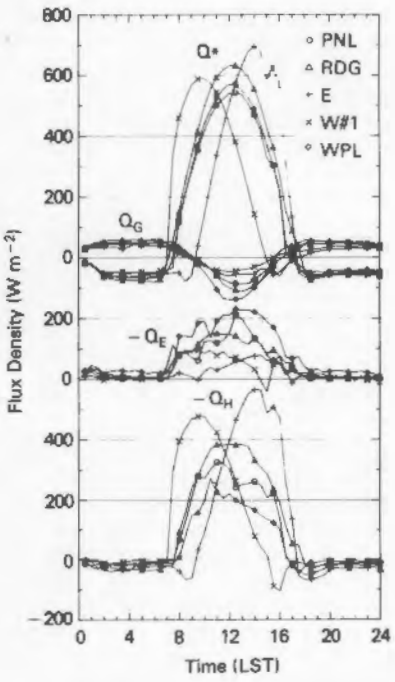

FIGURE 2. Net Radiation (Q*), Soil Heat Flux (Q_G), Latent Heat Flux (Q_E) and Sensible Heat Flux (Q_H) for Brush Creek Valley on September 25, 1984 (Y-axis values are in W/m^2).

Nighttime soil heat fluxes were toward the surface at rates of up to 50 to 60 W/m^2. This soil heat flux effectively counteracted most of the nighttime net radiative energy loss from the surface. The magnitude of the soil heat flux wave was highest at the more moist sites and was especially pronounced at the meadow site.

Latent heat fluxes, as expected, were relatively small in this semiarid valley. The largest latent heat fluxes (≈200 W/m^2) were measured in midday at the meadow site. Latent heat fluxes at the PNL, ridge-top, and meadow sites showed a near-symmetric shape but exhibited somewhat higher values in the afternoon. Latent heat fluxes were high on the west sidewall in the morning and on the east sidewall in the afternoon, in keeping with the asymmetric course of net radiation at the two sites.

Sensible heat fluxes differed significantly from site to site, with especially pronounced differences apparent between the east and west sidewalls. These differential heating rates on the opposing sidewalls produced pronounced cross-valley circulations (Bader and Whiteman 1986). Sensible heat fluxes that occurred during the daytime on the valley floor and ridge-top had a sinusoidal shape. Partitioning of much of the available energy ($Q^* + Q_G$) into latent heat flux at the meadow site reduced the sensible heat flux there. At the ridge-top site, the instantaneous sensible heat flux curve was symmetrical about solar noon. The maximum value of the curve was less than that at the east sidewall site. However, upward sensible heat flux persisted for a longer period of time on the ridge-top, where the effects of solar shading were absent.

Energy Balance Totals

Figure 3 shows the daily totals of the surface energy budget parameters. The 24-h soil heat flux totals ranged from 0.47 to 1.40 MJ/m^2, indicating a net cooling of the soil during this clear, fall day. Daily totals of sensible heat flux varied from 4.04 MJ/m^2 at the meadow site, where much of the available energy was used to support evapotranspiration, to 8.49 MJ/m^2 at the ridge-top site. The east sidewall site received a daily total almost as high (8.43 MJ/m^2). This site had a shorter day than the ridge-top site (i.e., a later local sunrise time and an earlier local sunset time), but the dry east sidewall was intensely heated in the afternoon and the lack of soil moisture and small amount of vegetation resulted in a large conversion of available energy into sensible heat flux. Sensible

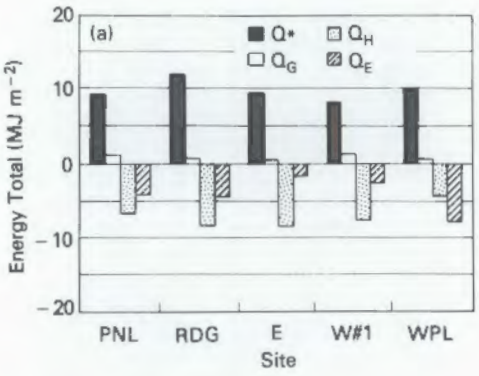

FIGURE 3. Daily Totals of Surface Energy Budget Parameters at the Five Bowen Ratio Sites, September 25, 1984.

heat flux totals at the five sites differed by as much as a factor of 2, while latent heat flux totals varied by a factor of 4.2. On clear days, such as September 25, 1984, the large sensible heat fluxes in this semiarid area are sufficient to destroy temperature inversions that form in the valleys at night and provide the source of energy to develop deep convective boundary layers over the western slope of the Rocky Mountains. The transfer of energy to and from the valley atmosphere (i.e., sensible heat flux) drives the local wind systems in the valley, producing along-valley, along-slope and cross-valley circulations. Work is under way using models (Bader 1987) and analysis of Colorado field data (Horst et al. 1987) to evaluate the energy budget of the valley atmosphere to gain basic knowledge about the dynamic responses of the valley atmosphere to the energy inputs. The influence of the circulations on transport and diffusion of pollutants is another key problem being addressed in the PNL ASCOT programs (Bader and Whiteman 1986).

Work is under way to develop methods for estimating the areal distribution of radiation and surface energy budget parameters in the valley from data collected at the five sites, using a digital terrain model of the valley. This work has been described in articles by Whiteman et al. (1987) and, in more detail, by Hubbe et al. (1987).

References

Bader, D. C. 1987. "Valley Mass and Energy Budgets Computed from Model Simulations." In Preprints, Fourth Conference on Mountain Meteorology, August 25-28, 1987, Seattle, Washington, pp. 15-19.

Bader, D.C., and C.D. Whiteman. 1986. "Model Simulation of Plume Dispersion in a Narrow Valley After Sunrise." In Preprints, Fifth Joint Conference on Applications of Air Pollution Meteorology, November 18-21, 1986, Chapel Hill, North Carolina.

Doran, J. C., and J. M. Hubbe. 1987. "Surface Heat Fluxes During the 1984 Brush Creek Field Study." In Pacific Northwest Laboratory Annual Report to the DOE Office of Energy Research, Part 3 - Atmospheric Sciences. PNL-6100 Pt. 3, p. 15, Pacific Northwest Laboratory, Richland, Washington.

Fritschen, L. J., J. R. Simpson, C. D. Whiteman and M. M. Orgill. 1985. "General Description and Location of Energy Balance Stations in a Deep Colorado Valley: ASCOT 84." In Preprints, 17th Conference on Agriculture and Forest Meteorology, May 21-24, 1985, Scottsdale, Arizona.

Horst, T. W., K. J. Allwine and C. D. Whiteman. 1987. "A Thermal Energy Budget for Nocturnal Drainage Flow in a Simple Valley." In Preprints, Fourth Conference on Mountain Meteorology, August 25-28, 1987, Seattle, Washington, pp. 15-19.

Hubbe, J. M., C. D. Whiteman, H. P. Foote and L. G. McWethy. 1987. "Applications of Digital Image Processing in Ongoing Research in Complex Terrain Meteorology." Paper presented at SPIE's 1987 Cambridge Symposium on Digital Image Processing and Visual Communications Technologies in Meteorology, October 25-30, 1987, Cambridge, Massachusetts.

Miller, D. H. 1981. Energy at the Surface of the Earth. International Geophysics Series, Volume 27, Academic Press, New York.

Oke, T. R. 1978. Boundary Layer Climates. Halsted Press, John Wiley and Sons, New York.

Whiteman, C. D., K. J. Allwine, J. M. Hubbe, H. P. Foote, M. M. Orgill and L. J. Fritschen. 1987. "Radiation and Surface Energy Budgets for a Colorado Valley." In Preprints, Fourth Conference on Mountain Meteorology, August 25-28, 1987, Seattle, Washington, pp. 11-14.

ESTIMATION OF THE NOCTURNAL THERMAL ENERGY BUDGET FOR BRUSH CREEK

T. W. Horst and K. J. Allwine

In September 1984 the ASCOT program made extensive measurements of the nocturnal wind and temperature fields in the Brush Creek valley of western Colorado. These measurements included an array of nine tethered balloons and four Doppler sodars deployed along the valley axis to measure vertical profiles of wind, temperature, and moisture; a Doppler lidar to measure the along-valley wind component throughout much of the valley; several laser anemometers to measure path-averaged valley, tributary, and slope winds; and several surface sites to measure surface fluxes of heat, moisture, and momentum and near-surface profiles of wind and temperature.

These data are being used to directly evaluate the nocturnal thermal energy budget of this simple valley, with the purpose of examining the relative importance of the various mechanisms that generate and maintain the valley inversion and thus also the nocturnal drainage flow. Time-averaged thermal energy budgets have been calculated for the period 2330 MST to 0630 MST for the nights of September 25-26 and 29-30; the results presented here are for the night of September 25-26. The weather on that night was relatively undisturbed, but with variable high thin cirrus and with winds above the ridge tops from the SW at 5 to 10 m/s.

Thermal Energy Budget

In order to examine the energy balance of the Brush Creek valley, we have calculated the cross-valley-integrated thermal energy budget for four consecutive segments of the Brush Creek valley, defined by the locations of the WPL, LANL, CSU, LLNL and PNL-V[(a)] tethered balloon sites. A schematic of one of these segments is shown in Figure 1. The segment is bounded in the along-valley direction by a pair of tethered balloon sites and in the cross-valley direction by the valley sidewalls. Each term of the thermal energy budget has been evaluated as a function of height above the valley floor by integrating across the width of the valley and then averaging in the along-valley direction between tethered balloon sites.

The thermal energy budget is

$$\rho C_p \frac{\partial \theta}{\partial t} = -\rho C_p \vec{U} \cdot \nabla \theta - \nabla \cdot \vec{F} , \qquad (1)$$

(a) These abbreviations identify the laboratories who operated measurement stations during the Brush Creek valley field experiment: the Wave Propagation Laboratory (WPL), Los Alamos National Laboratory (LANL), Colorado State University (CSU), Lawrence Livermore National Laboratory (LLNL), and the Pacific Northwest Laboratory (PNL).

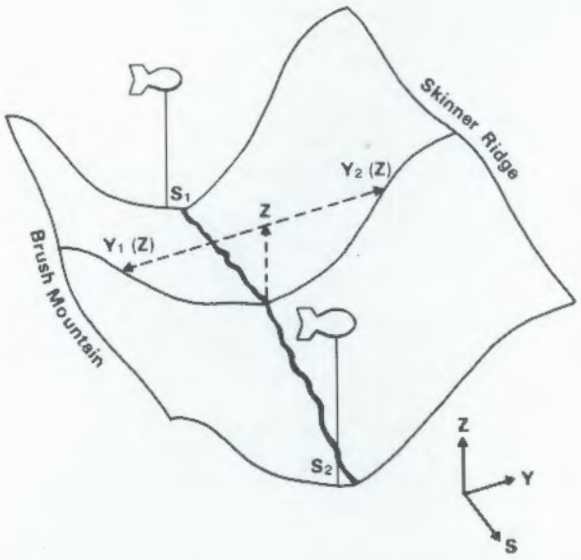

FIGURE 1. Schematic of Valley Segment Used for Calculation of the Cross-Valley-Integrated Thermal Energy Budget.

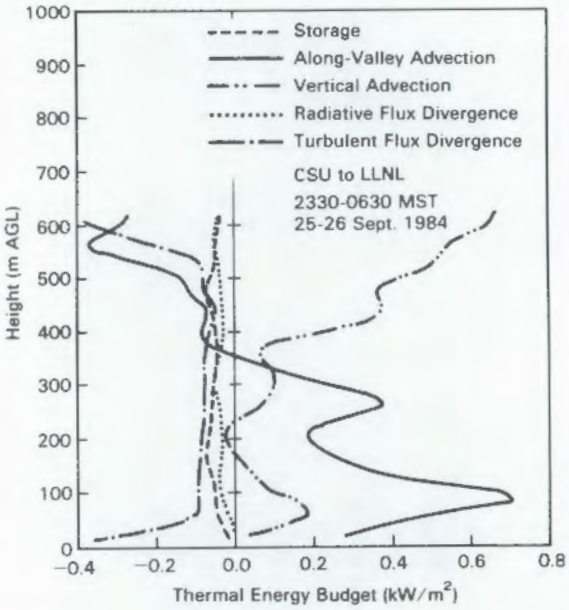

FIGURE 2. Cross-Valley-Integrated Thermal Energy Budget for CSU to LLNL Valley Segment, 2330 MST September 25, 1984 to 0630 MST September 26, 1984.

where F is the sum of the net radiation and turbulent energy fluxes, $F_n + \rho C_p \overline{w'\theta'}$, and the remaining notation is standard. The time-rate-of-change of thermal energy, along-valley thermal advection, and radiative flux divergence have been directly calculated from the data throughout the valley. The surface sensible heat flux has been estimated throughout the valley by spatial extrapolation of locally measured surface fluxes. Vertical thermal advection has been estimated by evaluating the valley mass budget to determine the vertical mass flux required to balance down-valley mass flux divergence. These estimates are shown in Figure 2 for a representative segment, that bounded by the CSU and LLNL sites.

The left-hand side of the thermal energy budget is an energy storage term. The valley atmosphere is found to cool through the night, reflecting an energy loss. Cross-valley-integrated thermal storage is roughly constant with height and appears to be a minor component of the budget. An interesting feature of the cooling rate profile is a local minimum near the level where the wind shifts from a down-valley to an up-valley direction about 400 m above the surface.

The radiative flux divergence term in the thermal energy budget has been computed with a radiative transfer model similar to that described by Cox (1973) and Griffith et al. (1980). The atmospheric sounding used for this calculation at each site is a composite of the tethered balloon measurements in the valley and a profile at higher altitudes that has been interpolated from a regional rawinsonde network. With the exception of a 10- to 20-m layer near the surface, radiative flux divergence causes cooling of the valley atmosphere. This is generally the smallest term in the thermal energy budget, but it is comparable in magnitude to the storage term and also has a local minimum at a height of 400 m.

The turbulent flux divergence was not measured directly, but has been estimated by assuming a constant surface sensible heat flux per unit horizontal surface area and arbitrarily assuming that the turbulent sensible heat flux is zero at a height of 20 m above the surface. The surface sensible heat flux was chosen to be 20 W/m^2 throughout the valley, based on a surface energy balance analysis for this night (Whiteman et al. 1987). The consequent profiles of cross-valley-integrated sensible heat flux divergence directly reflect the geometry of the valley, with higher values on the valley floor and on the ridge tops corresponding to larger horizontal surface area per unit height. The sensible heat flux divergence is comparable in magnitude to the preceding terms, but is generally the largest of the three.

The remaining term in the thermal energy budget is energy advection. If the potential

temperature is uniform in the cross-valley direction, cross-valley advection will be zero and the energy advection may be divided into along-valley and vertical components. It can be seen from Figure 2 that these are the dominant terms in the thermal energy balance.

Along-valley advection is the product of the along-valley wind and the along-valley potential temperature gradient. Down-valley drainage winds occur in the lowest 400 m of the valley depth, with a low-level maximum at a height of 60 m and up-valley winds above 400 m. The along-valley gradient of potential temperature, $\partial\theta/\partial s$, is somewhat variable with height and from segment to segment of the valley. Since a typical gradient of -0.2 K/km is based on a temperature difference of only 0.3 K between tethered balloon sondes with an along-valley separation of 1.5 km, part of this variation undoubtably reflects measurement uncertainty.

With the exception of the LANL to CSU valley segment, $\partial\theta/\partial s$ is negative, with the largest gradient near the surface, and along-valley thermal energy advection is positive in the down-valley drainage flow and negative above. In the LANL to CSU valley segment, however, $\partial\theta/\partial s$ is positive in the drainage flow and negative above. The positive $\partial\theta/\partial s$ is a consequence of strong subsidence warming between the LANL and CSU sites that depresses the isentropes near the CSU site.

Vertical advection is the product of the vertical wind and the vertical potential temperature gradient. The cross-valley-integrated vertical wind has been estimated for each valley segment from the divergence of the along-valley wind field; the nocturnal volume flux increases with distance down Brush Creek, implying a general subsidence. In two valley segments, including the CSU to LLNL segment, the vertical velocity is on the order of 1 cm/s in the lowest 100 m, becomes generally less than 0.5 cm/s between 100 and 200 m, and then increases to a value of 2 to 3 cm/s near the ridge top. As noted previously, between the LANL and CSU sites there appears to be much stronger subsidence within the drainage flow, up to 3 cm/s, decreasing to 2 cm/s near ridge top. The largest implied subsidence occurs between the LLNL and PNL-V sites, up to 9 cm/s near ridge top, corresponding to a large increase in the valley cross section with down-valley distance.

The vertical potential temperature gradient decreases from a maximum value of 50 to 60 K/km near the surface to 20 K/km at a height of 100 m to a minimum of 5 K/km at the top of the drainage flow. Above 400 m $\partial\theta/\partial z$ increases again to the isothermal value 10 K/km.

With the exception of the lowest 100 m of the LLNL to PNL-V valley segment, the vertical energy advection is positive. In the CSU to LLNL segment, Figure 2, the cross-valley-integrated vertical advection profile within the drainage flow is quite similar to that for along-valley advection, with a local minimum at the top of the drainage flow. Above the drainage flow, the cross-valley-integrated vertical advection increases to values substantially larger than those found within the drainage flow.

Discussion

As expressed in Equation (1), any net imbalance of the advection and flux divergence terms of the thermal energy budget should be reflected in the storage term. The measured storage term is smaller than the turbulent flux divergence and much smaller than the advection, implying that these latter terms are in balance. However, it is apparent that our present estimates for the terms of the Brush Creek thermal energy budget do not balance. The advection terms dominate our empirical thermal energy budget. Indirect support for dominance by the advection terms is also found in the energy storage term, i.e., $\partial\theta/\partial t$ has a minimum at the top of the drainage flow where along-valley advection is zero.

Although along-valley advection is the most directly measured term in the budget (with the exception of the storage term), the small temperature differences associated with $\partial\theta/\partial s$ are difficult to measure precisely with the tethered balloon sondes. Further, our present estimate of the vertical advection term depends on the assumption that the cross-valley distributions of vertical velocity and potential temperature gradient are uncorrelated. This situation is unlikely if the potential temperature is not uniform in the cross-valley direction, and the valley sidewalls are known to be colder than the center of the valley. Thus, subsidence that occurs preferentially near the sides of the valley or in the tributary box canyons could alter our thermal energy budget considerably.

A more detailed description of this analysis is given by Horst et al. (1987). These results are preliminary and intended to illustrate our approach to evaluating the thermal energy budget. We are continuing to refine our estimates of the terms of the budget and to quantify the uncertainties associated

with them. In particular our analysis will be extended to additional nights of the Brush Creek field study, and numerical simulations of the drainage flows in Brush Creek (Bader 1987) will be used to examine the assumptions on which our estimates are based.

Acknowledgments

We thank our colleagues in the ASCOT program for collaboration in the data collection and analysis and especially thank Prof. T. B. McKee for providing the radiative flux calculations.

References

Bader, D. C. 1987. "Valley Mass and Energy Budgets Computed from Model Simulations." Paper presented at the Fourth Conference on Mountain Meteorology, August 25-28, Seattle, Washington.

Cox, S. K. 1973. "Infrared Heating Calculations Within the Water Vapor Pressure Broadened Continuum." Quart. J. Roy. Met. Soc. 99:669-679.

Griffith, K. T., S. K. Cox and R. G. Knollenberg. 1980. "Infrared Radiative Properties of Tropical Cirrus Clouds Inferred from Aircraft Measurements." J. Atmos. Sci. 37:1077-1087.

Horst, T. W., K. J. Allwine and C. D. Whiteman. 1987. "A Thermal Energy Budget for Nocturnal Drainage Flow in a Simple Valley." Paper presented at the Fourth Conference on Mountain Meteorology, August 25-28, Seattle, Washington.

Whiteman, C. D., K. J. Allwine, J. M. Hubbe, H. P. Foote, M. M. Orgill and L. J. Fritschen. 1987. "Radiation and Surface Energy Budgets for a Colorado Valley." Paper presented at the Fourth Conference on Mountain Meteorology, August 25-28, Seattle, Washington.

EFFECTS OF VALLEY GEOMETRY ON VALLEY WINDS

D. C. Bader

The DOE ASCOT studies have focused on describing the mass and energy budgets of the valley wind systems in the Brush Creek valley in northwestern Colorado (Whiteman and Barr 1986). Recent attempts to quantify these budgets have employed a careful integration and analysis of data collected from a variety of different instrumentation (Horst et al. 1988). Unfortunately, some valley circulations occur on temporal and spatial scales that are not detected by the instrumentation. At times, the individual terms in the budget are dependent on these small-scale processes, making their evaluation difficult from data analysis alone. However, if the valley winds are correctly simulated by numerical models, resolution of atmospheric motions is limited only by the models' minimum resolution, which can be selected to resolve the scales of interest. A faithful simulation of the valley wind structure is essential in order to successfully evaluate the budget terms from the model results. This paper reports on model simulations that explore the effect of valley geometry on the valley wind system, a necessary prelude to performing the budget calculations.

The Model

The model is the same as that described by Bader et al. (1987). A nonhydrostatic dynamical equation set is employed on a terrain-following grid to simulate atmospheric boundary layer structure for regions of complex terrain. In all cases described here, the model was 4 km deep with a 50-m vertical grid spacing in the lowest 11 layers to provide sufficient resolution. The domain was aligned with the valley axis. It was assumed that the along-valley processes were of much larger scale than the cross-valley processes, allowing for a different grid spacing in those directions. It was also assumed that the flow was symmetric about the plane of the valley axis, requiring the simulation of only half the valley. In all four simulations the cross-valley spacing was 100 m while the along valley spacing was 750 m in three simulations and 1000 m in the fourth, which required a longer domain. The model was initialized with an isothermal layer ($d\theta/dz$ = 0.01 K/m) extending from the valley floor to several hundred meters above ridgetop. No external winds were prescribed. The boundary layer was cooled at the lower surface with a constant sensible heat flux to the ground of 40 W/m^2 for 2 h to produce a near steady state valley flow.

Figure 1 shows the four terrain configurations used for the study. In Figure 1a, a 12-km-long valley is cut into a 700-m-high, flat plateau. At the upper end, the sidewalls meet to form a V, with the floor widening to 1.5 km across at the valley mouth. The valley side and headwalls have slopes of 0.4. This basic structure is a first cut at approximating the topography of the lower end of Brush Creek valley without too much complexity. The second model valley (Figure 1b) added gently sloping regions connecting the upper sidewall to the model ridges, more like the actual shape of the real valley. In Figure 1c, the cross-valley width of the valley

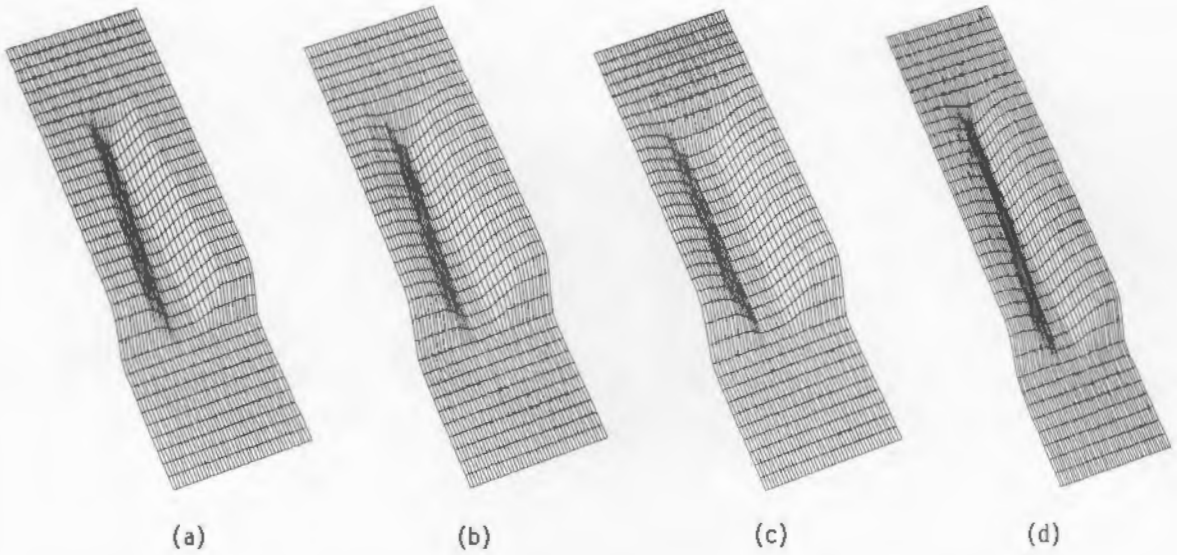

FIGURE 1. Terrain Configurations for a) Flat Upper Ridge Case, b) Sloping Upper Ridge Case, c) Constant Valley Width Case, and d) Longer Valley Case.

floor was not decreased with up-valley distance, to ascertain the effect of narrowing on valley flow. The last simulation included the V-shaped upper portion of the Brush Creek valley, which extended an additional 8 km from the point where the sidewalls met.

Results

Figure 2a shows a cross section taken at a point 2 km up-valley from the valley mouth for the flat ridge case. The solid lines are isotachs of along-valley wind speeds at 0.5 m/s intervals, while the dashed lines are isentropes (constant potential temperature) at 2-K intervals. Below 150 m is a strong inversion layer coinciding with a strong shear zone. A small jet region at 300 m contains a core valley wind with speed slightly higher than 2.5 m/s. The wind speed decreases slowly with height until it becomes near 0 at the ridge elevation. The lapse rate above the surface inversion remains nearly isothermal, with slightly stronger stability in the slope layer over the sidewall. This structure is very similar to that observed in the lower part of Brush Creek (Clements et al. 1988), except that the peak down valley wind speed is approximately 30 to 50% of that measured in the field. Analysis of the lidar data revealed that this peak is very narrow and may not be adequately resolved with the model's 100-m cross-valley resolution. However, the modeled speeds were also lower than the spatially averaged observed values.

Figure 2b shows the results when the upper sidewalls were more realistically modeled with a gentle slope. Although the temperature structure was similar to the previous case, the wind structure is slightly more pronounced with peak wind speeds near 3.0 m/s, However, these values were still not as high as those observed. Figure 2c shows the results from the case in which the valley floor was a constant width. In this case, the winds were the weakest found in any of the simulations. The decreased surface-to-volume ratio reduced the along-valley pressure gradient driving the wind. The results from the last simulation that included the narrow upper valley region are shown in Figure 2d. Peak speeds in this simulation exceeded 3.0 m/s and more closely approximated the observations than those in any of the other model runs. Once again, the temperature structure is very similar to that found in the other cases, a result that implies that the cross-valley temperature structure is not strongly dependent on along-valley geometry.

Conclusions

Four model simulations were run to examine the effect of valley geometry on nocturnal wind and temperature structure. The addition of sloping regions to the upper sidewall had only a minor effect on the resulting boundary-layer structure. The most significant influences were found to be valley length and the along-valley dependence of surface-to-volume ratio. A longer valley allows parcels to be

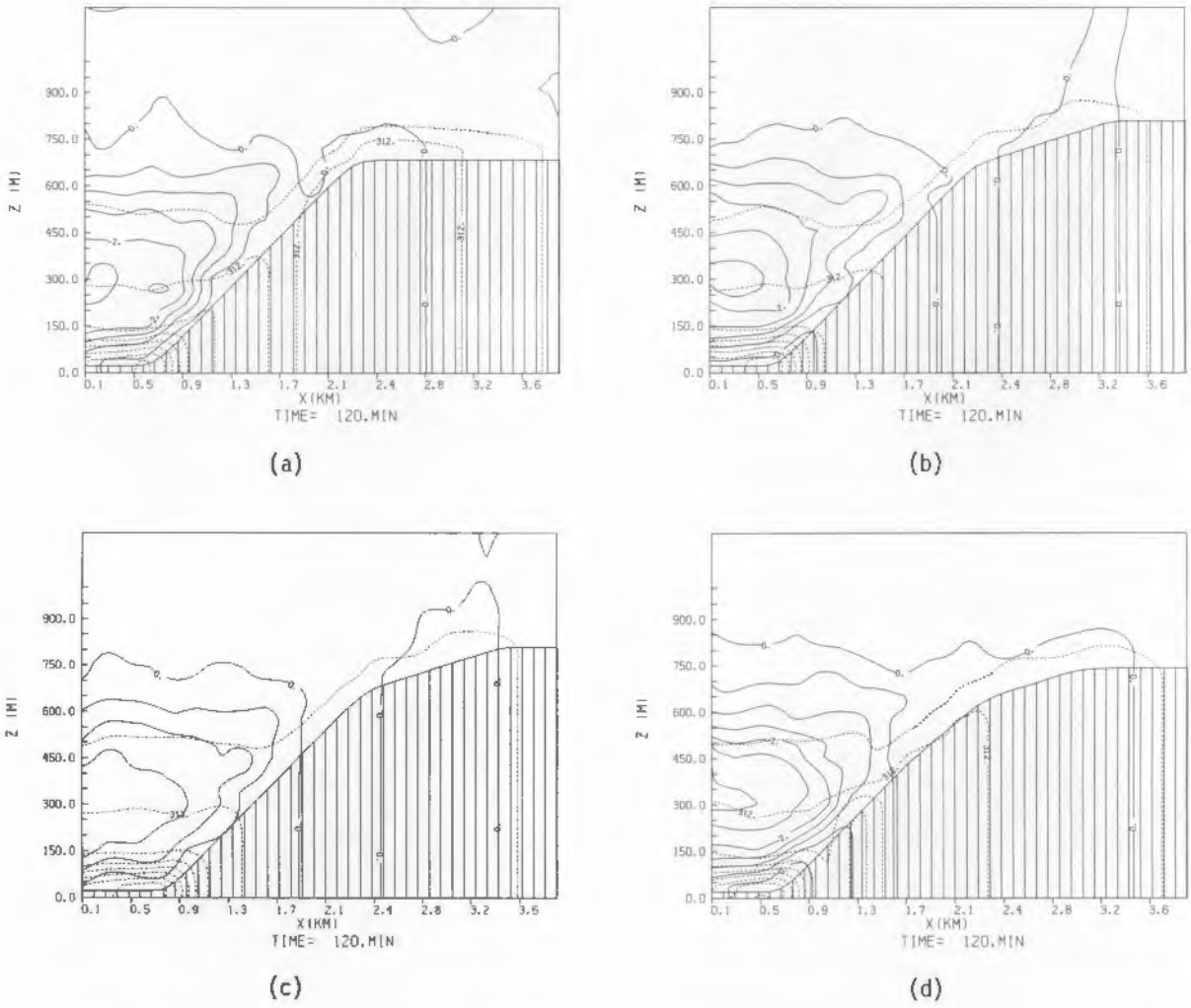

FIGURE 2. Valley Boundary Layer Structure 2 km Up-Valley from the Valley Mouth 2 h After the Start of the Simulation. Solid lines are isotachs of down-valley wind speeds in 0.5 m/s intervals. Dashed lines are potential temperature contours in 2-K intervals. Plots shown for a) flat upper ridge case, b) sloping upper ridge case, c) constant valley width case, and d) longer valley case.

accelerated through the thermally forced pressure gradient over a greater distance, thereby increasing the along-valley wind speed near the valley mouth. A valley that narrows with distance from the mouth produces a stronger along-valley pressure gradient and higher wind speeds than does one that has a constant width. Modeled cross-valley temperature structure is not strongly influenced by differences in along-valley geometry.

The results of these simulations will be used to evaluate the terms in the mass and energy budgets of the valley wind system. They also serve as a useful guide to estimating valley wind and temperature structure in valleys where little or no meteorological observations have been made.

References

Bader, D. C., T. B. McKee and G. J. Tripoli. 1987. "Mesoscale Boundary Layer Evolution over Complex Terrain. Part I: Numerical Simulation of the Diurnal Cycle." J. Atmos. Sci. 44:2823-2838.

Clements, W. E., J. A. Archuleta amd D. E. Hoard. "Mean Structure of the Nocturnal Drainage Flow in a Deep Valley." (submitted to J. Climate Appl. Meteor.).

Horst, T. W., and K. J. Allwine. 1988. "Estimation of the Nocturnal Thermal Energy Budget for Brush Creek." In this annual report.

Whiteman, C. D., and S. Barr. 1986. "Atmospheric Mass Transport by Along-Valley Wind Systems in a Deep Colorado Valley." J. Climate Appl. Meteor. 25:1205-1212.

MODEL STUDY OF CROSS-VALLEY PLUME DISPERSION AFTER SUNRISE

D. C. Bader

In a previous paper (Bader and Whiteman 1987), we used a numerical model to simulate the evolution of the daytime convective boundary layer and resulting plume dispersion in a cross section of a narrow mountain valley. In that study, it was shown that the preferential heating of one sidewall early in the morning can produce a pollutant fumigation episode over that sidewall from a plume initially located above the valley center. The simulation realistically reproduced the behavior of an observed tracer plume in Colorado's Brush Creek valley while also giving dispersion estimates for a hypothetical second plume located at a higher elevation than the first. The model demonstrated the strong dependence of source height on the subsequent morning dispersion, a result not obtained from the field experiment. In the present paper, we extend the modeling study to explore the dependence of convective boundary layer evolution and plume dispersion on the seasonal differences in solar heating of the Brush Creek valley.

The Model

The nonhydrostatic, boundary-layer version of the Colorado State University (CSU) Regional Atmospheric Modeling System (RAMS) was modified for this study. This multi-dimensional, primitive equation model utilizes a terrain-following coordinate system to allow the simulation of atmospheric winds and temperature in regions of complex terrain. A complete description of the basic model has been given by Tripoli and Cotton (1986) and Bader et al. (1987) and is not repeated here. The model was modified to include additional conservation equations for passive tracers that were used to simulate plume dispersion. The model valley was 700 m deep with sidewall slopes of 0.4. It was 1 km wide at the floor and had flat ridges extending from the sidewall crests to the model boundaries. Total domain width was 8 km and horizontal grid spacing was 100 m. Total domain depth was 4 km with 50-m grid spacing in the lowest 600 m above the lower surfaces. The valley surfaces were assumed to be dry with uniform albedo, an assumption that was not strictly valid, but was still appropriate for this type of study. Kinematic heat flux at each point along the surface was assumed to be 20% of the incident extraterrestrial solar radiation, with shaded surfaces contributing no heat. The valley axis was assumed to lie on a northwest-southeast line at 40°N. The time-dependent illumination of the valley surfaces was then calculated for two cases, the first day of summer and the first day of winter.

There were no initial cross-valley winds and there was no along-valley flow specified through the plane of the simulation. The turbulent effects of a 2 m s^{-1} wind along the lower surface were included to better specify surface mixing. The valley boundary layer was initialized with a structure similar to that observed in the Brush Creek valley. A potential temperature inversion of 8.25 K in the lowest 125 m above the valley floor was topped by a quasi-isothermal ($d\theta/dz$ = D.01 K/m) layer extending to 750 m above the valley floor. Figure 1 shows initial tracer concentrations for two circular Gaussian plumes with centerlines located at 125 m and 625 m above the valley floor. The contours shown represent 10% levels of the initial centerline concentrations. The broken line shows the 0.008 K/m lapse rate contour, which separates the remnants of the nocturnal stable layer (where mixing is suppressed) from the developing convective boundary layer. In the past, the region inside this contour has been referred to as the "stable core."

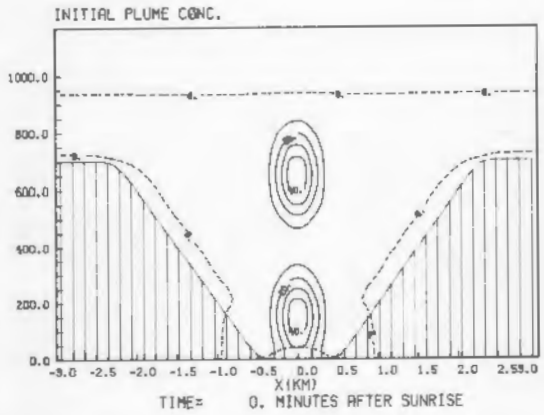

FIGURE 1. Initial Plume Concentrations and Outline of Stable Core for Both Cases. Solid lines are concentration contours at intervals of 10% of the initial centerline concentrations and the dashed line shows the 0.008 K/m stability level. Minimum concentration contour is 10%.

Results

Figure 2 shows the plume concentrations and stable core regions at 2 and 3 h after sunrise for the summer case. The southwest sidewall (to the left in the plots) was illuminated nearly 90 min before sunlight first struck the northeast sidewall. The convective layer developed over the lower part of the heated sidewall. This heating formed an upslope wind that carried the lower plume up the sidewall, while weak mixing distorted the upper plume. The stable core descended in the manner predicted by Whiteman (1982) so that the upper plume centerline was 50 m lower after 3 h than it was initially. Although the lower plume shifted from the valley center as a result of the uneven sidewall heating, the stable core containing the upper plume remained nearly symmetric, a result consistent with earlier simulations by Bader and McKee (1983, 1985).

The solar geometry for the winter case was such that the northeast sidewall remained shaded for only 30 min after the southwest sidewall was illuminated, thereby drastically reducing the differential heating seen in the summer case. As can be seen in Figure 3, the lower plume dispersed evenly in the convective boundary layer over the valley floor, while the upper plume diffused less rapidly in the stable core. Higher concentrations remained in the valley longer than in the summer, but the concentrations over the southwest slope were lower.

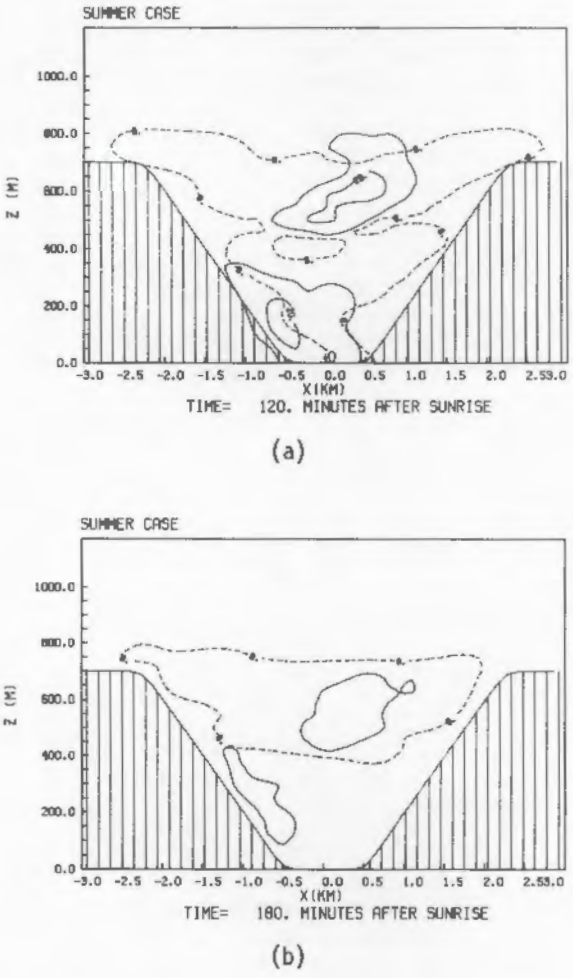

FIGURE 2. Summer Case Concentration Fields and Stable Core Depiction at a) 2 h After Sunrise and b) 3 h After Sunrise.

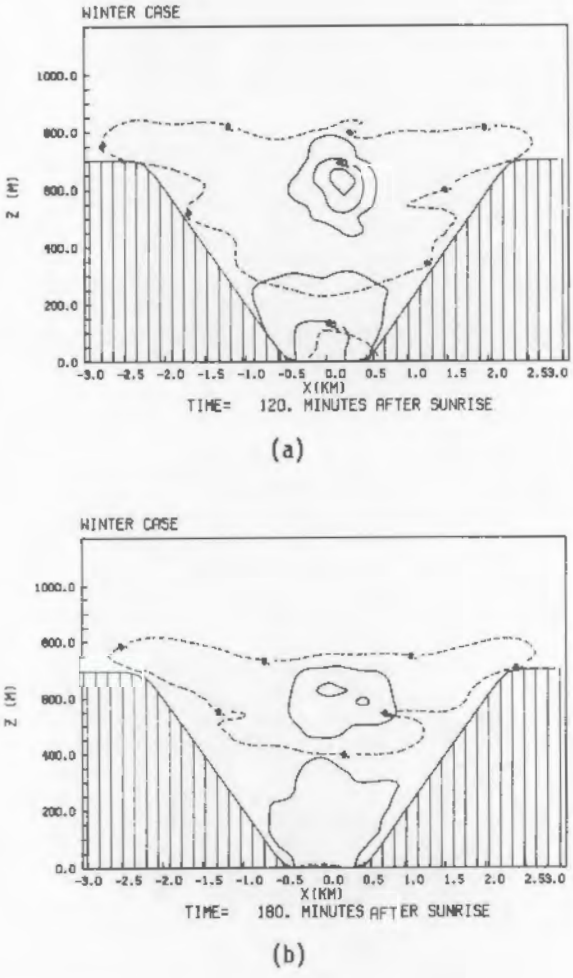

FIGURE 3. Winter Case Concentration Fields and Stable Core Depiction at a) 2 h After Sunrise and b) 3 h After Sunrise.

Conclusions

The dispersion of pollutants in a mountain valley is influenced by many factors, of which we have examined just two: plume elevation and solar geometry. This study shows that strongly asymmetric heating of the valley influences the dispersion of pollutants but not necessarily the valley's thermodynamic structure. In the future, we will extend these studies to three-dimensional simulations of dispersion both before and after sunrise in conjunction with other parts of the ASCOT program.

References

Bader, D. C., and C. D. Whiteman. 1987. "Model Simulation of Plume Dispersion in a Narrow Valley After Sunrise." In Pacific Northwest Laboratory Annual Report for 1986 to the DOE Office of Energy Research, Part 3 - Atmospheric Sciences. PNL-6100 Pt. 3, Pacific Northwest Laboratory, Richland, Washington.

Bader, D. C., and T. B. McKee. 1985. "Effects of Shear, Stability and Valley Characteristics on the Destruction of Temperature Inversions." J. Climate Appl. Meteor. 24:822-832.

Bader, D. C., and T. B. McKee. 1983. "Dynamical Model Simulation of the Daytime Boundary Layer Development in Deep Mountain Valleys." J. Climate Appl. Meteor. 22:341-351.

Whiteman, C. D. 1982. "Breakup of Temperature Inversions in Deep Mountain Valleys. Part I: Observations." J. Climate Appl. Meteor. 21:270-289.

MODIFICATION OF BOUNDARY LAYER STRUCTURE OVER COLD WATER

J. C. Doran

Numerical simulations of the behavior of winds and temperatures have been carried out for cases in which the wind flows from a strongly heated land area over a region of significantly colder water. These simulations were motivated by the Øresund experiment, a cooperative Nordic meteorological and tracer experiment carried out in the spring of 1984 (Gryning 1985). In that case, the body of water was a strait between Denmark and Sweden (the Øresund) that was bounded by heated land surfaces on both sides. Such conditions may be common in regions of other straits, offshore islands, and deep inland lakes.

The model used was a two-dimensional version of the Colorado State University Hydrostatic Mesoscale Model (McNider and Pielke 1985). The simulations showed that as warm air is advected over the water, it is cooled from below, resulting in the formation of a stable layer near the water's surface. This layer strengthens and deepens with increasing fetch. The turbulent exchange of heat and momentum is significantly decreased in this layer, and the downward transport of momentum from above is inhibited. Thus, although the wind speed initially increases as the wind passes from the rougher land surface over the water, the decreased turbulent exchange from above eventually results in a deceleration of the winds near the surface. This layer of decelerating winds slowly thickens as the over-water fetch increases (Figure 1). Such behavior should occur in the presence of moderate-to-strong ambient winds; for weaker winds, the more typical land-sea circulations will develop.

Comparisons with data obtained from a variety of instruments deployed over a 70-km extent in Sweden, Denmark, and over the Øresund, confirmed the general features of the wind and temperature fields simulated in the model. In particular, a series of measurements taken in the Øresund by a research vessel showed that regions of acceleration and deceleration of the near-surface winds, first identified in the simulations, are present (Doran and Gryning 1987). Moreover, the existence of several developing boundary layers, unstable over land and stable over water, have also been seen in both the observations and the model results. These layers have important

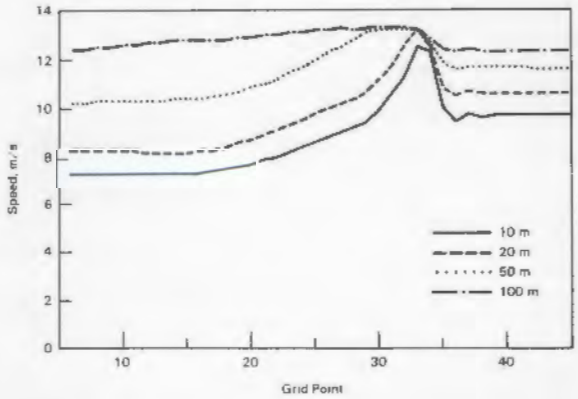

FIGURE 1. Wind Speed at Four Heights as a Function of Horizontal Position. Grid points 35 and higher represent land surface. Wind is flowing from right to left.

implications for the behavior of pollutants released into the atmosphere at various heights. The subsequently observed transport and dispersion will depend strongly on the location of the release and observation points with respect to the structure of these boundary layers.

References

Doran, J. C., and S.-E. Gryning. 1987. "Wind and Temperature Structure Over a Land-Water-Land Area." J. Climate Appl. Meteor. 26:973-979.

Gryning, S.-E. 1985. "The Øresund Experiment: A Nordic Mesoscale Dispersion Experiment Over a Land-Water-Land Area." Bull. Amer. Meteor. Soc. 66:1403-1407.

McNider, R. T., and R. A. Pielke. 1984. "Numerical Simulation of Slope and Mountain Flows." J. Climate Appl. Meteor. 23:1441-1453.

TEMPERATURE INVERSION BREAKUP IN SWITZERLAND'S DISCHMA VALLEY

C. D. Whiteman

In deep mountain valleys the post-sunrise breakup of the nocturnal temperature inversion differs from the well-known inversion breakup over the plains. Over the plains the inversion is destroyed by the upward growth from the ground of a convective boundary layer, through the process of penetrative convection. In the valley, however, the destruction is affected by upslope motions that develop over the heated sidewalls. These upslope flows remove air mass from the valley and require a compensatory subsidence over the center of the valley atmosphere. Thus, valley inversion destruction is characterized by the upward growth of convective boundary layers into the temperature inversion layer from the sidewalls and valley floor, and subsidence of the top of the temperature inversion layer. Observations of inversion breakup in several mountain valleys has shown that the relative importance of these two processes varies from case to case (Machalek 1974, Whiteman 1982, Brehm and Freytag 1982).

Cooperative investigation of a recent set of observations of inversion breakup in a Swiss valley with a German investigator, Dr. Hans Mueller, has added new evidence that links the inversion destruction pattern to two factors: the thermal energy budget of the valley and a thermal energy amplification factor that depends on the topographic shape of the valley. The results of this analysis will soon be published (Mueller and Whiteman 1988).

Inversion destruction in the Swiss valley on August 11, 1980, occurred over a 4-1/2-hour period following sunrise, and was accomplished primarily by subsidence of the top of the temperature inversion. This inversion destruction pattern is in sharp contrast to summertime inversion destruction patterns in Colorado mountain valleys (Whiteman 1982), where convective boundary layer growth is the primary destruction process. In Colorado, inversion destruction by subsidence was observed only in winter when the ground was covered with snow. The apparent connection between patterns of winter inversion destruction in Colorado and summer inversion destruction in the Swiss valley appeared to be related to the surface energy balance. This concept was tested using the inversion destruction model of Whiteman and McKee (1982), as extended using the concept of topographic amplification of thermal energy developed by an Austrian researcher (Steinacker 1984).

Model results support the concept that the observed pattern of inversion destruction is preferred when the rate of input of sensible heat flux is low. In the Colorado winter case, when the ground is snow-covered the energy available for sensible heat flux is reduced by the reflection of the incoming solar beam. In the moist summertime Dischma Valley environment, on the other hand, the energy available for sensible heat flux is reduced by the strong partitioning of available energy into evaporative flux. High ground moisture was present in the Dischma Valley experiment, which followed 3 days of rain, totaling 215 mm (Freytag and Hennemuth 1982). Model calculations for the breakup of the Dischma Valley inversion indicate that only 6% of the extraterrestrial solar radiation flux is required to be converted to sensible heat within the valley to explain the observed rate of inversion destruction. The model-estimated values are supported by surface energy budget measurements made in the valley by Halbsguth et al. (1984).

References

Brehm, M., and C. Freytag. 1982. "Erosion of the Night-Time Thermal Circulation in an Alpine Valley." Arch. Meteor. Geophys. Bioklimat., Ser. B 31:331-352.

Freytag, C., and 8. Hennemuth, eds. 1982. DISKUS, Gebirgswindexperiment im Dischmatal - Datensammlung Teil 2: Bodennahe Messungen und Flugzeugmessungen. Wiss. Mitt. Met. Inst., München 46, 192 pp.

Halbsguth, G. , M. J. Kerschgens, H. Kraus, G. Meindl and E. Schaller. 1984. "Energy Fluxes in an Alpine Valley." Arch. Met. Geoph. Biocl., Ser. A 33:11-20.

Machalek, A. 1974. "Inversionsuntersuchungen in einem Gebirgstal." Wetter und Leben 26(3):157-168.

Mueller, H., and C. D. Whiteman. 1988. "Breakup of a Nocturnal Temperature Inversion in the Dischma Valley During DISKUS." Accepted for publication in J. Climate Appl. Meteor.

Steinacker, R. 1984. "Area-Height Distribution of a Valley and Its Relation to the Valley Wind." Beitr. Phys. Atmosph. 57(1):64-71.

Whiteman, C. D. 1982. "Breakup of Temperature Inversions in Deep Mountain Valleys: Part I. Observations." J. Appl. Meteor. 21(3):270-289.

Whiteman, C. D., and T. B. Mckee. 1982. "Breakup of Temperature Inversions in Deep Mountain Valleys: Part II. Thermodynamic Model." J. Appl. Meteor. 21(3):290-302.

THE TURBULENCE LENGTH SCALE IN NOCTURNAL SLOPE FLOW

T. W. Horst and J. C. Doran

During FY 1986, the turbulence structure of nocturnal slope flow was predicted with a turbulence covariance model for stably stratified flow developed by Brost and Wyngaard (1978). These predictions were found to compare well with observations from the Rattlesnake Mountain slope wind site (Horst and Doran 1987, 1988). One of the parameters of this model is a turbulent length scale, which for flow over flat terrain is

$$\ell = \frac{z}{(1 + z/\ell_B)} \quad . \qquad (1)$$

Here z is height above the surface and ℓ_B is a buoyancy length scale, $\ell_B = C_b [(\overline{w^2})^{(1/2)}]/N$, where C_b is a constant equal to 1.69, $\overline{w^2}$ is the variance of the vertical wind component, and N is the Brunt-Vaisala frequency, $N = [g/T\ \partial\theta/\partial z]^{(1/2)}$. We extended Equation (1) to slope flow by replacing z with the distance n normal to the surface and expressing the Brunt-Vaisala frequency as $N = [g/T\ \partial\theta/\partial n \cos(a)]^{(1/2)}$, where a is the slope angle.

The preceding expression for ℓ_B follows quite readily from consideration of a balance between inertial accelerations, $\sim\overline{w^2}/\ell_B$, and buoyancy accelerations, $\sim g/T\ \ell_B\ \partial\theta/\partial z$ (Nieuwstadt 1984). A more general derivation for ℓ_B is based on the equation for conservation of turbulent kinetic energy (TKE) and assumes that Rf, the ratio of buoyant turbulence production to shear production, approaches a constant in the stably stratified limit (Wyngaard 1983). Application of the latter approach to slope flow gives a buoyancy length scale

$$\ell_B = \qquad (2)$$

$$C_b \left[\frac{\overline{w^2}}{\frac{g}{T} \frac{\partial\theta}{\partial n} \left[\cos(a) - \frac{H}{\overline{w\theta}} \cos(\theta_H) \sin(a)\right]} \right]^{1/2} .$$

Here $\overline{w\theta}$ is the heat flux normal to the slope, H is the magnitude of the turbulent heat flux parallel to the slope, and θ_H is the angle between H and the downslope direction. $H/\overline{w\theta}$ is typically on the order of -3.

The factor $[\cos(a) - H/\overline{w\theta} \cos(\theta_H) \sin(a)]$ is the ratio of the vertical to the normal heat flux and comes from the buoyant production term of the slope flow TKE budget. It appears in that term because the vertical heat flux is not normal to the flow, but is equal to $\overline{w\theta}$ $\cos(a) - H \cos(\theta_H) \sin(a)$. Below the slope flow wind maximum, the slope-parallel heat flux H is downslope, $\cos(\theta_H) \simeq 1$, while above the wind maximum it is upslope, $\cos(\theta_H) \simeq -1$. Since the normal heat flux $\overline{w\theta}$ is always negative, the vertical heat flux below the wind maximum is also negative, and the buoyancy term destroys TKE, the usual situation in stably stratified flow. Above the wind maximum, however, the vertical heat flux becomes positive for slope angles exceeding arctan $[H/\overline{w\theta} \cos(\theta_H)]^{-1}$, or roughly 20°, and the buoyancy term changes sign and produces TKE. The consequences for turbulent transport of this behavior of the buoyant production term were discussed by Horst and Doran (1987, 1988).

For small slope angles (roughly <10°) the turbulent length scale based on Equation (2) is nearly identical with our original formulation, and consequently the results of model calculations using Equation (2) are similar to those obtained with the original length scale. For larger values of the slope angle, however, the turbulent length scale and the model results based on Equation (2) can differ significantly from the original. In particular, when the vertical heat flux above the

wind maximum is positive there can be no stably stratified limit for Rf, and the assumption under which Equation (2) was derived is no longer applicable.

The most significant differences between the predictions of the two model formulations occur for K_h, the eddy thermal diffusivity, as a function of n/λ. λ is a local Monin-Obukhov length defined in terms of the local values of the heat flux $\overline{w\theta}$ and the stress τ; n/λ is another measure of the relative roles of TKE production by buoyancy and shear. Observations and model results are plotted in Figure 1 for both flat terrain and for a 21° slope (above the wind maximum). For small values of n/λ the predictions of the two slope flow models are essentially identical, the difference increasing with n/λ. Above n/λ = 0.8, the vertical heat flux becomes positive and there is no model solution with Equation (2).

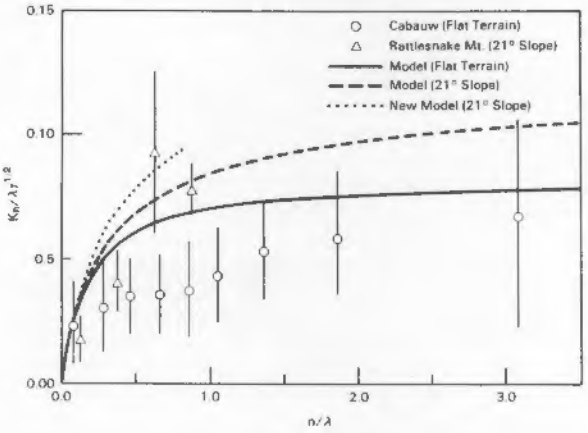

FIGURE 1. The Normalized Eddy Diffusivity for Heat K_h as a Function of n/λ for Both Flat Terrain and a 21° Slope.

Determination of the proper formulation for the turbulent length scale requires a more extensive data base than presently available from the Rattlesnake Mountain slope wind site and could be obtained through either additional field studies or through simulation with a more detailed turbulence model. In any case it appears that the principal conclusions of Horst and Doran (1987, 1988) do not depend on this issue.

References

Brost, R. A., and J. C. Wyngaard. 1978. "A Model Study of the Stably Stratified Planetary Boundary Layer." J. Atmos. Sci. 35:1427-1440.

Horst, T. W., and J. C. Doran. 1987. "PNL Studies on the Turbulence Structure of Nocturnal Slope Flow." In Pacific Northwest Laboratory Annual Report for 1986 to the DOE Office of Energy Research, Part 3 - Atmospheric Sciences, pp. 13-15. PNL-6100 Pt. 3, Pacific Northwest Laboratory, Richland, Washington.

Horst, T. W., and J. C. Doran. 1988. "The Turbulence Structure of Nocturnal Slope Flow." J. Atmos. Sci. 45:605-616.

Nieuwstadt, F. T. M. 1984. "The Turbulent Structure of the Stable, Nocturnal Boundary Layer." J. Atmos. Sci. 41:2022-2216.

Wyngaard, J. C. 1983. "Lectures on the Planetary Boundary Layer." In Mesoscale Meteorology - Theories, Observations and Models, pp. 603-650. D. K. Lilly and T. Gal-Chen, eds., D. Reidel, Boston, Massachusetts.

Large-Scale Atmospheric Transport and Processing of Emissions

LARGE-SCALE ATMOSPHERIC TRANSPORT AND PROCESSING OF EMISSIONS

Current research on large-scale atmospheric transport and processing of emissions through storms is a natural outgrowth of the long-term emphasis in atmospheric sciences research at PNL on atmospheric cleansing processes. This research has expanded from its initial focus on localized precipitation scavenging of nuclear materials to the removal of widespread fossil and other energy effluents as responsibilities have evolved for DOE. When national attention focused on acid rain, PNL, together with other DOE laboratories, joined in planning and conducting the interagency efforts within the National Acid Precipitation Assessment Program (NAPAP). DOE's program within NAPAP, Processing of Emissions by Clouds and Precipitation (PRECP), examines the source-receptor relationships of the regional-scale acid rain impacts issue.

PRECP's scientific domain addresses the physical and chemical processes within the cloud and precipitation systems; cloud dynamics defining inflow and outflow characteristics, microphysics and in-cloud scavenging properties, aqueous phase chemistry, regional wet deposition patterns, and storm chemistry climatology receive direct attention. A major effort in PRECP has been to conduct large-scale experiments involving surface-based measurements and aircraft probing frontal and convective storm systems. These activities are a combined effort of Argonne and Brookhaven National Laboratories (ANL and BNL) and PNL. The magnitude of the field experiments has also prompted cooperative efforts with other agency scientists who are concentrating on other aspects of the storm systems. Modeling research, which organizes field research results into a descriptive and predictive framework, has emphasized cloud and precipitation chemistry and microphysics. These modeling efforts have also benefitted from strong interfaces with subcontracted university researchers and other scientists on related research topics such as photochemistry, synoptic- and regional-scale circulations, and cloud dynamics. This close cooperation is permitting us to integrate a comprehensive modeling description of the combined processes leading to acid deposition. In future PRECP research, model experiments will simulate storm processing of pollutants interactively with analysis of field experiments to improve understanding and contribute input modules to assessment codes that agencies will ultimately use for policy and regulatory considerations.

The importance of large-scale transport is becoming increasingly evident as PRECP results demonstrate that a significant fraction of energy contaminants can be vented through cloud systems, redistributed throughout the troposphere, and carried to large distances. A multi-agency field study of large convective storms in the midwestern United States is being organized by ANL, BNL, and PNL, which will comprehensively measure with several aircraft and multiple Doppler radar the dynamical, microphysical, and chemical processes responsible for convective cloud development, contaminant and oxidant ingestion, transformations, and wet deposition or redistribution throughout the troposphere of resultant chemical species. The experiment will extend our model descriptions of these processes, particularly the venting process determining the fraction of pollutants passing through the storm to be made available for long-range transport. Later, a series of even larger scale experiments of contaminant scavenging and redistribution by frontal passages through the eastern United States and Canada will be planned with Canadian scientists.

A valuable source of data for continental- to hemispheric-scale transport was the Chernobyl event. The Soviet nuclear accident permitted measurement of primary nuclear contaminants following transport, dispersion, and wet and dry removal over Europe, Asia, and North America. Studies of the processes involved in producing their distributions in air, clouds, and on the surface are continuing as the large number of contributors to the measurements, who were rapidly brought together in a cullaborative effort, make progress in processing data and sharing results.

Undoubtedly, there will be an important role for tracers in future long-range transport studies where exchange of contaminants between multiple layers through the atmosphere, having differing wind, mixing, and moisture conditions, must be characterized. Recent long-range tracer experiments in ANATEX, approaching continental scales, required extremely sensitive tracer detection for transport and dispersion studies at these distances, even in clear-air conditions. Tracers that can also be used in storm conditions, with known scavenging characteristics and even greater detectability, will be necessary for the future.

The interpretation of transport, dispersion, and removal processes on very large scales must also extend beyond the dynamical description of individual case studies. The statistics and theory for considering multiple processing of events, widespread and repeated releases, and the ultimate fate and balance of source-to-sink cycling of contaminants on a continental or global basis must be firmly established before meaningful conclusions can be drawn.

The projects whose progress is reported in the following articles are:

- **PRECP**
- **Soviet Accident Fallout Measurements**
- **ANATEX.**

PRECP: STATUS AND FUTURE DIRECTIONS

M. Terry Dana and A. C. D. Leslie

PRECP's primary objective--to provide essential information for the quantitative description of wet deposition as a function of air-pollution loadings, geographical location, and atmospheric processing--has been implemented through research in several areas: definition and reduction of inadequacies in models of atmospheric processing of pollutants by clouds and precipitation through field, laboratory, and theoretical studies; contribution to understanding of pollutant processing through field observations and resultant data bases; and reexamination of acidic deposition data bases for indications of nonlinearities. The major thrust of this effort has been directed toward field studies, of which five have been conducted:

- PRECP-I (April-May 1985): storm inflow and outflow, scavenging ratios
- PRECP-II (June 1985): convective storm processing, pollutant redistribution (with the PRESTORM experiment managed by NSF/NOAA)
- PRECP-III (January-February 1986): winter storm processing, oxidant profiles, deposition by snowfall
- PRECP-IV (January-March 1986): low-latitude winter storm inflow and outflow, rain band chemistry, model evaluation data base (with the GALE study managed by NOAA/NSF)
- PRECP-V (June 1987): convective storm processing, oxidant profiles, pollutant redistribution.

Analyses of the results of these studies are continuing (see the articles in this section), and planning for the final PRECP field effort under NAPAP, 3CPO (PRECP-VI) (see the article by Leslie and Dana in this section) is under way at the time of this writing.

Major findings of the completed field efforts--supported by the laboratory, modeling, and theoretical studies--include:

- Boundary layer air and a significant fraction of its associated pollutants are vertically redistributed to the upper troposphere, where they are no longer available for local scavenging, and may be transported very long distances to affect the atmospheric chemistry in other regions, countries, or continents.
- The delivery of pollutants to the surface can be controlled as much by oxidant (e.g., hydrogen peroxide) levels as by concentrations of primary pollutants; the potential nonlinearities are of concern to emission control strategies.

The first of these findings provides a major thrust for extension of the PRECP project beyond NAPAP, which is scheduled for conclusion at the end of FY 1989. There is increasing concern about the interactions of anthropogenic and natural atmospheric chemicals, which can affect atmospheric quality at great distances from their sources or may lead to global climatic changes and biosphere disruptions. Examples include CO_2 and global warming, sulfate and climate cooling, methane and stratospheric clouds, chlorofluorocarbons (CFC) and the ozone layer, and climatic effects of elemental carbon, sulfate, and other species in the Arctic and Antarctic regions. PRECP intends to extend its consideration of cloud and precipitation processing of pollutants to this larger scale; understanding of the contributions of these processes to the global atmosphere will require a carefully planned program of field and laboratory measurement and theoretical and modeling studies, directed toward long-range-planned, cooperative field experiments in 1989 and beyond. Interagency and international cooperation is necessary if an understanding of meteorological systems and pollutant budgets on the international scale is to be obtained. A logical progression of "Global PRECP" field efforts could include:

- Northeastern U.S./Southeastern Canada Scavenging Experiment (Fall 1989). Jointly with the Atmospheric Environment Service, characterizing inflow into storms moving over eastern North America, and outflow to the Atlantic and toward the Arctic; a significant spatial expansion would include the use of existing Canadian sampling networks.
- Pollution of the Arctic (Fall 1992). Interagency study with long-range sampling aircraft, examining transport of North American pollution to the Arctic, its involvement with and effect on cloud processes, albedo, and surface ecology.

- Stratospheric Ozone and Pollution. Interagency study to understand the effects of wet processes on CFC and ozone chemistry.

- Flux of Atmospheric Trace Chemicals to Europe. International study, combining techniques and objectives of the previous studies to understand transatlantic pollutant budgets and the extent of North American pollutant effects on Europe.

During the balance of the NAPAP-related phase of PRECP, continued analyses of the data bases created during the six field projects will provide additional understanding of the mechanisms involved with the two major findings above, will provide data for model evaluation, and possibly will lead to additional insights related to acidic deposition phenomena. In addition, model simulations will be completed for convective and frontal storm cases experienced during the field projects, offering tests of the postulated controlling mechanisms in support of NAPAP's goal of providing reliable prediction for regulatory decision-making.

SCAVENGING RATIOS FOR SO_2, $SO_4^=$, AND NO_3^- CALCULATED FROM RELEVANT AIRCRAFT AND SURFACE MEASUREMENTS

W. E. Davis, J. M. Thorp, R. N. Lee, and M. Terry Dana

One of the major problems facing acid precipitation researchers is the modeling of wet deposition. To better understand and predict the effects of wet deposition, various chemistry and wet removal computer models are being developed that will represent the chemical transformations and precipitation removal of pollutants from the atmosphere. A parameter that, in applications of such models, can serve as a relatively reliable indication of precipitation scavenging is the scavenging ratio: the ratio of the concentration of a chemical in precipitation to its concentration in air.

One objective of PRECP has been to form a data base, through field studies of wet deposition episodes and analyses of the field results, to aid in model development and testing. The first of these field studies, PRECP-I, was conducted during April and the first part of May 1985. In PRECP-I, atmospheric chemistry measurements were made on the ground and by aircraft in the inflow air aloft (as well as in clouds and precipitation) to provide data for making computations of "improved" scavenging ratios; i.e., based on storm inflow rather than surface-level air concentrations.

Scavenging ratios, even improved ratios, fall far short of explaining the processes that take place within the storm. Because the ratio is formed by integrating a number of effects over time, the amount of information that is lost is significant. For example, the chemical reactivities are not considered; in-cloud processes involving particle and drop size spectra, collision efficiencies, and thermophoretic and diffusiophoretic effects are also not treated individually. To move from an integrated measurement to measuring the specific effects, however, increases the number of measurements and the degree of difficulty by at least an order of magnitude. The scavenging ratio, despite its shortcomings, allows the model developer an end-point comparison with results from his scavenging model and, for application purposes, may provide a relatively stable or reliable parameterization of the many complex processes involved. In a sense, the scavenging ratio represents a "black box" description of the scavenging process. One measures the air concentrations entering the box and the precipitation concentrations that come out of the box, but within the box the processes are integrated. Subsequent field studies (PRECP-II and PRECP-VI) have been designed to provide some insight in understanding the processes taking place within the box.

Scavenging ratios for various species have been made by a number of authors (Engelmann 1971, Barrie 1985, Barrie and Neustadter 1983, Gatz 1974, Krey and Toonkel 1974, Misra et al. 1985, Niemann 1983, and Westhuizen 1969). Previous calculations of scavenging ratios have been based on the concentrations of species in surface air measurements. These ratios varied by orders of magnitude. At least two problems in previous scavenging ratio calculations may explain the large variations in the ratios: the locations of the air concentration measurements and precipitation measurements. In previous work the air concentrations measured at the surface have been assumed to be the same concentrations feeding the storm. The relationship should be formed instead from the air concentration feeding into the storm, processed in the storm, and then deposited in the precipitation. That is, the concentration in the precipitation is the result of integral processing of the inflow air by the storm. The second problem is caused by the precipitation sampling. The concentration in the precipitation should be related to the concentration of the inflow air to the storm; thus, if there are different sources of inflow air during the sampling period, the precipitation sampling must be conducted sequentially in order to separate periods of precipitation that are related to different phases of the storm. For example, in a typical

frontal storm situation, the inflow air to the precipitation region ahead of the warm front is likely to come from a source region different from the air feeding into the warm sector and its associated precipitation. Likewise, precipitation associated with the cold front in such a situation would be affected by inflow air from yet another source region. The precipitation measurements should be particular to the event and not to a combination of all events. In an attempt to solve these problems, the aircraft used in PRECP-I were placed in sampling positions of the boundary-layer air that was to feed the storm. Also, the ground samples of precipitation were taken on an event basis at times correlated with the predicted wet deposition of the sampled air.

Scavenging Ratios

The scavenging ratio (by volume), k, is defined as the ratio of the pollutant concentration in the water to the concentration in the air.

$$k = \text{concentration in water}(\mu M/m^3)/\text{concentration in air}(\mu M/m^3). \quad (1)$$

In Equation (1) there is an implied assumption that by the integral process discussed above, the air concentration of species and the surface precipitation concentration of species are related in some consistent manner. The parameters involved in the process include the air concentration fluxes, in-cloud microphysics, pollutant particle sizes, and reaction efficiencies; however, these parameters are not available. In the face of this lack of knowledge, we assume that the air concentrations, measured from aircraft placed in an inflow region, feed the precipitation. Further, we assume that the precipitation, sampled at carefully selected locations and times, is representative for the species scavenged from the inflow air. We then have the information needed to calculate the improved scavenging ratio.

PRECP-I

The PRECP-I field study was carried out from two centers of operation: Columbus, Ohio, and Philadelphia, Pennsylvania. The Columbus center was primarily used as a base for aircraft sampling in conjunction with surface precipitation sampling deployed throughout the Northeast or around Columbus. The Philadelphia site was used to determine the effect of the Philadelphia pollutant plume on the local precipitation. Since one of the major purposes of the field study was to provide data for calculating improved scavenging ratios, the discussions in this paper will refer only to the missions flown from the Columbus center of operations.

Two aircraft, a DC-3 from PNL and a Queen Air from BNL, were used to make the air concentration measurements of pollutant species in the inflow air. Figure 1 shows the composite flight patterns for all missions flown by the DC-3 during PRECP-I. The rather extensive areal coverage of the flights was necessitated by the lack of precipitation near Columbus during the field period. (It was the driest April on record at Columbus.) Data from these flights combined with the appropriate surface sampling data were used for the computation of scavenging ratios. The selection of missions that provided usable data was based on the requirement that the inflow air sampled by the aircraft was related to the precipitation sample collected at the surface. Trajectories within the boundary-layer air were used to determine if these criteria were met. Table 1 lists the 7 cases that met the requirements for computing scavenging ratios.

Summary of Results

Table 2 shows the average scavenging ratio assuming a log-normal distribution for all case studies. The individual scavenging ratios for NH_4^+ and $SO_4^=$ range over several orders of magnitude. The NO_3^- appeared to produce somewhat more stable values, as shown by the geometric standard deviation. The results with the smallest standard deviations were total NO_3^- and total sulfur. Total NO_3^- was computed by combining NO_3^- and HNO_3, and $SO_4^=$ was combined with SO_2 to yield total sulfur (see Misra et al. 1985). The ratio for total NO_3^- appeared to be the most stable for all of the experiments with an average of the events of 2.4e06 and a geometric standard deviation of 1.4.

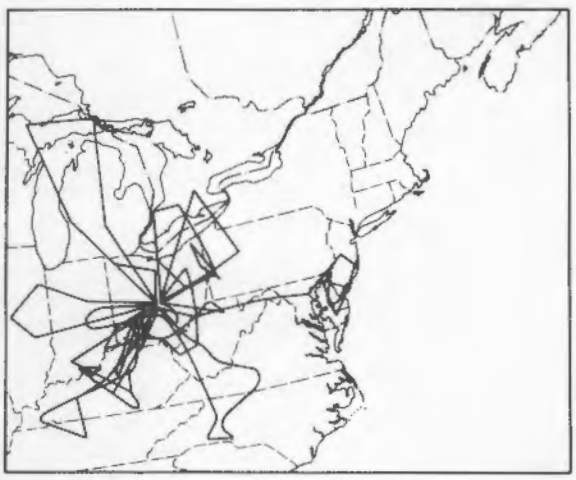

FIGURE 1. Composite Flight Patterns for All Missions Flown by the DC-3 During PRECP-I.

TABLE 1. Condensed Mission Summaries for PRECP-I, Columbus (CMH), April Through May 1985

	Mission Accomplishment/Meteorological Situation
Date: April 5 Time, GMT: 15 to 20Z Altitude, 1000 ft: 3.0 Mix Depth, 1000 ft: ~6.6	Aircraft characterization by PNL and BNL of inflow to cold front with surface precipitation collection for scavenging ratio determinations. Surface samples were taken at 4 sites At 12Z, Ohio was covered by the warm sector of a frontal system with a slow-moving cold front approaching from the west.
Date: April 7 Time, GMT: 19 to 24Z Altitude, 1000 ft: 3.0 to 4.0 Mix Depth, 1000 ft: ~6.0 to 7.5	Aircraft sampling of showers and cloud water, coupled with isolated surface precipitation in eastern Ohio for scavenging ratio determination. Surface precipitation samples at Site 21 were taken at about the same time as the aircraft samples. Low freezing level. Convective showers of rain and snow occurred in the postfrontal cold air. This air did not have its origin in the Ohio valley.
Date: April 11 Time, GMT: 10 to 16Z Altitude, 1000 ft: 3.0 to 4.0 Mix Depth, 1000 ft: ~4.0 to 6.0	Aircraft sampling of clouds and precipitation, coupled with surface precipitation collection for calculation of scavenging ratios. PNL made 2 flights to sample light showers and clouds in southern and eastern Ohio and western West Virginia. Ground Sites 1, 2, and 3 collected precipitation. A weak cold front in Michigan moved to central Ohio by 12/00Z. Showers occurred in eastern Ohio, western Pennsylvania, and West Virginia earlier in the day.
Date: April 19 Time, GMT: 15 to 20/01 Altitude, 1000 ft: 3.3 to 3.5 Mix Depth, 1000 ft: 6.5 to 8.5	On consecutive days PNL and BNL aircraft sampled inflow, clouds, and precipitation over eastern Ohio, western Pennsylvania and southern Ontario in an area of convective showers associated with a stationary front. One surface sample was collected at Site 41.
Date: April 20 Time, GMT: 15 to 19Z Altitude, 1000 ft: 3.5 to 4.0 Mix Depth, 1000 ft: 8.5	Stationary front across Michigan. High pressure continued over Ohio. Convective showers occurred over Ohio, Pennsylvania and New York.
Date: April 24 Time, GMT: 16 to 21Z Altitude, 1000 ft: 8.5 Mix Depth, 1000 ft: ?-?	Clear air and show sampling over Pennsylvania and West Virginia. PNL and BNL sampled air, clouds and precipitation in southern Ohio and across West Virginia. Ground precipitation samples were collected as Sites 1,2,3,4, and 7 in southern Ohio. At 18Z a cold front was in eastern Indiana. It passed through the CMH area at about 25/00Z. A weak stationary front was located in eastern West Virginia.
Date: April 18 Time, GMT: 12 to 22Z Altitude, 1000 ft: 2.5 Mix Depth, 1000 ft: 7.0 to 6.0	Inflow and outflow aircraft measurements of orographic flow over the Appalachian Mountains in Indiana and North Carolina. PNL and BNL flew to North Carolina and Indiana respectively, to sample the orographic inflow and outflow east and west of the Appalachians. Surface Site 66 collected one sample from precipitation that occurred on the 27th and 28th. The stationary front across southern Ohio began to move slowly south like a weak cold front into Kentucky and West Virginia during the morning. Widely scattered showers accompanied the front and its associated trough.

TABLE 2. Event Geometric Averaged Scavenging Ratios for PRECP-I

Date	NH_4^+	$SO_4^=$	NO_3^-	Total NO_3^-	Total S
April 5	1.4e05	3.8e05	2.3e06	2.2e06	2.5e05
April 7		7.8e05	2.6e06	2.4e06	3.6e05
April 11		1.3e06	9.3e06	2.3e06	1.7e05
April 19-20	5.1e06	6.6e05	8.4e06	1.4e06	4.7e05
April 24	1.3e06	1.6e06	1.4e07	2.8e06	6.5e05
Geometric mean[a]	4.3e05	9.7e05	7.1e06	2.4e06	3.8e05
Geometric Standard Deviation	4.1	1.9	2.3	1.4	1.8

(a) For all ratios.

This reflects a narrow range of scavenging ratio for total NO_3^-, which ran from a minimum of 9.2e05 to a maximum of 4.9e06. For $SO_4^=$, on the other hand, the mean was 9.7e05 and the geometric standard deviation was 1.9. The combined SO_2 and $SO_4^=$ had a mean of 3.8e05 and a geometric standard deviation of 1.8. The combined sulfur scavenging ratio was better behaved in that it did not vary as much as the ratio formed from $SO_4^=$ alone.

The results when compared with those of Misra et al. (1985) show a close correspondence for the average values for total sulfur, where geometric means of 2.2 to 3.7e05 were reported versus our 3.8e05. However, the geometric standard deviations of 3.2 to 3.7 were much different from our 1.8, reflecting, in our opinion, an improved inflow sampling. The same was true of total NO_3^- where Misra et al. arrived at a geometric mean of 0.7 to 3.4e06 versus our 1.9e06. Again their standard deviation was much higher: 2.6 to 3.4 versus our 1.4.

Conclusions

Case studies selected from PRECP-I yielded a number of improved scavenging ratios. The results were not equally consistent between ions: the average of the events of the total NO_3^- scavenging ratios was quite consistent with a geometric mean of 2.4e06 and standard deviation of 1.4, while the total sulfur results had a geometric mean of 3.8e05 and a larger standard deviation of 1.8. The total NO_3^- and sulfur results indicate average values comparable with those of Misra et al. (1985). The reason for the discrepancy may be their necessary use of surface air concentrations in forming the ratio. Since no surface air concentrations were measured at our sampling sites, a firm conclusion cannot be reached with regard to large variations in the scavenging ratio when using surface air data. It does appear that, by properly matching both the inflow air concentrations and the surface precipitation measurements, a useful and improved scavenging parameter results.

References

Barrie, L. 1985. "Scavenging Ratios, Wet Deposition, and In-cloud Oxidation: An Application to the Oxides of Sulphur and Nitrogen." J. Geo Res. 90:5789-5799.

Barrie, L., and J. Neustadter. 1983. "The Dependence of Sulphate Scavenging Ratios on Meteorological Variables." In Precipitation Scavenging, Dry Deposition and Resuspension. H. R. Pruppacher et al., eds., Elsevier, New York.

Engelmann, R. J. 1971. "Scavenging Prediction Using Ratios of Concentrations in Air and Precipitation." J. Appl. Meteor. 10:493-497.

Gatz, D. F. 1974. "Scavenging Ratio Measurements in METROMEX." In Precipitation Scavenging (1974). R. G. Semonin and Beadle, coords., CONF-74 1003, National Technical Information Service, Springfield, Virginia.

Krey, P., and L. E. Toonkel. 1974. "Scavenging Ratios." In Precipitation Scavenging (1974). R. G. Semonin and Beadle, coords., CONF-74 1003, National Technical Information Service, Springfield, Virginia.

Misra, P. K., W. H. Chan, D. Chung and A. J. S. Tang. 1985. "Scavenging Ratios of Acidic Pollutants and Their Use in Long-Range Transport Models." Atmos. Environ. 19(9):1471-1475.

Niemann, B. L. 1983. "Scavenging Ratios for Exceptional Wet Sulfate Episodes in Eastern North America From Three Event Networks." In Precipitation Scavenging, Dry Deposition and Resuspension. H. R. Pruppacher et al., eds., Elsevier, New York.

Van der Westhuizen, M. 1969. "Radioactive Nuclear Bomb Fallout - A Relationship Between Deposition, Air Concentration, and Rainfall." Atmos Environ. 3:241-249.

THE PRECP-V FIELD EXPERIMENT SERIES

K. M. Busness, D. S. Daly, M. Terry Dana, W. E. Davis, A. C. D. Leslie, and J. M. Thorp

The fifth in the series of PRECP field experiments (PRECP-V) was conducted in the Columbus, Ohio, area June 1 through June 26, 1987. The three major objectives were as follows:

- To study the chemical composition of the inflow and outflow of summer convective storms, to estimate the extent that various species are processed and removed, and to determine whether significant amounts of pollutants are transported to the upper troposphere. This goal followed up the measurements made during PRECP-II (Dickerson et al. 1987), which indicated strongly that boundary layer air is transported to the upper troposphere. These measurements did not definitively document, however, higher-level injection of NO_x, which may be produced in the process by lightning, and SO_2, some of which can be subject to rapid oxidation to sulfate and subsequent removal.

- To measure the concentrations of gaseous H_2O_2 in and around convective storms; in particular, to measure vertical profiles from the boundary layer to 6 km. Recent measurements (Heikes et al. 1987) indicated that H_2O_2 concentrations increase above the boundary layer, suggesting that entrainment of air into convective storms may provide a substantial source of H_2O_2 for oxidation of SO_2.

- To develop and test methods for the study of convective storms in preparation for PRECP-VI, to be conducted during the summer of 1988 (see the next article in this section).

The Columbus area was chosen because of its location within a region of significant anthropogenic pollution and the availability of satisfactory aircraft logistical support and meteorological services. In addition, familiarity with the area was obtained during the PRECP-I field series, based in Columbus in April and May 1985.

Aircraft Operations

The three aircraft employed during PRECP-V were the PNL DC-3, the NOAA King Air, and the NCAR Sabreliner. Table 1 summarizes the measurement capabilities of these aircraft. Integration of these capabilities into aircraft operations is illustrated by Figure 1, which shows the primary flight plan, that for the study of convective storms. The DC-3 was used for chemical documentation of low-level inflow from the boundary layer, while the King Air concentrated on mid-level inflow and outflow and the Sabreliner attempted to document outflow in the anvil region. While convective storms were the primary objective for study, flight operations were planned for cases of warm, cold, and stationary fronts, and for clear-air sampling, where H_2O_2 profiles were the primary goal. Table 2 is a summary of aircraft missions conducted during PRECP-V.

Ground Operations

A limited network of precipitation sampling sites was established for the experiment series. The primary objective of ground sampling was to document pollutant outflow in precipitation associated with storms sampled by aircraft. These measurements were confined, however, to the Columbus area, and to the MAP3S site at Oxford, Ohio, because of personnel limitations and because the PRECP-I experience showed the impracticality of sampling far afield of the experiment base when resources are limited. Table 3 lists the established sampling sites and the instrumentation used. With the exception of site 05, which was new for PRECP-V, the sites are the same as those used during PRECP-I. Table 4 lists the dates and types of precipitation samples collected during PRECP-V.

The network, shown in Figure 2, formed a rough "Y" shape with Oxford at the western extreme, and three sites surrounding Columbus except to the east. Figures 3 and 4 show the rainfall rates and major ion concentrations by OSCAR sequential stages for the event of June 25 at two sites: D5 and 06.

An additional goal of the ground operations was testing of prototype computer-controlled automatic rain samplers (CCARS), which will be employed during the PRECP-VI field project. The base sampling site (05), at the Battelle Columbus Laboratory's West Jefferson facility, included two wet-only automatic collectors that were capable of supporting one CCARS each and additional sampling by OSCAR sequential samplers (Easter et al. 1984), and a

TABLE 1. Aircraft Instrumentation

Parameter	Instrument		
	Sabreliner	King Air	DC-3
Aircraft Position, Velocity, Altitude	Inertial navigational system, LORAN-C	LORAN (radio)	ONI LORAN-C
Temperatures	Non-deiced sensor (fuselage mount) Deiced sensor (fuselage mount) Cabin temperatures	Rosemount resistance sensor	Rosemount sensor - regular and fast response
Data Acquisition	Sabreliner ADS (Motorola-based) with Dylon Tape Controller and Kennedy Tape Drive; displayed on HP Computer with HP Disk Drive, Printer, Terminal Emulator, and Panasonic Twin Monitor Video		PMS Data Acquisition system (analog and spect. probes); HP 9920 + (analog and LORAN)
Wind Speed and Direction		LORAN	LORAN-C
Dew Point and Humidity	Dew Point Hygrometers (2 units in fuselage mount)	Thermo-electric sensor	EG&G Cambridge
Pressure	Static: Digital Pressure Transducer (fuselage port), pressure transducers (fuselage port, boom mount, interior cabin monitor) Dynamic: Pitot tube and transducer (fuselage and boom mounts)	Pressure transducer, differential pressure transducer	Pressure transducer
Air Flow	Flow angle sensors for gust boom flow: attack (gust probe and differential pressure transducer); sideslip (gust probe and differential pressure transducer)		Flowmeter Totalizer
Communications	---------- FM Radio (163.275/172.075 MHz, 151.2 Hz Guard Frequency ----------		
Radiation Fluxes	Two Pyranometers (upward and downward looking); two radiometers	Photo cell	Radiometer
Photography	Video Camera and Recorder - Color Camera Starboard (Date and Time Recording); Video Camera Module - Cockput Forward Facing with Video Tape Recorder (Date and Time Recording VHF and Audio Capahility)		
Cloud Physics and Other	Icing Rate Detector - fuselage mount; heated wire sensor for cloud liquid water - wing mount; aerosol filter pack system	Heated wire sensor for cloud liquid water; light attenuation for fine and coarse particles; impaction for aerosols	ASRC-SUNYA collectors and hot-wire sensor for cloud liquid water; water vapor sensor; aerosol analyzer for submicron (0.01 to 1 μm) particle; spectrometer probes for small (0.1 to 3 μm) and large (0.5 to 47 μm) particles; air exhauster and filter for aerosols/metals/gases; PNL collector for precipitation.

TABLE 1. (contd)

Parameter	Instrument		
	Sabreliner	King Air	DC-3
Air Chemistry Gases			
0_3	Ozone Analyzer	UV absorption sensor	Two sensor: Bendix, Monitor Labs
CO	Modified TECO	Modified TECO	Dasibi sensor
$NO-NO_x$	$NO-NO_x$ Modified Monitor Instrument	$NO-NO_x$ Modified Monitor Instrument	PNL Chemiluminescent analyzer
SO_2	Modified Meloy	Fluorescence and filter capture	Meloy sensor
H_2O_2		Wet chemistry	
HNO_3		Filter capture	
Hydrocarbons		Grab sample	

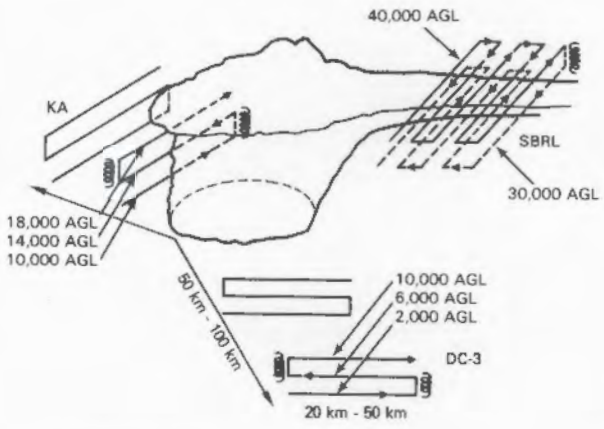

DC-3: Low-Level Inflow
KA: King Air Mid-Trap Inflow (and Low-Level Outflow)
SBRL: Sabreliner Upper-Level Outflow, Ice

FIGURE 1. Primary Flight Plan for PRECP-V Missions.

bulk sampler for special sampling for measurement of SO_2 and H_2O_2 in rain. In addition to the normal wet-only event sampling at the Oxford site, the site operator performed sequential sampling with OSCAR samplers on request from the Columbus base.

References

Dickerson, R. R., G. J. Huffman, W. T. Luke, L. J. Nunnermacker, K. E. Pickering, A. C. D. Leslie, C. G. Lindsey, W. G. N. Slinn, T. J. Kelly, P. H. Daum, A. C. Delany, J. P. Greenberg, P. R. Zimmerman, J. F. Boatman, J. D. Ray and D. H. Stedman. 1987. "Thunderstorms: An Important Mechanism in the Transport of Air Pollutants." Science 235:460-465.

Easter, R. C., M. T. Dana, J. M. Thorp, K. M. Busness, J. M. Hales, G. S. Raynor, C. M. Berkowitz, R. L. Tanner and J. D. Shannon. 1984. Overview of the Oxidation and Scavenging Characteristics of April Rains (OSCAR) Experiment. PNL-4869, Pacific Northwest Laboratory, Richland, Washington.

Heikes, B. G., G. L. Kok, J. G. Walega and A. L. Lazrus. 1987. "H_2O_2, O_3, and SO_2 Measurements in the Lower Troposphere Over the Eastern United States During Fall." J. Geophys. Res. 92(D1):915-931.

TABLE 2. PRECP-V Missions

Date	Time	KA	DC	SL	Mission Purpose
06/02/87	1800-2100	N	Y	Y	Convective storms study
06/03/87	1030-1430	Y	Y	Y	Convective inflow/outflow
06/04/87	1830-2150	Y	N	N	Clear air for vertical profiles of H_2O_2 and SO_2
06/06/87	1827-2154	Y	N	N	Clear air for H_2O_2 vertical profiles
06/08/87	1730-2100	Y	Y	Y	Intercomparison
06/08/87	2200-2530	Y	Y	Y	Charact. inflow/outflow/entrainment
06/09/87	1504-2031	Y	Y	Y	Charact. boundary level inflow
06/12/87	1330-1630	Y	Y	Y	Convective systems
06/12/87	1930-2130	N	N	Y	Deter. ootflow from conv. cells along warmfront
06/14/87	1421-1628	Y	Y	N	EPA flight (mission uncompleted)
06/16/87	1648-2049	Y	Y	Y	Convective systems study
06/17/87	1706-2143	Y	Y	N	EPA flight - S path
06/18/87	1703-1949	Y	Y	N	Clear air profile
06/19/87	1700-2149	Y	Y	Y	Convective systems study
06/20/87	1704-2318	Y	Y	Y	Convective, inflow/outflow/entrainment
06/21/87	1757-2205	Y	Y	Y	Convective systems
06/23/87	1754-1941	N	N	Y	Clear air profile
06/24/87	1213-[a]	Y	Y	Y	I ntercomparison; EPA flight (T path)
06/25/87	1526-1840	N	Y	N	Clear air profile

(a) On 6/24/87, first portion was an intercomparison (from 1224-1329); KA had mechanical problems and did not return to Columbus until 6/28/87.

N = no, Y = yes

TABLE 3. PRECP-V Ground Sampling Network

Site No.	Name	Coordinates[a]		Equipment[b]
05	West Jefferson	39°57′	083°15′	R, B, A, O, C, S
06	Pickaway Airport	39°31′	082°59′	R, B, A, O
07	Delaware USDA[c]	40°21.5′	083° 3′	R, B, A, O
08	Oxford MAP3S	39°32′	084°44′	R, B, A, O

(a) Latitude, Longitude.

(b) R = Belfort weighing rain gauge
B = Bolk (wet + dry) collector
A = Automatic (ACM) Collector(s)
O = OSCAR Sequential Collector (occasional at sites 06-07)
C = CCARS collectors
S = Special collectors for SO_2 and H_2O_2.

(c) U.S. Department of Agriculture Experiment Station-also a National Atmospheric Deposition Program (NADP) site.

TABLE 4. Precipitation Sampling Summary--PRECP-V

Prec. Date (a)	ID Date (b)	Site	Prec., cm	Rainfall Start (GMT)	Rainfall Stop (GMT)	Number of Samples by Sample Type/ Number of Sequential Stages											
						OBS	OAS	OAN	MAS	HAS	HAN	IBS	HAE	OBE	OAE	MAE	IAE
2	2	5	0.74	1650	1820									1			
3	3	5	4.5	0342	0930		1/9	1/9						1	1		
3	3	6	0.41	0230	0700									1	1		
3	3	8	1.6	0430	0700		1/3										
(c)	8	6	0.3	(c)	(c)										1		
9	9	5	0.1	0900	(d)	1/1	1/1	1/1							1		
9	9	6	(d)	(d)	(d)										1		
9	9	7	2.1	0142	0940										1		
9	9	8	0.13	1425	1430		1/1							1			
12	12	5	0.18	0900	1120		1/2	2/(2,1)			1/1				1		
12	12	5	0.51	1335	1524			2/(1,1)									
12	12	7	3.6	0600	1530										1		
12	12	8	0.66	1210	1300		1/1							1			
12	13	6	1.6	0930	1830										1		
16	16	5	1.5	2230	2310		1/8	2/(6,5)							1	1	
16	16	7	0.97	2042	2140										1	1	
19	20	6	0.41	2320	2330										1	1	
20	20	7	0.71	1945	2221		1/2			1/2							
20	20	8	0.38	0305	0400		1/2							1			
21	21	5	1.6	2145	2200		1/6	2/(3,4)		1/6		1/6	1		1	1	1
21	21	6	0.58	2300	0200										1		
22	22	5	1.1	2342	0015		1/5										
22	22		0.25	0010	0500			1/1									
21	22	6	1.4	1755	2200										1	1	
21	22	7	0.36	2221	1300										1	1	
22	22	8	1.4	2020	0800		1/6							1			
25	26	5	2.3	1750	2250		1/9	2/(8,9)		1/1		1/9	1		1	1	1
25	26	6	1.9	1750	1840		1/8		1/8								

(a) Date of precipitation end (all June).

(b) Collection date (all June).

(c) Unknown.

(d) Insufficient sample for analysis.

SAMPLE TYPE CODE = XYZ:

X
- O = for standard ion analysis
- M = for trace element analysis
- I = for dissolved SO_2 analysis
- H = for H_2O_2 analysis

Y
- A = automatic sampler
- B = bulk sampler

Z
- E = event sample
- N = CCARS sequential sample
- S = OSCAR sequential sample

FIGURE 2. Network of Ground Precipitation Sampling Sites.

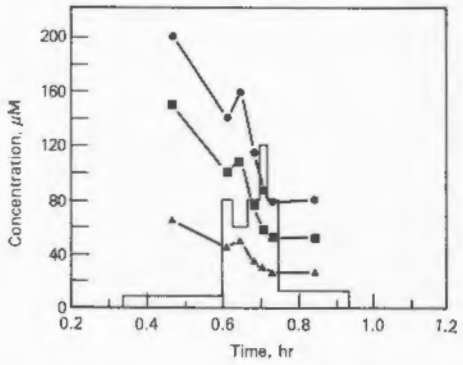

FIGURE 3. Rainfall Rates (mm/hr, stair step) and Concentrations (μM) for June 25 Site 05 Sequential Samples. $SO_4^=$ (+); NO_3^-(◇); NH_4^+ (Δ). Time scale is the same as for Figure 3.

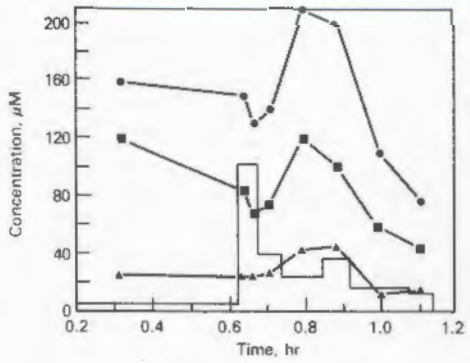

FIGURE 4. Rainfall Rates (mm/hr, stair step) and Concentrations (μM) for June 25 Site 06 Sequential Samples. $SO_4=$ (+); NO_3^-(◇); NH_4^+ (Δ). Time scale is the same as for Figure 3.

PLANS FOR THE 3CPO/PRECP-VI FIELD EXPERIMENT, SUMMER 1988

A. C. D. Leslie and M. Terry Dana

PRECP has to date conducted five field programs since 1985. A significant amount of planning has been conducted in FY 1987 (and will continue through FY 1988) for the sixth field program, PRECP-VI, which will be undertaken in May 1988.

Built on the foundations of operational experience gained in previous programs--in particular PRECP-II and PRECP-V--the goal of PRECP-VI now is to provide as complete a description as is technically possible of the chemical, microphysical, and dynamic processes involved in the deposition and redistribution of pollutants by convective systems. Within this principal goal are the following two subobjectives:

- To create a comprehensive data base on precipitation scavenging by convective storms for detailed evaluation of the RADM Scavenging Module and development of other cloud physics, chemistry, and scavenging codes.
- To investigate and quantify the phsiochemical mechanisms leading to the wet removal of pollutants in Midwestern convective storms.

To help enable a realistic accomplishment of these goals--which are most certainly ambitious--planning was initiated that has enabled the PRECP-VI program to form a synergistic force behind the creation of a much more extensive field program than PRECP-VI alone. A synthesis has been brought about of a joint participation of PRECP atmospheric chemists, and of physicists and meteorologists from other government, university and private agencies. A program known as the Cloud Chemistry and Cloud Physics Organization (3CPO) has thereby been constructed.

3CPO originated in a meeting of members of the NAPAP and PRECP community held on December 16, 1986, at Argonne National Laboratory (ANL), in which the combined scientific experience of those gathered could be drawn upon in the planning of a summer-1988 PRECP-VI field study. The goal then of PRECP-VI was a study of scavenging by convective storms. During the discussions there was a general recognition that for a description of scavenging processes by convective storms to be definitive, cloud physics and storm dynamics information would be required. However, the collection of this type of data was beyond the financial and personnel resources of PRECP. A mutually beneficial cooperative program, which would

draw in many of the resources needed, would enable a more complete study to be made encompassing the microphysical, dynamical, as well as chemical aspects of scavenging processes. Initial contacts were made with members of the Hailswath II, STORM, FIRE and PACE research communities to explore this cooperative concept. An open workshop was held at ANL on February 11 and 12, 1987, to further examine the potential of cooperative study and to initiate planning. Twenty-seven individuals from 14 different organizations (government and private) attended. At this meeting it became clear that a cooperative field program would be able to assemble an array of measurement facilities not affordable in total by any single research group. In essence, complementary information would be collected both from the PRECP research aircraft and by others using surface facilities including--but not limited to--surface Doppler radar, meteorological sites, wind profilers and CLASS soundings. Airborne and surface measurements would augment each other. Participants agreed on the timing and location of a joint field study and identified functional and cooperative roles. Participants and their roles are listed in Table 1.

TABLE 1. Summary Listing of Current 3CPO Participants

Subject/Principal Investigator	Funding Source	Current Funding Status
Anvil outflow/Dickerson	NSF/Moyers	yes
Cloud-venting modeling/Vukovich	EPA	yes
PRECP/Daum	DOE	yes
Anvil studies/Heymsfield	NCAR	yes
Cloud merger/Westcott-Ackerman	NSF/Nelson	no
Storm venting/Kropfli	EPRI	probable
Precip. efficiency/C. Knight	NCAR	yes
Rain chemistry/Bowersox	DOE	yes
Storm outflows/Achtemeier	NSF/Nelson	no
Storm outflows/Emmitt-Garstang	NSF/Nelson	no
Lidar/Hardesty	?	no
PACE/Changnon	Illinois	yes
Lagrangian studies/Vali	NSF(?)	no
Hailstones/N. Knight	NCAR	yes
Modeling/Moncreiff	NCAR	yes
Modeling/Lamb	NSF/Nelsnn	no
Cloud chemistry/Czys	NSF/Nelson	no
Composite Cb met./Lyons-Pielke	EPRI	?
Tracers/Stith and Poellot	EPRI	?
Doppler and PAM/Seliga-Heydin	NSF/Taylor	?
Profiler/Strauch	NCAR	no
Profiler/Ecklund et al.	NOAA	yes
Tracers/Gaustein-Turekian	?	yes
Carbon aerosols/Hansen-Novakov	?	partially
Anvil outflow meas./Harris-Hobbs	EPRI	?
Multi-Doppler analysis/Johnson-Ray	?	?
Aerosol chem./Johnson-Kumar	EPRI	favorable
Chill/profiler/Larsen-Ullrich	NSF	partially
Mini-profilers/Green et al.	NOAA	yes

A further 3CPO planning meeting was held at the end of FY 1987, on September 29. The purpose of this meeting was to commence the consolidation of the research plans of the groups who intended to participate.

Summary

The 3CPO program was conceptualized, interested participants formulated their plans, and the initial coordination of an overall 3CPO program plan was solidly put in place during FY 1987. The overall objectives of 3CPO that were thus developed in FY 1987 were:

1. To describe the air, water and pollutant flow and deposition fields in summer convective storms in the Midwestern U.S.

2. To identify and quantitatively describe the dominant chemical and microphysical processes determining the fraction of water and pollutants deposited in precipitation at the surface in such storms.

3. To examine the influence of horizontal and vertical air motions within an existing convective storm on the formation of new cells and to evaluate their role on the formation and maintenance of the storm.

4. To obtain data that will permit testing of numerical models of the wet scavenging process.

The 3CPO project is planned to be conducted between May 1 and June 30, 1988, centered on Champaign in east-central Illinois. The most intensive measurements will be conducted when the NOAA P-3 research aircraft is present from May 15 through June 15. The location of the surface-based facilities is shown in Figure 1. The extended area of operations is within the larger block. It is contemplated that aircraft operations will extend to various parts of the horizontal boundary under particular meteorological situations, but will be conducted intensively within the region of the fixed surface facilities. This area of east-central Illinois is well suited for convective storm research for a number of reasons. It is in a flat region of the country, thus allowing the storms to be observed in the absence of orographic complications. Moreover, the simple terrain minimizes radar ground clutter effects and provides favorable conditions for research aircraft operations. The area is situated in a relatively polluted region of the United States, but contains few major sources; thus relatively homogeneous pollutant concentration fields can be expected for any storm event. This will be a distinct

FIGURE 1. Location of Surface-Based Facilities.

advantage for the planned precipitation-scavenging evaluations and for basic cloud research. On the other hand, the region is known to lie on the climatological "shoulder" of the northeastern United States wet deposition pattern, suggesting that a diversity of pollution environments will be experienced from one storm to the next. This will certainly be an attractive feature from a model evaluation perspective. Finally, east-central Illinois provides a prime field study site because of the large body of logistic support available from the Illinois State Water Survey (ISWS) in Champaign and their history of previous measurements.

PRECP initiated 3CPO as an attempt to draw a broad base of technical capability to a central location on a data-sharing effort, in support of PRECP's goals of precipitation-scavenging research and model evaluation. In addition to DOE, the agencies and groups participating in 3CPO include NOAA, NCAR, NSF, the Electric Power Research Institute (EPRI), the Federal Aviation Administration (FAA), the Illinois State Water Survey (ISWS), the University of Maryland, Yale University, R*SCAN, and Simpson Weather Associates. Field measurements will be centered primarily on a 62.5 x 62.5 mile (100 x 100 km) square near Champaign, Illinois.

These measurements will include detailed surface-network measurements of meteorological parameters, rain chemistry, and pollution features, aircraft measurements of cloud physics and pollution fields, and numerous types of radar measurements of storm features and flow patterns.

Aircraft and surface facilities to be deployed (as of 3/88) during 3CPO are shown in Table 2.

3CPO is still coming into final shape because of funding reallocations. It appears, however, that 3CPO is likely to provide the most comprehensive set of measurements yet obtained on the combined chemical and dynamical behavior of summertime convective storms.

MODELING OF POLLUTANT REMOVAL AND REDISTRIBUTION BY CONVECTIVE STORMS

R. C. Easter and C. G. Lindsey

One of the modeling activities within the PNL component of PRECP involves the study of pollutant removal and redistribution by storms on the meso-gamma spatial scale. The objective of this modeling component is to define and advance understanding of the relations between pollutant inflows and outflows for individual storm systems (e.g., isolated convective storms or frontal rainbands). Pollutant outflows include both wet deposition to the surface and vertical redistribution of non-deposited pollutants. For several reasons, activities

TABLE 2. Aircraft and Surface Facilities

Facility	Function
PNL Gulfstream-1	Perform boundary-layer pollution-inflow measurements, and release chaff to assist NOAA/EPRI radar studies of vertical venting by storms (its first mission as a research aircraft)
NOAA P-3 Aircraft	Make mid-level pollution and Doppler radar measurements
NCAR Sabreliner Aircraft	Obtain high-altitude, pollution-venting measurements
South Dakota School of Mines' T-28 and Beach-Baron-type meteorological aircraft	Operate within the ISWS Precipitation Augmentation for Crops Experiment ("PACE")
Automated Balloon System (CLASS)	Take upper-air wind and thermodynamic measurements
Two NSF Doppler Radar Units ("HOT" and "CHILL") Doppler	"HOT": Serve as surveillance radar; "CHILL": Provide wind-field measurements in coordination with the P-3
Real-time Aircraft Tracking System (RATS) on CHILL and HOT Radars	Display real-time position of research aircraft
X-Band Polarized Doppler Radar	Conduct chaff measurements of cloud venting (EPRI/NOAA)
Two Phased-Array Radar Profilers from NOAA	Obtain real-time measurement of winds aloft
Two DOE Surface-Pollution Measurement Laboratories	
Surface Array of CCARS (Computer Controlled Automatic Rain Sampler)	An inexpensive, rapidly deployable field research tool (recently developed by PNL)
A Surface Network of 25 to 50 Portable Meteorology Stations from Simpson Weather Associates (probable)	

within this component have concentrated on modeling of convective storms. The meteorological complexity of these storms makes modeling an attractive approach for understanding the overall effects of the numerous processes occurring in the storms. The work has developed our capability for analyzing results from the PRECP-II (Pre-STORM) and the upcoming PRECP-VI (3CPO) convective storm field studies. Finally, the results should be applicable to scavenging modules for regional acid deposition models.

The convective storm modeling work has utilized the PLUVIUS-II reactive scavenging model (Easter and Luecken 1987) coupled with the Colorado State University (CSU) cloud model (Tripoli and Cotton 1982). The PLUVIUS model solves a set of mass-conservation equations for specified pollutant species. These equations describe the effects of transport by storm-scale motions and falling precipitation, cloud microphysical processes, physical attachment and mass transfer to cloud and precipitation particles, and chemical reactions within liquid particles. The PLUVIUS model is a kinematic model, so storm dynamical fields must be provided from another source. Dynamical fields from CSU cloud model simulations have been used in this work. The CSU model results were obtained through a PRECP subcontract with Dr. W. R. Cotton. Under this subcontract, Dr. Cotton's group has provided simulations of two previously studied convective storms. Dr. Cotton's group has also been working on simulations of the June 26 case (a classical cold front) from the Pre-STORM field experiment. A two-dimensional simulation of this case has been completed, and a three-dimensional, channel symmetric simulation is under way.

The results presented in this article involve the two "past case studies" provided by CSU. Both of these cases are two-dimensional simulations of intense convective storms, which develop sustained updrafts in excess of 20 m/s. The first of these cases is a cold-based continental convective cloud (the Colorado storm), which has been extensively analyzed by the CSU group (Tripoli and Cotton 1986). The second case is a warm-based, maritime tropical convective cloud (the Florida storm) described by Cotton et al. (1982). Because warm rain processes were dominant in the Florida case, ice-phase microphysical processes were deactivated in this simulation. The two cases provide an interesting contrast in two ways. First, ice processes are important in the Colorado storm but not in the Florida storm. Second, the Colorado storm develops a stronger, more sustained circulation than the Florida storm.

The scavenging simulations with the PLUVIUS model have focused on the processing of sulfur species. The simulations involve four pollutant species: sulfur dioxide (SO_2), sulfate aerosol, hydrogen peroxide (H_2O_2), and ozone. Ammonia and nitric acid are not included in the simulations. (Although they affect sulfur scavenging through their influence on cloud and rain pH, they generally neutralize much of each other's impact.) Besides gas and aerosol forms, the species can be dissolved or bound in any of the water forms treated in the CSU model: cloud water, rain, graupel, aggregates, and ice crystals. The scavenging processes included in the model for these species are impaction and nucleation scavenging of aerosols (nucleation scavenging efficiency of 0.9 assumed), reversible gas scavenging (treated as equilibrium for cloud water and nonequilibrium for rain), aqueous chemical reactions between SO_2, H_2O_2, and ozone, and cloud microphysical processes that transfer water from one form to another.

Simulations were performed with a number of different initial pollutant conditions representing moderate to heavy pollution levels for the eastern United States. The same sets of pollutant conditions were used with both the Colorado and Florida cases. This study did not attempt to investigate effects caused by different pollutant conditions in Colorado and Florida. The two storm cases are treated simply as two examples of intense convective clouds and are used to study pollutant processing by such clouds under pollutant conditions occuring in the eastern United States.

Two sets of initial conditions for sulfur species were used. In the heavily polluted ("hi-S") case, surface mixing ratios were 10 ppb for SO_2 and 4 ppb for sulfate. In the moderately polluted ("lo-S") case, surface mixing ratios were 3 ppb for SO_2 and 1.5 ppb for sulfate. Both SO_2 and sulfate have exponential profiles with 2- and 3.5-km scale heights, respectively. The profiles for the lo-S case are shown in Figure 1. Ozone was 70 ppb, independent of height, in all the simulations. The H_2O_2 profile used in most of the simulations (the "A" profile) had a peak mixing ratio above the boundary layer, based on recent observational data (Heikes et al. 1987). Peak mixing ratios of 1.5 ppb ("lo-HP" case) and 3 ppb ("hi-HP" case) were used. Figure 1 shows the H_2O_2 profile for the 1.5 ppb case.

Model results are discussed below with respect to the following topics: the relative importance of different scavenging mechanisms to sulfur wet deposition, the sensitivity of sulfur wet deposition to H_2O_2 levels and H_2O_2

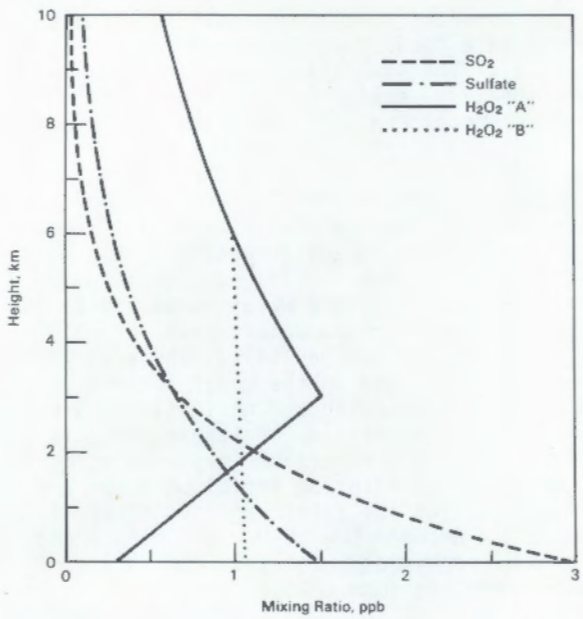

FIGURE 1. Initial Pollutant Profiles for Scavenging Simulations. SO_2 and sulfate aerosol profiles are for the "lo-S" case. For H_2O_2, both the "A" and "B" profiles for the "lo-HP" case are shown.

profile shapes, and the wet removal and vertical redistribution efficiencies of the storms.

The relative importance of different sulfur scavenging mechanisms to sulfur wet deposition is summarized in Table 1. The two most important mechanisms are sulfate aerosol scavenging and SO_2 scavenging through the reaction with H_2O_2. Aerosol scavenging is most important in the Colorado storm simulations, while SO_2-H_2O_2 scavenging is most important in the Florida storm. This difference reflects the greater amount of liquid water (in which the reaction can occur) in the Florida storm. Scavenging of SO_2 through the reaction with O_3 is of lesser importance in most of the simulations; the exceptions are the Florida storm simulations with lower H_2O_2 levels. The greater importance of SO_2 scavenging in the Florida simulations again reflects the greater amount of liquid water. The direct, nonreactive scavenging of SO_2 is also of lesser importance, contributing at most 10% to the sulfur wet deposition. The secondary importance of the SO_2-O_3 and nonreactive SO_2 scavenging mechanisms under the high liquid

TABLE 1. Contributions of Different Scavenging Mechanisms to Sulfur Wet Deposition

Simulation Conditions			Sulfur Wet Dep[a]	Contribution of Scavenging Mechanism to Sulfur Deposition (% of Total)			
Storm	Sulfur	H_2O_2	(μmol/ℓ)	Aerosol[b]	SO_2-H_2O_2[c]	SO_2-O_3[d]	S(IV)[e]
Colorado	lo-S	hi-HP	14.4	54	35	4	7
Colorado	lo-S	lo-HP	13.1	60	23	7	10
Colorado	hi-S	hi-HP	34.1	61	31	2	6
Colorado	hi-S	lo-HP	30.1	69	19	3	9
Florida	lo-S	hi-HP	13.1	40	51	6	3
Florida	lo-S	lo-HP	12.3	42	37	16	5
Florida	hi-S	hi-HP	31.2	44	44	8	4
Florida	hi-S	lo-HP	26.8	51	27	16	6

(a) Event averaged concentration = (total sulfur deposition)/(total water deposition).

(b) Sulfate aerosol scavenging.

(c) SO_2 scavenging through reaction with H_2O_2.

(d) SO_2 scavenging through reaction with O_3.

(e) Nonreactive SO_2 scavenging.

water conditions of these intense convective storms is significant.

The sensitivity of sulfur wet deposition to H_2O_2 levels (1.5 versus 3 ppb maximum H_2O_2) is shown in Table 2. Normalized sensitivity coefficients are shown for sulfur as a result of the SO_2-H_2O_2 reaction, for sulfur as a result of all SO_2 scavenging mechanisms, and for total sulfur (which includes the sulfate aerosol scavenging). The sensitivity coefficients for sulfur from the SO_2-H_2O_2 reaction are fairly high (0.55-0.92), as is expected when SO_2 levels generally exceed H_2O_2 levels. For sulfur as a result of all SO_2 scavenging, the coefficients drop considerably, because increasing H_2O_2 causes the other SO_2 scavenging mechanisms to be less effective. For total sulfur wet deposition, the coefficients are lower still (0.09-0.22), because sulfate aerosol scavenging determines much of the total deposition. These low sensitivity coefficients are significant because they suggest that uncertainties in predictions or measurements of H_2O_2 levels will translate to considerably smaller uncertainties in total sulfur wet deposition.

Recent observations of H_2O_2 profiles (Heikes et al. 1987) show that the peak H_2O_2 levels often occur above the boundary layer. Because peak SO_2 levels generally occur within the boundary layer, this has raised questions about the effect on scavenging from the differing vertical profiles of SO_2 and H_2O_2. To investigate this effect, simulations were made with an alternative H_2O_2 profile shape. The alternative profile (the "B" profile, see Figure 1) decreases monotonically with height but has the same total H_2O_2 in the 0- to 6-km layer as the "A" profile. Thus, differences between the "A" and "B" profile simulations are due to the distribution of H_2O_2 but not the overall amount. The results from these simulations are summarized in Table 3. For the Colorado storm, wet-deposited sulfur from SO_2 scavenging is 9 to 19% greater with the "B" profile, but total wet-deposited sulfur is only 4 to 7% greater. For the Florida storm, there is a much smaller difference between the "A" and "B" profile results. These results suggest that in vigorous convective storms under polluted conditions, total sulfur wet deposition has a low sensitivity to the H_2O_2 profile shape.

TABLE 2. Sensitivity of Sulfur Wet Deposition to Initial H_2O_2 Levels

Simulation Conditions		Normalized Sensitivity Coefficient		
Storm	Sulfur	Total Sulfur	Sulfur from From All SO_2 Scavenging	Sulfur from SO_2-H_2O_2 Reaction
Colorado	lo-S	0.13	0.31	0.75
Colorado	hi-S	0.18	0.51	0.92
Florida	lo-S	0.09	0.14	0.55
Florida	hi-S	0.22	0.43	0.75

TABLE 3. Effect of H_2O_2 Profile Shape on Sulfur Wet Deposition

Simulation Conditions			Increase (%) in Sulfur Deposition from H_2O_2 Profile "A" Simulation to H_2O_2 "B" Simulation	
Storm	Sulfur	H_2O_2	Total Sulfur	Sulfur from SO_2 Scavenging
Colorado	lo-S	hi-HP	5	11
Colorado	lo-S	lo-HP	4	9
Colorado	hi-S	hi-HP	7	19
Colorado	hi-S	lo-HP	4	14
Florida	lo-S	hi-HP	-1	-2
Florida	lo-S	lo-HP	0	0
Florida	hi-S	hi-HP	3	5
Florida	hi-S	lo-HP	2	4

Wet removal and vertical redistribution (venting) efficiencies provide another way to analyze pollutant processing by storms. A convective storm can be viewed as a black box having a number of pollutant inflows and outflows. The primary inflow for sulfur species is low-level air, which contains the highest concentrations of sulfur species. The outflows of primary interest are wet deposition and outflow to mid and high levels. The wet removal efficiency (E_{wet}) for a species is the ratio of the wet deposition rate to the low-level inflow. The venting efficiency (E_{vent}) is the ratio of the outflow above some level to the low-level inflow. For these simulations, low-level has been defined as below 4 km. Venting efficiencies have been calculated for venting above 4 km and above 8 km.

Table 4 summarizes E_{wet} and E_{vent} values for water, sulfate aerosol, and SO_2. One of the most noticeable features in these results is the marked difference between the Colorado and Florida storms. The Colorado storm has much higher E_{vent} (all species) and much lower SO_2 E_{wet}. The higher E_{vent} values are due primarily to the stronger, more sustained

TABLE 4. Wet Removal and Venting Efficiencies for the Convective Storm Simulations

Species	Pollutant Conditions		Wet Removal Efficiency (%)		Venting Efficiencies (%)			
					Colorado		Florida	
	Sulfur	H_2O_2	Colorado	Florida	4 km	8 km	4 km	8 km
Water	all	all	46	52	31	28	2	1
Sulfate	all	all	75	90	16	16	0	5
SO_2	lo-S	hi-HP	40	94	46	42	5	3
SO_2	lo-S	lo-HP	32	86	51	47	9	4
SO_2	hi-S	hi-HP	24	62	60	55	16	8
SO_2	hi-S	lo-HP	17	47	66	59	22	10

updraft structure that develops in the Colorado storm. The E_{vent} values also display some inverse dependence on E_{wet} values (if most material is wet deposited, then little is available for venting, and vice-versa). In the Colorado storm, the 4-km E_{vent} values are not significantly larger than the 8-km values, so most of the venting is to above 8 km. In the Florida storm, the SO_2 venting is evenly distributed between mid levels (4 and 8 km) and high levels (above 8 km). The higher E_{wet} for SO_2 in the Florida storm is due primarily to the greater amount of liquid water in this case, and secondarily to the higher efficiency with which cloud water is removed (as indicated by the higher E_{wet} for sulfate aerosol). The E_{wet} for SO_2 are strongly dependent on the relative amounts of SO_2 and H_2O_2, reflecting the dominance of the H_2O_2 reaction in SO_2 scavenging. The large variability in both E_{wet} and E_{vent} for SO_2, both between storms and as a function of initial SO_2 and H_2O_2 levels, is significant. A fuller understanding of this variability will be required to accurately simulate these processes in regional acid deposition models.

These results demonstrate the insights that modeling can provide about how storms process pollutants. Modeling results from more extensive theoretical studies and from analyses of PRECP field experiments are expected to be of significant utility.

References

Cotton, W. R., M. A. Stephens, T. Nehrkorn and G. J. Tripoli. 1982. "The Colorado State University Three-Dimensional Cloud/Mesoscale Model-1982. Part II: An Ice Phase Parameterization." J. Rech. Atmos. 16:295-320.

Easter, R. C., and D. J. Luecken. 1987. "A Simulation of Sulfur Wet Deposition and Its Dependence on the Inflow of Sulfur Species to Storms." Submitted to Atmos. Environment.

Heikes, B. G., G. L. Kok, J. G. Walega and A. L. Lazrus. 1987. "H_2O_2, O_3 and SO_2 Measurements in the Lower Troposphere Over the Eastern United States During Fall." J. Geophys. Res. 92:915-931.

Tripoli, G. J., and W. R. Cotton. 1982. "The Colorado State University Three-Dimensional Cloud/Mesoscale Model-1982. Part I: General Theoretical Framework and Sensitivity Experiments." J. Rech. Atmos. 16:185-219.

Tripoli, G. J., and W. R. Cotton. 1986. "An Intense, Quasi-Steady Thunderstorm Over Mountainous Terrain. Part IV: Three-Dimensional Numerical Simulation." J. Atmos. Sci. 43:894-912.

THEORETICAL RESULTS FOR THE RELATIONSHIP BETWEEN CONCENTRATION FLUCTUATIONS AND RESIDENCE TIMES OF ATMOSPHERIC TRACE GASES

W. G. N. Slinn

No doubt there is an enormous number of different gases in the atmosphere: this number is comparable to the total number of chemical compounds known, since each has a finite vapor pressure. Moreover, there is no doubt that each gas has a finite lifetime in the atmosphere, since otherwise, the concentrations of continuously emitted gases would increase without bounds. This article deals with

relating the atmospheric lifetime of gases to measured fluctuations in their concentrations.

That concentration fluctuations of a gas should be related to its atmospheric residence time, T_r, seems intuitively reasonable: if a gas has a very long residence time in the atmosphere (e.g., oxygen's 10^4 years), then it seems reasonable that fluctuations in its concentration would be small; conversely, for a relatively short-lived gas (e.g., 1 day to 1 week for SO_2), it seems reasonable that its concentration would vary quite substantially. The purpose of this article is to place this intuitively reasonable result on a firm theoretical foundation.

As demonstrated by Figure 1, experimental results confirm the intuitively reasonable relation between concentration fluctuations and atmospheric residence times. The chosen measure for the concentration fluctuations is the coefficient of deviation, f_c, which is the standard deviation of the concentration fluctuations, σ_c, divided by the mean concentration, $\bar{C}$. For Figure 1, the atmospheric residence time for each gas is based on estimates of total atmospheric burden divided by production or removal rates. Figure 1 includes a plot of Junge's empirical fit to the data (Junge 1974).

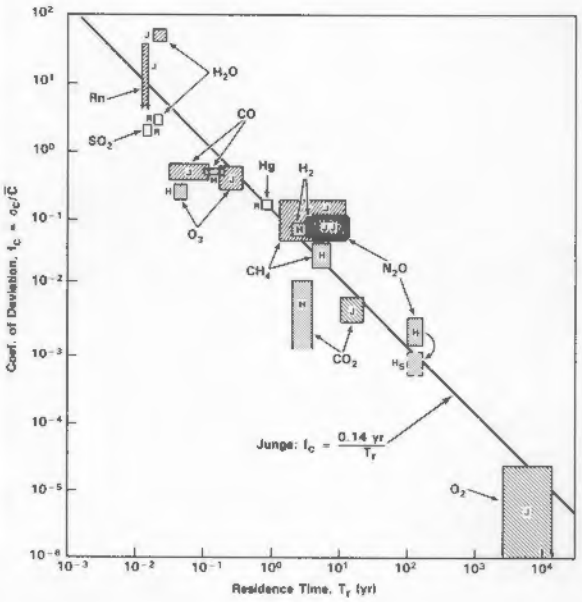

FIGURE 1. Junge's Empirical Relationship Between Concentration Variability and Residence Time for Trace Gases in the Atmosphere. For descriptions of the estimates of F_c for different gases see Junge (1974) = J, R. Jaenicke (1982) = R, and Hamrud (1983) = H and H_s.

Junge's relationship,

$$f \equiv \frac{\sigma_c}{\bar{C}} = \frac{b}{T_r} \quad , \qquad (1)$$

with b the same constant for all gases, has recently been used to estimate the atmospheric residence time of new gases for which only concentration fluctuations have been measured. Junge's relationship has therefore become a valuable predictive tool for new gases released to the atmosphere, and consequently, there is also substantial practical value in developing a theoretical understanding of Junge's empirical result. This article demonstrates a simple derivation of Junge's result and reveals its limitation (Slinn 1988).

A number of authors attempted to derive Junge's result both analytically (Gibbs and Slinn 1973, Baker et al. 1979, Jaenicke 1982, Slinn 1983) and numerically (Junge 1974, Hamrud 1983), but none has been entirely successful. However, Hamrud's analysis is particularly illuminating: he emphasized that Junge's result is more appropriately interpreted, not as a relationship for fluctuations in time at a particular point, but as a measure of the spatial variability of the concentrations. If Hamrud's interpretation is coupled with a part of Jaenicke's concept of finite sampling time, then the following simple model can be developed.

Simple Model

As suggested in Figure 2, suppose that the concentration of a trace gas decreases exponentially with distance downwind from a point

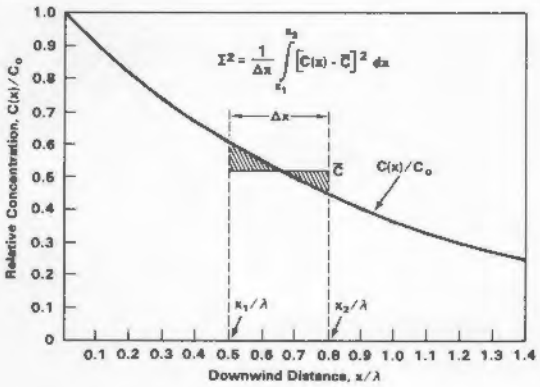

FIGURE 2. The Peculiar Variance Used to Derive Junge's Result.

source at $x = 0$, viz., $C = C_o \exp(-x/\lambda)$, with λ the characteristic removal length. It will be seen that neither the initial concentration, C_o, nor the sampling location, x, appears in the final result; therefore, for a linear system, the result will be valid for an arbitrary upwind distribution of sources and arbitrary source strengths, at least for the one-dimensional case. Consequences of additional dimensions and an arbitrary functional form for the dependence of the concentration on the downwind distance will be mentioned in a later paragraph. To introduce the residence time, we can let $s = x/\bar{u}$ be the time along the trajectory (with $\bar{u}$ an average wind speed). Then $C = C_o \exp(-s/T_r)$, with $T_r = \lambda/\bar{u}$ interpreted to be the residence time.

Now define a mean concentration, averaged over a sampling distance Δx (or over a corresponding range of sampled times, $\Delta s = \Delta x/\bar{u}$):

$$\bar{C} = \frac{1}{\Delta x}\int_{x_1}^{x_2} C(x)\,dx = \frac{C_o\lambda}{\Delta x}\left[e^{-x_1/\lambda} - e^{-x_2/\lambda}\right] . \tag{2a}$$

Similarly, although it is rather peculiar, define the mean-square concentration:

$$\overline{C^2} = \frac{1}{\Delta x}\int_{x_1}^{x_2} C^2(x)\,dx = \frac{\lambda}{2\Delta x} C_o^2\left[e^{-2x_1/\lambda} - e^{-2x_2/\lambda}\right] . \tag{2b}$$

From Equation (2) we can define a coefficient of deviation (though it, too, is rather peculiar), $F_c = [(\overline{C - \bar{C})^2}]^{1/2}/\bar{C}$, and obtain

$$F_c^2 + 1 = \frac{\overline{(C^2)}}{(\bar{C})^2} = \frac{\Delta x}{2\lambda}\,\frac{\left[1 - \exp\{-2(\Delta x)/\lambda\}\right]}{\left[1 - \exp\{-(\Delta x)/\lambda\}\right]^2} , \tag{3a}$$

or in alternative notation,

$$F_c^2 + 1 = \frac{\Delta s}{2T_r}\,\frac{\left[1 - \exp\{-2(\Delta s)/\lambda\}\right]}{\left[1 - \exp\{-(\Delta s)/\lambda\}\right]^2} , \tag{3b}$$

which is plotted in Figure 3.

Results and Discussion

Figure 3 suggests that the simple result [Equation (3)] contains the essence of Junge's result. A second-order expansion of Equation (3) for $\Delta x \ll \lambda$ (or $\Delta s \ll T_r$) gives

$$F_c \to \frac{1}{\sqrt{12}}\,\frac{\Delta x}{\lambda} = \frac{1}{\sqrt{12}}\,\frac{\Delta s}{T_r} . \tag{4}$$

Interestingly, this result [and Equation (3)] suggests that Junge's result should not be used to estimate residence times of gases, unless account is taken for the distribution of sampling locations (or corresponding sampled times).

For a general functional form for the concentration, $C = C(x)$, it can be seen that the λ^{-1} in Equation (4) is replaced by $(1/C)(dC/dx)$. If cross-wind diffusion were important (e.g., downwind of a finite-area source), it might be thought that F_c would then be smaller (because $d(\ln C)/dx$ would then be larger than λ). However, this peculiar F_c would then depend on the region sampled, and F_c could be larger if cross-wind locations were sampled. Cases of larger F_c for finite-area sources are demonstrated by Hamrud's numerical analyses. Here, in Figure 3, we

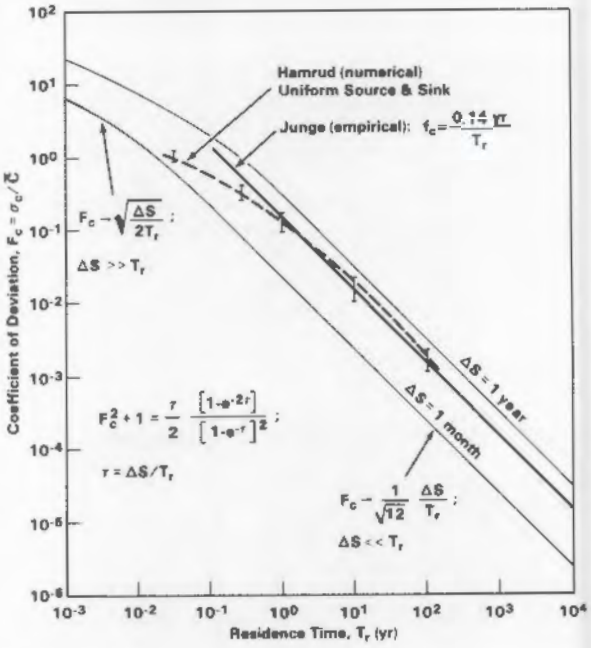

FIGURE 3. Comparisons of the Result, Equation (3) (and its limiting forms), for Two Sampled Times, with Junge's Empirical Result and Hamrud's Numerical Calculations [for his case of "tropospheric variability," "ocean source," and "uniform sink" (viz., his σ_t, Case 3)].

at least demonstrate the general agreement between the results from this simple model, Equation (3), and Hamrud's calculations for a uniform source (and uniform sink).

In Jaenicke's (1982) important work, Junge's result is assumed to be derived from sampling the concentration between zero and some t_{max}. He states that "it immediately becomes obvious that a time t_{max} has to be introduced as upper limit of the averaging period" (presumably because of a minimum detection limit of the sampling instrument). He then makes what appears to the present author to be an unrealistic assumption that, for the sampled concentrations between zero and t_{max}, "observations at any time are of equal probability." Finally, Jaenicke apparently did not notice that Junge's definition for the "coefficient of deviation" is peculiar. In contrast, in the interpretation presented here, it is suggested that Junge's empirical result depends on his peculiar definition of concentration deviations, viz., based only on the mean concentration [cf. Equation (2)]. In essence, the interpretation presented here is that if one takes a finite sample of any decaying function and calculates first and second moments from the portion of the function that has been sampled, then these moments contain information about the decay rate (coupled with the sampling time). As a result of this different interpretation, the model presented is exceedingly simple: there is no need to introduce assumptions about instrument sensitivity or sampling probability. Thus, Jaenicke's assumptions appear to be unnecessarily restrictive, and he failed to notice that Junge's definition is peculiar.

Moreover, this peculiar definition appears to be the cause of previous difficulties in deriving Junge's result (Gibbs and Slinn 1973, Baker et al. 1979, Slinn 1983). These other derivations have calculated the variance from an ensemble (or time) average over the concentration fluctuations at a single point; i.e., they have relied on the common meaning for variance. In contrast, what has been calculated here is a deviation from the sample mean, over a finite sampling interval. For a stationary process, the usual variance is independent of the sampling time (which, theoretically, is infinitely long). In contrast, if the interpretation given here for Junge's result is correct, then his coefficient of deviation would become large, without bound, for large Δx (or Δs). Nevertheless, this peculiar definition for F_c can yield useful estimates of T_r, either from Equation (3) (knowing Δx or Δs), or from noticing that, for $\Delta s \ll T_r$, $dF_c/d(\Delta s) \rightarrow (1/\sqrt{12})\ T_r^{-1}$, independent of the sampled times.

References

Baker, M. B., H. Harrison, J. Vinelli and K. B. Erickson. 1979. "Simple Stochastic Model for the Sources and Sinks of Two Aerosol Types." Tellus 31:39-51.

Gibbs, A. G., and W. G. N. Slinn. 1973. "Fluctuations in Trace Gas Concentrations in the Troposphere." J. Geophys. Res. 78:574-576.

Hamrud, M. 1983. "Residence Time and Spatial Variability for Gases in the Atmosphere." Tellus 35B:295-303.

Jaenicke, R. 1982. "Physical Aspects of the Atmospheric Aerosol." In Chemistry of the Unpolluted and Polluted Troposphere, H. W. Georgii and W. Jaeschke, eds., pp. 341-373. D. Reidel Publ. Co., Boston, Massachusetts.

Junge, C. E. 1974. "Residence Time and Variability of Tropospheric Trace Gases." Tellus 26:477-487.

Slinn, W. G. N. 1983. "Air-to-Sea Transfer of Particles." In Air-Sea Exchange of Gases and Particles, P. S. Liss and W. G. N. Slinn, eds., pp. 299-405. D. Reidel Publ. Co., Boston, Massachusetts.

Slinn, W. G. N. 1988. "A Simple Model for Junge's Relationship Between Concentrations Fluctuations and Residence Times for Tropospheric Trace Gases." Tellus 40B (in press).

FOUNDATIONS FOR AN INTEGRAL DESCRIPTION OF CONCENTRATION FLUCTUATIONS IN DISPERSIVE MEDIA

W. G. N. Slinn

Perhaps the most obvious characteristic of the concentrations of any chemical in any environmental fluid (the atmosphere, rivers, lakes, estuaries, the oceans) is that the concentrations fluctuate in time: concentrations are **stochastic**. Causes of these time variations include time variations in source strengths, turbulence in the fluid, and the stochastic nature of processes that remove or destroy the chemical (for example, sources of these stochastic removal processes in the atmosphere are precipitation scavenging and dry deposition). This article addresses the stochastic nature of a chemical's concentration in environmental fluids.

In spite of the obvious stochastic nature of chemical concentrations in environmental fluids, emphasis of environmental scientists during the past century or so has been on measuring, understanding, and modeling the mean values of the concentrations, with the average usually taken over a finite sampling time or distance, or taken over a time period (hour, day, year) relevant to some receptor's response to the chemical. A major reason for this emphasis on mean values is that understanding the concentration variations is extremely difficult.

Recently, however, there have been both theoretical and practical requirements for understanding and modeling higher moments (variance, skewness, kurtosis, etc.) of the concentration. An example of theoretical requirements was given in the previous article in this report, where it was shown that information about the variance of a chemical's concentration in the atmosphere can be used to estimate the chemical's atmospheric residence time. An example of the practical need to know concentration statistics is in recent air pollution regulations based on concentration extremes, such as the requirement that a specific chemical's hourly concentration not exceed a specified value more frequently than a specified number of hours per year. There is therefore need to develop methods for modeling concentration statistics, and the need is expected to intensify as more regulations attempt to protect against chemical concentrations exceeding values determined to be threshold values for deleterious effects to human and environmental health.

The purpose of this article is to outline a new theoretical foundation (Slinn 1988) for the mathematical description of a trace chemical's concentration statistics in environmental fluids. It may be true that all processes can theoretically be described in complete detail (viz., deterministically); for example, even the outcome of the tossing of a coin could be predicted accurately if all forces and all boundary and initial conditions were specified exactly. However, for the case of a chemical's concentration in an environmental fluid, it is impractical to try to specify all conditions completely. Moreover, even in the unlikely case that complete descriptions of forces and initial and boundary conditions could be obtained, and even in the more unlikely case that the needed calculations could then be performed, it is doubtful that the answers would be desired: rather than the complete and exact description of a stochastic variable, we typically desire information only about a few statistical properties, such as the value of the first few moments (mean, variance, etc.) of the probability density function for the concentration variations. In this article, a new method for obtaining these moments is described. Before describing the method for a dispersive medium, however, it is useful to reformulate the problem for a nondispersive medium.

Concentrations in a Nondispersive Medium

Let C be the concentration of the trace material of interest, where "trace" means that the material has negligible influence on the dynamics of the host fluid. In this section, diffusion is ignored, and therefore, C is assumed to satisfy the continuity equation

$$\frac{\partial C}{\partial t} + \vec{v}_E \cdot \nabla C = \dot{G} - \dot{L} , \qquad (1)$$

in which $\vec{v}_E(\vec{r},t)$ is the (Eulerian) velocity field of the fluid, and $\dot{G}$ and $\dot{L}$ are (deterministic) volumetric gain and loss rates, respectively. For Equation (1), C can be either mass density or mass mixing-ratio, and the fluid can be compressible or incompressible: for these different cases, the only difference in Equation (1) is a term in $\dot{L}$ linear in C, which will not influence the following analysis (Slinn 1988). Baker (1980) has examined the statistics of Equation (1), for spatially independent $\vec{v}_E$ and special cases of $\dot{G}$ and $\dot{L}$, by solving Equation (1) using Fourier-transform methods. In the following discussion, Lagrange's method will be used, and the restriction to spatially independent $\vec{v}_E$ can be relaxed.

Lagrange's solution to Euler's continuity equation, Equation (1), can be obtained either by using Lagrange's method for solving first-order partial differential equations (Slinn 1988) or by first transforming Equation (1) to Lagrangian coordinates and then solving the resulting ordinary differential equation (Slinn 1988). In either case, we use the notation $\vec{v}_E[\vec{r}(t), t] = \vec{v}_L(t)$ for the (Lagrangian) velocity of fluid particle at $\vec{r}(t)$. For the important special case with the gain rate, $\dot{G}$, independent of C and the loss rate, $\dot{L}$, linear in C [viz., $\dot{L} = \ell(\vec{r}, t)C$], then the solution to Equation (1) is

$$C(\vec{r},t) = C_o[\vec{r} - \langle\vec{v}_L\rangle t, 0] \exp\{-\langle\ell\rangle t\} + \int_0^t d\tau\, \dot{G}\,[\vec{r} - \langle\vec{v}_L\rangle\tau, t - \tau] \exp\{-\langle\ell\rangle\tau\} , \qquad (2)$$

in which the (prior) time average of a quantity q is defined via

$$\langle q(t;T)\rangle = \frac{1}{T}\int_{t-T}^{t} d\tau\, q(\tau) , \qquad (3)$$

i.e., evaluated backward along the "trajectory" that arrives at $\vec{r}$ at time t.

Two special versions of Equation (2) will be used frequently in the analysis below. First, since any initial concentration, C_o, arises from prior emissions, then Equation (2) can be written as

$$C(\vec{r},t) = \int_0^\infty d\tau\ \dot{G}[\vec{r} - \langle\vec{v}_L\rangle\tau, t - \tau]\ \exp\{-\langle\ell\rangle\tau\}; \tag{4}$$

i.e., the sum of the gains at all prior locations and times, suitably decayed by removal en route. Second, for the special case of a single, continuous point source at $\vec{r}_o$, i.e.,

$$\dot{G}(\vec{r},t) = \dot{g}(t)\ \delta(\vec{r} - \vec{r}_o)\ , \tag{5}$$

in which δ is a Dirac function, then Equation (4) yields

$$c(\vec{r},t) = \tag{6}$$

$$\int_0^\infty d\tau\ \dot{g}(t - \tau)e^{-\langle\ell\rangle\tau}\ \delta[\vec{r} - \{\vec{r}_o + \langle\vec{v}_L\rangle\tau\}]$$

where lower-case c has been used to emphasize that Equation (6) is the solution for a continuous, point source.

As a simple illustration of these results for a nondispersive medium, consider the case of a uniform wind field $\vec{v}_L = u_o\hat{i}$, a constant loss rate ℓ_o, and a constant (subscript zero) point source of pollution at $\vec{r}_o = (x_o,0,h)$. Then Equation (6) becomes

$$c(\vec{r},t) = \tag{7}$$

$$\int_0^\infty d\tau\ g_o\ \delta[x - x_o - u_o\tau]\ \delta(y)\ \delta(z - h)e^{-\ell_o\tau}.$$

But for any strictly monotonic function of ξ that vanishes at $\xi = \eta$, we have

$$\delta[f(\xi)] = \delta(\xi - \eta)/|f'(\xi = \eta)| \tag{8}$$

(which follows easily if δ is interpreted as a probability density function or pdf); therefore,

$$\delta[x - x_o - u_o\tau] = \frac{1}{u_o}\ \delta\left[\tau - \left\{\frac{x - x_o}{u_o}\right\}\right]\ . \tag{9}$$

Also, $\int_0^\infty \delta(\tau - \tau_o)\ f(\tau)\ d\tau = f(\tau_o)\ h(\tau_o)\ ,$ (10)

where $h(\tau_o)$ is the unit (Heaviside) step function. Consequently, Equation (7) yields

$$c(\vec{r},t) = \frac{g_o}{u_o}\ \exp\left[-\ell_o\left\{\frac{x - x_o}{u_o}\right\}\right] \tag{11}$$

$$\cdot\ h(x - x_o)\ \delta(y)\ \delta(z - h)\ ,$$

which is transparent. Note that Equation (11) does not describe diffusion, a condition to be rectified in the next section.

Formulation for Stochastic Processes

For definiteness, consider the case of a single, continuous point source (emission rate $\dot{g}(t)$ in, say, moles per unit time). Since linearity has been assumed (e.g., with $\dot{L} = \ell C$), we can find the solution for an arbitrary spatial distribution of sources via superposition. The (deterministic) result for a single source at $\vec{r}_o$ [cf. Equation (6)], viz

$$c(\vec{r},t) = \tag{12}$$

$$\int_0^\infty d\tau\ \dot{g}(t - \tau)\ e^{-\langle\ell\rangle\tau}\ \delta[\vec{r} - \{\vec{r}_o + \langle\vec{v}_L\rangle\tau\}]\ ,$$

can be interpreted as the resulting concentration for a single realization of a stochastic process, i.e., with known (deterministic) $\dot{g}$, ℓ, and $\vec{v}_L$. Now consider a great number (an "ensemble") of realizations of Equation (12), for each of which

$$\underset{\sim}{c}(\vec{r},t) = \tag{13}$$

$$\int_0^\infty d\tau\ \underset{\sim}{\dot{g}}(t - \tau)\ e^{-\underset{\sim}{\ell}\tau}\ \delta[\vec{r} - \{\vec{r}_o + \underset{\sim}{\vec{v}}_L\tau\}]\ ,$$

(in which the tildes identify random variables). We now seek statistical properties of the random concentration $\underset{\sim}{c}$ (especially its mean and variance) over the ensemble of realizations, with different gain and loss rates and with different trajectories, caused, e.g., by "turbulent diffusion."

If $\underset{\sim}{\dot{g}}$, $\langle\underset{\sim}{\ell}\rangle$, and $\langle\underset{\sim}{\vec{v}}_L\rangle$ are independent random variables, then from Equation (13) the ensemble- (as opposed to the time-) average of $\underset{\sim}{c}$ is

$$\mathcal{E}\{\underset{\sim}{c}\} = \int_0^\infty d\tau\ \mathcal{E}\{\underset{\sim}{\dot{g}}(t - \tau)\}\ \mathcal{E}\{e^{-\underset{\sim}{\ell}\tau}\} \tag{14}$$

$$\cdot\ \mathcal{E}\{\delta[\vec{r} - \vec{r}_o - \underset{\sim}{\vec{v}}_L\tau\}\ .$$

Similarly, for the autocorrelation of $\underset{\sim}{c}$,

$$\mathcal{E}\{\underset{\sim}{c}(\vec{r}_1,t_1)\ \underset{\sim}{c}(\vec{r}_2,t_2)\} = \int_0^\infty d\tau_1 \int_0^\infty d\tau_2 \qquad (15)$$

$$\cdot\ \{\dot{\underset{\sim}{g}}(t_1-\tau_1)\ \dot{\underset{\sim}{g}}(t_2-\tau_2)\}\quad \mathcal{E}\{e^{-\underset{\sim}{\ell}\tau_1}\ e^{-\underset{\sim}{\ell}\tau_2}\}$$

$$\cdot\ \mathcal{E}\{\delta(\vec{r}_1-\vec{r}_o-\langle\vec{\underset{\sim}{v}}_L\rangle\tau_1)\ \delta(\vec{r}_2-\vec{r}_o-\langle\vec{\underset{\sim}{v}}_L\rangle\tau_2)\}.$$

If $\dot{\underset{\sim}{g}}$, $\underset{\sim}{\ell}$, and $\vec{\underset{\sim}{v}}_L$ are not independent random variables (e.g., if $\dot{\underset{\sim}{g}}$ describes particle resuspension and if $\underset{\sim}{\ell}$ includes dry deposition, then these would be proportional to the velocity), then in Equation (14), for example, correlations between the variables would be needed. Here, however, only the simpler case of independent random variables will be considered.

To understand the meaning of the term $\mathcal{E}\{\delta(\vec{r}-\vec{r}_o-\langle\vec{\underset{\sim}{v}}_L\rangle\tau)\}$ in Equation (14), and the similar term in Equation (15), first simplify notation by letting $\vec{x} = \vec{r} - \vec{r}_o$ and

$$\vec{\underset{\sim}{\xi}} = \langle\vec{\underset{\sim}{v}}_L\rangle\tau \equiv \int_{t-\tau}^{t} \vec{\underset{\sim}{v}}_L(\tau')\,d\tau' \equiv \vec{\underset{\sim}{\xi}}(t,\tau)\ . \qquad (16)$$

Then, using Fourier transforms with parameter $\vec{k}$, we see

$$\mathcal{F}_{\vec{k}}\mathcal{E}\{\delta(\vec{x}-\vec{\underset{\sim}{\xi}})\} = \mathcal{E}\left\{\int d\vec{x}\ e^{i\vec{k}\cdot\vec{x}}\ \delta[\vec{x}-\vec{\underset{\sim}{\xi}}(t,\tau)]\right\}$$

$$= \mathcal{E}\{e^{i\vec{k}\cdot[\vec{x}=\vec{\underset{\sim}{\xi}}]}\} = \int d\vec{\xi}\ \underset{\sim}{f}_{\vec{\underset{\sim}{\xi}}}(\vec{\underset{\sim}{\xi}}=\vec{x})\ e^{i\vec{k}\cdot\vec{\xi}}$$

$$= \mathcal{F}_{\vec{k}}\ \underset{\sim}{f}_{\vec{\underset{\sim}{\xi}}}(\vec{\underset{\sim}{\xi}}=\vec{x})\ , \qquad (17)$$

where the second to last equality follows from the definition of the expected value, in which $\underset{\sim}{f}$ is the pdf for the random variable $\vec{\underset{\sim}{\xi}} = \langle\vec{\underset{\sim}{v}}_L\rangle\tau$. In words, the result Equation (17) shows that the expected value of this delta function of the random variable $\vec{\underset{\sim}{\xi}}$ is just the probability that the trace material has traveled from its source at $\vec{r}_o$ to the sampler at $\vec{r}$:

$$\mathcal{E}\{\delta[\vec{r}-(\vec{r}_o+\vec{\underset{\sim}{\xi}})]\} = \underset{\sim}{f}_{\vec{\underset{\sim}{\xi}}}[\vec{\underset{\sim}{\xi}}=(\vec{r}-\vec{r}_o)]\ , \qquad (18)$$

which, in hindsight, seems rather obvious.

In a similar manner, by taking a double Fourier transform of Equation (15), it is straightforward to show that $\mathcal{E}\{\delta_1\delta_2\}$ is the joint pdf for $\vec{\underset{\sim}{\xi}}_1$ and $\vec{\underset{\sim}{\xi}}_2$ (Slinn 1988). Further, there appear to be no conceptual difficulties in extending this method to the evaluation of moments of any order. The present method therefore appears able to yield all statistical moments of the exact solution to the convective-diffusion equation (diffusion having been incorporated not with a diffusivity, but via the randomness of the trajectories). The method also explicitly accounts for stochastic gain and removal. In addition, a distributed source can be described simply by changing from $\dot{g}(t)$ to a function such as $\dot{g}(\vec{r}_o,t)d\vec{r}_o$, describing the spatial distribution of sources, and by integrating over all source areas, $\vec{r}_o$. These results are perhaps not particularly surprising to those who heuristically start from an integral-equation formulation of dispersion (e.g., for a restricted case, see Pasquill and Smith 1983, p. 141), but it is satisfying to see the general formulation derived directly from the continuity equation.

References

Baker, M. B. 1980. "A Simple Analytical Model for Transport by Fluctuating Winds." J. Appl. Meterol. 19:1064-1073.

Pasquill, E., and F. B. Smith. 1983. Atmospheric Diffusion, Third Ed., John Wiley & Sons, New York.

Slinn, W. G. N. 1988. "Concentration Statistics for Dispersive Media." Tellus 40B (in press).

ELIMINATION OF THE NONPHYSICAL "SLOW-DOWN SINGULARITY" THROUGH INCORPORATION OF ALONG-WIND DIFFUSION

W. G. N. Slinn

This article has two goals: to demonstrate how the theory displayed in the previous article can be applied to solve practical problems, and to demonstrate how the "slow-down singularity" can be eliminated by accounting for along-wind diffusion. This slow-down singularity is familiar in assessments of the consequences of pollution releases to the atmosphere (e.g., for nuclear accidents); it is the prediction, derived from Gaussian plume models, that the airborne concentration of the pollutant becomes very large when the wind speed is low (and follows because the Gaussian plume model predicts that the concentration is inversely proportional to the wind speed). After demonstrating how the new theory is capable of eliminating this nonphysical slow-down singularity, it will be shown how the result can also be derived using the K-theory of diffusion. Finally, more general results, which can be used at regional to global spatial scales, will be demonstrated (Slinn 1988).

Results Using the Integral Description

The analysis starts from Equation (14) of the previous article, written here for the case of a steady source at (0,0,h) and deterministic gain and loss. To bound the cases of plume reflection versus complete absorption at z = 0, Equation (14) is written as

$$\mathcal{E}\{\underset{\sim}{c}(\vec{r},t)\} = \int_0^\infty d\tau\; g_o e^{-\ell_o \tau} \left[f_{\underset{\sim}{\xi}}\{x,y,(z-h)\} + \epsilon\, f_{\underset{\sim}{\xi}}\{x,y,(z+h)\} \right] , \tag{1}$$

with $\epsilon = 1$ for perfect reflection and $\epsilon = -1$ for perfect absorption at the surface. To proceed, we need the pdf for

$$\underset{\sim}{\xi}(t,\tau) = \int_{t-\tau}^{t} \underset{\sim}{v}_L(t')\, dt' . \tag{2}$$

A number of assumptions are now introduced. First, assume that the components of $\underset{\sim}{\xi}$ (or at least the first two moments) are independent of the absolute time, dependent only on the time since release, τ. Second, based on the central-limit theorem (or on data in Monin and Yaglom, 1971), assume that the pdf for $\underset{\sim}{\xi}$, $f_{\underset{\sim}{\xi}}$, is Gaussian; therefore, we need only the mean and variance of $\underset{\sim}{\xi}$. Third, assume that the mean-wind is steady along the x-axis, so that

$$\mathcal{E}\{\underset{\sim}{\xi}\} = \mathcal{E}\left\{ \int_0^\tau \underset{\sim}{v}_L(\tau')\, d\tau' \right\} = u_o \tau \hat{i} . \tag{3}$$

Fourth, assume that the random components of $\underset{\sim}{v}_L$ (about the mean) are independent and possess the same statistics; therefore, using primes to identify these components, we need evaluate only

$$\mathcal{E}\{\underset{\sim}{\xi}'(\tau_1)\; \underset{\sim}{\xi}'(\tau_2)\} = \int_0^{\tau_1} d\tau_1' \int_0^{\tau_2} d\tau_2' \cdot \mathcal{E}\{\underset{\sim}{u}_L'(\tau_1')\; \underset{\sim}{u}_L'(\tau_2')\} . \tag{4}$$

Finally, assume

$$\mathcal{E}\{\underset{\sim}{u}_L'(\tau_1')\; \underset{\sim}{u}_L'(\tau_2')\} = \sigma_u^2 \cdot \exp\{-|\tau_1 - \tau_2|/T_L\} , \tag{5}$$

where T_L is a characteristic (Lagrangian) time-scale for the fluid's "memory" of velocity fluctuations. With Equation (5) in Equation (4) and evaluating for $\tau_1 = \tau_2 = \tau$, we then obtain

$$\sigma_{\underset{\sim}{\xi}}'^2(\tau) = 2(\sigma_u T_L)^2 \left[\frac{\tau}{T_L} - 1 + \exp\left\{ -\frac{\tau}{T_L} \right\} \right] . \tag{6}$$

In summary, for the pdf in Equation (1) we take

$$f_{\underset{\sim}{\xi}}\{x,y,(z \mp h)\} = \frac{1}{(2\pi)^{3/2}\, \sigma_x \sigma_y \sigma_z} \cdot \exp\left[-\frac{(x - u_o\tau)^2}{2\sigma_x^2} - \frac{y^2}{2\sigma_y^2} - \frac{(z \mp h)^2}{2\sigma_z^2} \right] . \tag{7}$$

If Equation (7) is used in Equation (1), the result is difficult to integrate, except numerically. For $\tau \gg T_L$,

$$\sigma_x^2 \to 2[\sigma_u T_L]^2 \frac{\tau}{T_L} \equiv 2K\tau , \tag{8}$$

and this in Equation (1) yields

$$\mathcal{E}\{c\} = \frac{q_o}{4\pi K} \exp\left\{ \frac{u_o x}{2K} \right\} \left[\frac{1}{r_1} \exp\left\{ -r_1 \left(\frac{u_o^2}{4K^2} + \frac{\ell_o}{K} \right)^{1/2} \right\} + \frac{\epsilon}{r_2} \exp\left\{ -r_2 \left(\frac{u_o^2}{4K^2} + \frac{\ell_o}{K} \right)^{1/2} \right\} \right] \tag{9}$$

with $r_{1,2}^2 = x^2 + y^2 + (z \mp h)^2$. (10)

Derivation Using K-Theory

Equation (10) can also be derived from K-theory of diffusion, but not without difficulty. To demonstrate, consider the simpler problem in unbounded space

$$\bar{u} \frac{\partial c}{\partial x} = K \nabla^2 c + \dot{Q}\, \delta(\vec{r}) . \tag{11}$$

A Fourier transform of Equation (11), with parameters (ξ, η, ζ), gives

$$\hat{c} = \frac{\dot{Q}/K}{\left[\xi^2 + \frac{iu}{K} \xi + \eta^2 + \zeta^2 \right]} , \tag{12}$$

and therefore,

$$c(\vec{r}) = \frac{e^{\bar{u}x/(2K)}}{(2\pi)^3} \int_{-\infty}^{+\infty} d\xi' \int_{-\infty}^{+\infty} d\eta \int_{-\infty}^{+\infty} d\zeta \cdot \frac{\dot{Q}/K \; e^{i(\xi' x + \eta y + \zeta z)}}{[(\xi')^2 + \eta^2 + \zeta^2 + \frac{u^2}{4K^2}]} \tag{13}$$

The integrals in Equation (13) can be performed by transforming to spherical coordinates (k, θ, ϕ); after integrating over ϕ and θ, the remaining integral is

$$c(\vec{r}) = \frac{\dot{Q}}{2\pi^2 Kr} \exp\left\{\frac{\bar{u}x}{2K}\right\} \int_0^{\infty} dk \cdot \frac{k}{k^2 + a^2} \sin kr \; , \tag{14}$$

which is a known integral. The result for this simple case is therefore

$$c(\vec{r}) = \frac{\dot{Q}}{4\pi Kr} \exp\left\{\frac{\bar{u}x}{2K}\right\} \exp\left\{-\frac{\bar{u}r}{2K}\right\} \; , \tag{15}$$

which is essentially the same as Equation (9), albeit for a simpler case.

Discussion of Results and the Results for a More General Case

In Figure 1, the result of Equation (9) with $\ell_o = 0$ is plotted along with the familiar Gaussian-plume result (in which x-diffusion is ignored),

$$\chi = \frac{\dot{Q}}{2\pi\bar{u}\sigma_y\sigma_z} \exp\left\{-\frac{y^2}{2\sigma_y^2}\right\} \left[\exp\left\{-\frac{(z-h)^2}{2\sigma_z^2}\right\} + \epsilon \exp\left\{-\frac{(z+h)^2}{2\sigma_z^2}\right\}\right] , \tag{16}$$

for the corresponding case with $\sigma_y = \sigma_z = 2Kx/\bar{u}$ and for $\epsilon = 1$ (i.e., no deposition). And although the desire, here, is more to show applications of the formalism than consequences of the results, the comparison in Figure 1 reveals the following:

- x-diffusion can be ignored beyond a few "stack heights," h, from the source.
- x-diffusion should not be ignored for $x \lesssim h$. Ignoring x-diffusion is the cause of the nonphysical "slow-down singularity" (i.e.,

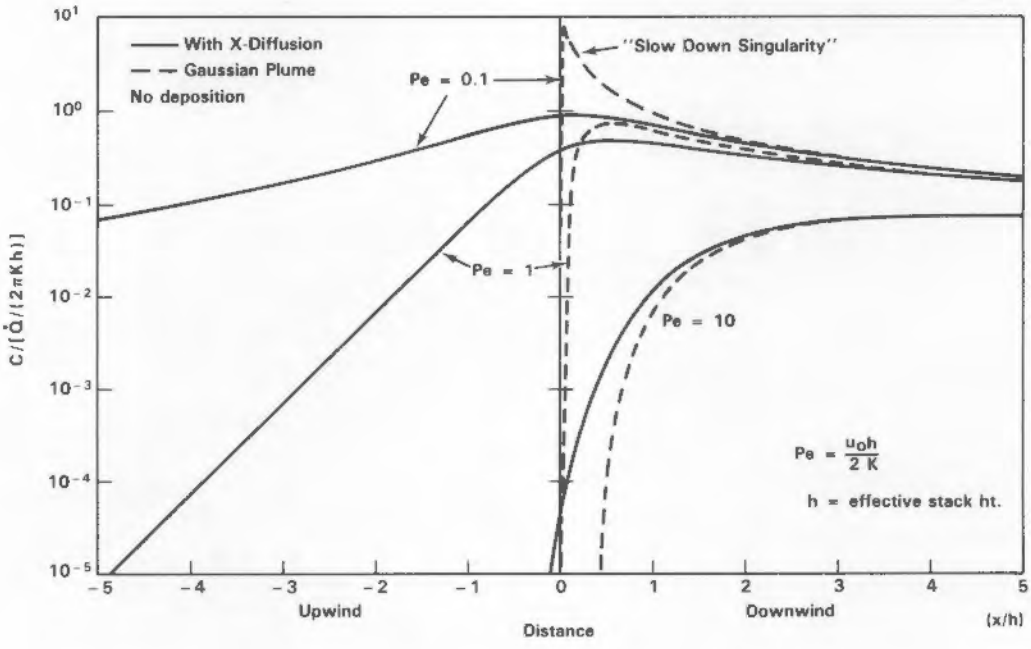

FIGURE 1. Comparisons Between Results for the Distance Dependence of the Normalized Concentration Predicted by the Current Theory Equation (9) with Results for a Gaussian Plume, Equation (16). The comparison reveals that the "slow-down" singularity of the Gaussian plume model is eliminated by inclusion of x-diffusion.

$\chi \to \infty$ with $\bar{u} \to 0$), familiar in assessing accident consequences, e.g., for nuclear facilities. Also, ignoring x-diffusion may cause some of the difficulties in deriving σ-values from concentration data.

- x-diffusion should not be ignored in the "acid-rain issue," since the resulting concentration is modeled totally inadequately in the (climatologically averaged) upwind direction, $x < 0$.

For large travel times, such as for the acid-rain issue, it would of course be inappropriate to use the same K or σ values for all directions: horizontal diffusion is then typically very much larger than vertical diffusion. As an illustration, if K_z is ignorable, then Equation (14) of the previous article, evaluated with constant gain and removal and with

$$f_{\underset{\sim}{\xi},\Pi} = \frac{1}{2\pi\sigma_x\sigma_y} \exp\left\{-\frac{(x - u_o\tau)^2}{2\sigma_x^2} - \frac{y^2}{2\sigma_y^2}\right\} , \quad (17)$$

where $\sigma_x^2 = 2\alpha\tau$ and $\sigma_y^2 = 2\beta\tau$, gives

$$\mathcal{E}\{\underset{\sim}{c}(x,y)\} = \frac{q_o}{2\pi\sqrt{\alpha\beta}} \exp\left\{\frac{xu_o}{2\alpha}\right\}$$

$$\cdot K_o\left[\left\{\left(\frac{x^2}{\alpha} + \frac{y^2}{\beta}\right)\left(\ell_o + \frac{u_o^2}{2\alpha}\right)\right\}^{1/2}\right] ,$$

in which K_o is the modified Bessel function of second kind. If we also have $\sigma_z^2 = 2\gamma\tau$, then the generalization of Equation (9) is

$$\mathcal{E}\{\underset{\sim}{c}(\vec{r})\} = \frac{q_o}{4\pi} \frac{e^{u_o x/(2\alpha)}}{\sqrt{\alpha\beta\gamma}}$$

$$\cdot \left[\frac{1}{r_1'} \exp\left\{-r_1'\left(\ell_o + \frac{u_o^2}{4\alpha}\right)^{1/2}\right\} \quad (18)\right.$$

$$\left. + \frac{\epsilon}{r_2'} \exp\left\{-r_2'\left(\ell_o + \frac{u_o^2}{4\alpha}\right)^{1/2}\right\}\right] ,$$

with $(r_{1,2}')^2 = \frac{x^2}{\alpha} + \frac{y^2}{\beta} + \frac{(z \mp h)^2}{\gamma}$.

References

Monin, A. S., and A. M. Yaglom. 1971. Statistical Fluid Mechanics: Mechanics of Turbulence, ed. J. L. Lumley, Vol. 1. The MIT Press, Cambridge.

Slinn, W. G. N. 1988. "Concentration Statistics for Dispersive Media." Tellus 40B (in press).

SOME PRACTICAL CONSEQUENCES OF THE RANDOMNESS OF PRECIPITATION SCAVENGING

W. G. N. Slinn

For many chemical species, precipitation scavenging is the dominant atmospheric cleansing process; i.e., precipitation events control their lifetime in the troposphere. Examples include species indicted in the acidic deposition issue (e.g., $SO_4^=$, NO_3^-, H^+, etc.), as well as chemicals related to other energy generation activities, such as nuclear energy production, oil shale development, and methanol use as a transportation fuel. One of the most obvious features of precipitation events is their randomness in time, and the purposes of this article are to demonstrate how this randomness can be described mathematically and to reveal some of the practical consequences of the theoretical results.

This demonstration starts from results described elsewhere in this report (see "Foundations for an Integral Description of Concentration Fluctuations in Dispersive Media," in this annual report). In particular, the analysis starts from the following result for the ensemble mean of the concentration, for a deterministic source at the origin:

$$\mathcal{E}\{\underset{\sim}{c}(\vec{r},t)\} = g_o \int_o^\infty d\tau \; \mathcal{E}\{e^{-\underset{\sim}{\ell}\tau}\} \; f_{\underset{\sim}{\xi}}(\vec{\xi} = \vec{r}) \quad (1)$$

in which g_o is the deterministic source strength (in, e.g., moles per second), $\underset{\sim}{\ell}$ is the stochastic loss rate (e.g., caused by precipitation scavenging), and f is the probability density function (pdf) describing the probability that the chemical will be transported from the source to the receptor (or sampling station). In this demonstration, two cases are presented: first, for the case in which atmospheric diffusion is ignored and precipitation scavenging has a quite general statistical description, and second, for the case with diffusion and with a specific and realistic description of precipitation scavenging.

The Case with Negligible Diffusion

If diffusion is negligible, i.e., if

$$f_{\underset{\sim}{\xi}}(\vec{\xi} = \vec{r}) = \delta(x - u_o\tau)\;\delta(y)\;\delta(z) , \quad (2)$$

in which u_o is the mean wind speed, then Equation (1) with Equation (2) becomes

$$\mathcal{E}\{\underset{\sim}{c}\} = \frac{q_o}{u_o} \mathcal{L}_{\frac{x}{u_o}} \{f_{\underset{\sim}{\ell}}(\langle \ell \rangle)\} \, \delta(y) \, \delta(z) \ , \qquad (3)$$

in which $\mathcal{L}$ is the Laplace transform with parameter (x/u_o) and $f_{\underset{\sim}{\ell}}$ is the pdf for the random loss rate.

As one example of Equation (3), suppose $\underset{\sim}{\ell}$ is deterministic. Then

$$\mathcal{E}\{\underset{\sim}{c}\} = \frac{q_o}{u_o} \, \delta(y) \, \delta(z) \, \exp\{-x\ell_o/u_o\} \ , \qquad (4)$$

which is transparent.

As a more informative example, suppose $\underset{\sim}{\ell}$ has a gamma distribution, i.e.,

$$f_{\underset{\sim}{\ell}}(\langle \ell \rangle) = \frac{\gamma^{b+1}}{\Gamma(b+1)} \langle \ell \rangle^b \, e^{-\gamma \langle \ell \rangle} \, h(\langle \ell \rangle) \ , \qquad (5)$$

in which $h(\langle \ell \rangle)$ is the Heaviside function and the mean value of $\underset{\sim}{\ell}$ is, say, $(b + 1)/\gamma = \ell_o$. Then Equation (3) yields

$$\mathcal{E}\{\underset{\sim}{c}\} = \frac{q_o}{u_o} \, \delta(y) \, \delta(z) \left[1 + \frac{\ell_o x}{(b + 1)u_o}\right]^{-(1+b)} . \qquad (6)$$

As an example of Equation (6), if $b = 1$, then

$$\mathcal{E}\{\underset{\sim}{c}\} = \frac{q_o}{u_o} \, \delta(y) \, \delta(z) \left[\frac{1}{1 + \ell_o x/(2u_o)}\right]^2 \ , \qquad (7)$$

which shows that a distribution of $\underset{\sim}{\ell}$-values results in a very much slower decrease in the concentration with increasing x (i.e., roughly as $1/x^2$) compared to the exponential decrease of (4), appropriate when $\underset{\sim}{\ell}$ is deterministic.

This result has already been emphasized by others (e.g., Rodhe and Grandell 1972, Rodhe 1980, Davis 1981) for the case of precipitation scavenging and follows quite generally from Jensen's lemma for a convex removal function. A convex function of ℓ, $\chi(\ell)$, is one whose chord lies above or on the graph of χ. Jensen's inequality (see any advanced statistical text) states that if χ is a convex function of ℓ (e.g., here, $\chi(\ell) = \exp(-\tau\ell)$, then

$$\mathcal{E}\{\chi(\underset{\sim}{\ell})\} \geq \chi[\mathcal{E}\{\underset{\sim}{\ell}\}] \ . \qquad (8)$$

Applied in the present case, Equation (8) states that the ensemble average of the concentration is usually larger than estimates derived using the average removal rate.

The reasonableness of this result can be seen from an alternative definition of a convex function: its graph is above its tangent. Consequently, for any point λ where the slope is evaluated,

$$\chi(\ell) \geq \chi(\lambda) + \chi'(\lambda) \, [\ell - \lambda] \ . \qquad (9)$$

Therefore, if λ is taken to be $\mathcal{E}\{\underset{\sim}{\ell}\}$, then Equation (9) yields

$$\mathcal{E}\{\chi(\underset{\sim}{\ell})\} \geq \chi[\mathcal{E}\{\underset{\sim}{\ell}\}] + 0 \ . \qquad (10)$$

For some dependencies of the concentration on the removal rate, use of the mean removal-rate may be an adequate approximation; however, for a convex functional-dependence on ℓ, use of the mean removal-rate not only ignores the stochastic nature of the removal process, but does so with a consistent bias toward more rapid removal.

Diffusion Plus Stochastic Loss

As an illustration of how this formalism can be used to model precipitation scavenging, suppose that, in addition to a deterministic loss rate ℓ_o (e.g., caused by chemical conversion), there is a Poisson-distributed stochastic loss: with average frequency λ_p (the average frequency with which the trace material encounters relatively short-duration precipitation bands), there are random pulses (at times $\underset{\sim}{t}_i$) of removal with random integrated removals $\underset{\sim}{\epsilon}_i$; i.e.,

$$\underset{\sim}{\ell}(\tau) = \ell_o + \underset{\sim}{\epsilon}_i \, \delta(\tau - \underset{\sim}{t}_i) \ . \qquad (11)$$

Then

$$\int_0^\tau \underset{\sim}{\ell}(\tau') \, d\tau' = \ell_o \tau + \sum_{i=1}^{\underset{\sim}{n}(\tau)} \underset{\sim}{\epsilon}_i \ , \qquad (12)$$

where $\underset{\sim}{n}(\tau)$ is the (random) number of "storms" (or rain cells) encountered during the time interval $(0,\tau)$, considered to be long compared to the duration (typically $\sim 10^3$ s) of an individual rain cell. If Equation (12) is used in Equation (1) and if y- and z-diffusion are ignored, then Equation (1) becomes

$$\mathcal{E}\{\underset{\sim}{c}\} = g_o \int_0^\infty d\tau \, e^{-\ell_o \tau} \, \mathcal{E}\left[\exp\left\{-\sum_{i=1}^{\underset{\sim}{n}(\tau)} \underset{\sim}{\epsilon}_i\right\}\right] \qquad (13)$$

$$\cdot \frac{1}{\sqrt{2\pi}\sigma_x} \exp\left\{-\frac{(x - u_o\tau)^2}{2\sigma_x^2}\right\} \delta(y) \, \delta(z) \ .$$

Before trying to evaluate Equation (13), look at the random variable that appears therein:

$$\underset{\sim}{\Pi} = \exp[-\underset{\sim}{\Sigma}], \text{ with } \underset{\sim}{\Sigma} = \sum_{i=1}^{\underset{\sim}{n}(\tau)} \underset{\sim}{\epsilon}_i \ ,$$

which is known as a compound Poisson process. As is derived in many statistical texts (e.g., Ross 1983), the "moment-generating function" of $\underset{\sim}{\Sigma}$ is

$$\Phi_\tau(s) = \mathcal{E}\{\exp[s\ \underset{\sim}{\Sigma}]\}$$

$$= \sum_{n=0}^{\infty} \mathcal{E}\{\exp[s\ \underset{\sim}{\Sigma}]/\underset{\sim}{n} = n\}\ \text{Prob}\{\underset{\sim}{n} = n\}$$

$$= \sum_{n=0}^{\infty} \mathcal{E}\{\exp[s(\underset{\sim}{\epsilon}_1 + \underset{\sim}{\epsilon}_2 + \ldots + \underset{\sim}{\epsilon}_n)]/\underset{\sim}{n} = n\}$$

$$\cdot\ e^{-\lambda_p \tau}\ (\lambda_p \tau)^n / n! \qquad (14)$$

$$= \sum_{n=0}^{\infty} [\mathcal{E}\{\exp(s\ \underset{\sim}{\epsilon}_1)\}]^n\ e^{-\lambda_p \tau}\ (\lambda_p \tau)^n / n! \qquad (15)$$

$$= \sum_{n} [\phi_{\underset{\sim}{\epsilon}}]^n\ e^{-\lambda_p \tau}\ (\lambda_p \tau)^n / n! \qquad (16)$$

$$= \exp\{\lambda_p \tau\ [\phi_{\underset{\sim}{\epsilon}}(s) - 1]\}\ , \qquad (17)$$

where Equation (14) follows from the definition of a Poisson process, Equation (15) follows from the assumption that the statistical distribution is the same for all $\underset{\sim}{\epsilon}_i$, and in Equation (16), $\phi_{\underset{\sim}{\epsilon}}$ is the moment-generating function of $\underset{\sim}{\epsilon}$:

$$\phi_{\underset{\sim}{\epsilon}}(s) = \mathcal{E}\{\exp(s\underset{\sim}{\epsilon})\} \equiv \int_{-\infty}^{+\infty} e^{s\epsilon}\ f_{\underset{\sim}{\epsilon}}(\epsilon)\ d\epsilon \ . \qquad (18)$$

For example, if the random fraction, $\underset{\sim}{\epsilon}$, is uniformly distributed in (0,1), then

$$\phi_{\underset{\sim}{\epsilon}}(s) = \int_0^1 e^{s\epsilon}\ d\epsilon = \frac{1}{s}\ [e^s - 1] \ . \qquad (19)$$

Now, returning to Equation (13), we see that the expected value in the integrand is the moment-generating function Φ_τ, with $s = -1$.

Equation (13) can now be evaluated for different distributions of $\underset{\sim}{\epsilon}_i$ (and, in fact, for more general loss rates). As perhaps the simplest example, if $\sigma_x = 2K\tau$ and if $\underset{\sim}{\epsilon}$ is uniformly distributed in (0,1) [i.e., use Equation (19) with $s = 1$], then the resulting integral is known (e.g., Erdélyi 1954):

$$\frac{\mathcal{E}\{\underset{\sim}{c}\}}{\delta(y)\ \delta(z)} = \begin{cases} \dfrac{q_o}{u_o}\ \dfrac{1}{(1+\delta)^{1/2}}\ \exp\left\{-\dfrac{u_o x}{2K}\ [(1+\delta)^{1/2} - 1]\right\}\ , & x > 0 \\[2ex] \dfrac{q_o}{u_o}\ \dfrac{1}{(1+\delta)^{1/2}}\ \exp\left\{+\dfrac{u_o x}{2K}\ [(1+\delta)^{1/2} + 1]\right\}\ , & x < 0 \end{cases} \qquad (20)$$

where

$$\delta = \frac{4K}{u_o^2}\left[\ell_o + \frac{\lambda_p}{e}\right] \ , \qquad (21)$$

which is essentially the inverse of the Péclét number (the ratio of transport to diffusive "speeds").

It is informative to examine Equation (20) in some detail. For $x > 0$ and δ small,

$$\exp\left\{-\frac{u_o x}{2K}\ [(1+\delta)^{1/2} - 1]\right\} \qquad (22)$$

$$\simeq \exp\left\{-\frac{x}{u_o}\left(\ell_o + \frac{\lambda_p}{e}\right)\right\} \ ,$$

showing that the concentration is reduced at the rate $(\ell_o + \lambda_p/e)$, which is slightly slower than the average removal rate [for $\mathcal{E}\{\underset{\sim}{\epsilon}\} = 1/2$] of $\ell_o + \lambda_p/2$, where, again, λ_p is the average frequency of precipitation events. This result is therefore consistent with Jensen's inequality, Equation (8). For $x > 0$ and δ large (large diffusion compared to transport or, e.g., frequent precipitation events), then Equation (20) gives an e-fold length of essentially $(eK/\lambda_p)^{1/2}$, which can be substantially larger (viz., slower removal) than the value u_o/Λ frequently used in Gaussian plume models modified to account for precipitation scavenging, with Λ an average scavenging rate. Figure 1 summarizes this case of stochastic scavenging, but with only x-diffusion. For a more general case (stack of height h, image source, diffusivities α, β, γ in the x, y, and z directions), see Slinn (1988).

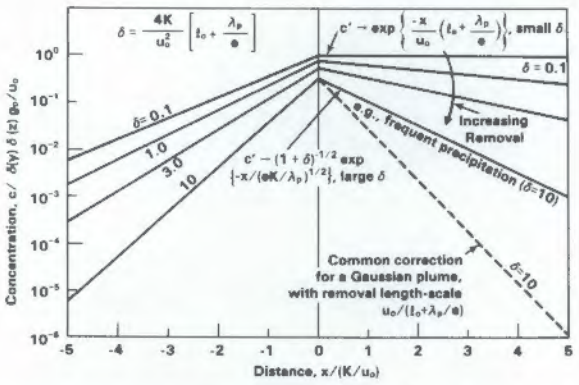

FIGURE 1. Plots of Equation (20) Showing the Dependence of the Mean Concentration on Distance for Different Levels of Stochastic Scavenging and Compared with the Frequently Used Gaussian Plume Model Incorrectly "Corrected" for Precipitation Scavenging.

References

Davis, W. E. 1981. "Another Look at the Use of Average Precpitation for Use in Wet Deposition." In Pacific Northwest Laboratory Annual Report for 1980, Part 3 - Atmospheric Sciences. PNL-3700 Pt. 3, pp. 58-60, Pacific Northwest Laboratory, Richland, Washington.

Rodhe, H., and J. Grandell. 1972. "On the Removal Time of Aerosol Particles from the Atmosphere by Precipitation Scavenging." Tellus 24(5):442-454.

Erdélyi, A., ed. 1954. Tables of Integral Transforms. McGraw-Hill, New York.

Rodhe, H. 1980. "Estimates of Wet Deposition of Pollutants Around a Point Source." Atmos. Environ. 14:1197-1199.

Ross, S. M. 1983. Stochastic Processes. John Wiley & Sons, New York.

Slinn, W. G. N. 1988. "Concentration Statistics for Dispersive Media." Tellus 408 (in press).

EXPLORATORY THEORETICAL STUDIES OF CONCENTRATION DEVIATIONS

W. G. N. Slinn

Earlier in this annual report, the general theory for an integral method of evaluating moments (of arbitrary order) of the concentration for a trace species in dispersive media was presented [see "Foundations for an Integral Description of Concentration Fluctuations in Dispersive Media" (Slinn 1988b)]. To this point in this annual report, however, the general theory has been illustrated only with evaluations of first-order moments, viz., evaluations of mean concentrations. The purpose of this article is to demonstrate how the general theory can be used to provide estimates of second moments.

It can be seen (Slinn 1988a) that evaluations of second- and higher-order moments of the concentration are quite involved; therefore, only two relatively simple examples will be illustrated. In the first, we seek an estimate of the magnitude of concentration fluctuations arising from diffusion, alone, without a mean wind. In the second example, we add a mean wind and a stochastic gain term. Judged by the difficulty of these calculations for these two relatively simple cases (and containing simplified expressions for the variance of the velocity fluctuations), it appears that the majority of applications of the theory will need to be performed numerically.

Random Walk from a Continuous Point Source

A familiar analogy for the random-walk problem is in terms of a single, inebriated pedestrian. For the present problem, imagine a continuous stream of drunkards leaving a saloon: the drunkards take random steps along a sidewalk (the y-axis), some fall into the street, and the problem is to find the mean concentration of drunkards still on the sidewalk, plus a measure of the fluctuations in the concentration, at any point.

Mathematically, we start with Equation (14) of the article referenced above (Slinn 1988b). For a constant loss rate, ℓ_o, a constant gain rate, g_o, and the origin of the y-axis at the saloon door, this equation becomes

$$\mathcal{E}\{\underset{\sim}{c}\} = g_o \int_0^\infty d\tau\, e^{-\ell_o \tau}\, \mathcal{E}\{\delta[y - \underset{\sim}{\eta}(\tau)]\}\ , \qquad (1)$$

with $\underset{\sim}{\eta} = \langle v_L \rangle \tau$. Now use

$$\mathcal{E}\{\delta[y - \underset{\sim}{\eta}]\} = f_{\underset{\sim}{\eta}}[\underset{\sim}{\eta} = y] \qquad (2)$$

$$= \frac{1}{\sqrt{2\pi}\,\sigma_y(\tau)} \exp\left\{-\frac{y^2}{2\sigma_y^2}\right\}\ ,$$

with $\sigma_y^2 = 2\beta\tau$. The resulting integral is available in Laplace-transform tables; the result is

$$\mathcal{E}\{\underset{\sim}{c}\} = \frac{g_o}{2\sqrt{\ell_o \beta}} \exp\left\{-\left[\frac{\ell_o y^2}{\beta}\right]^{1/2}\right\} . \qquad (3)$$

As two asides, note that there is no steady-state solution unless there is loss, and note that if σ_y^2 = constant, then the solution would have been

$$\mathcal{E}\{\underset{\sim}{c}\} = \frac{g_o}{\ell_o} \frac{1}{\sqrt{2\pi}\,\sigma_y} \exp\left\{-\frac{y^2}{2\sigma_y^2}\right\} .$$

To obtain a measure of the concentration fluctuations, we evaluate Equation (15) (Slinn 1988b), viz.,

$$\mathcal{E}\{\underset{\sim}{c}(y_1,t_1)\ \underset{\sim}{c}(y_2,t_2)\}$$

$$= g_o^2 \int_0^\infty d\tau_1\, e^{-\ell_o \tau_1} \int_0^\infty d\tau_2\, e^{-\ell_o \tau_2} \qquad (4)$$

$$\cdot\ \mathcal{E}\{\delta[y_1 - \underset{\sim}{y}(\tau_1)]\ \delta[y_2 - \underset{\sim}{y}(\tau_2)]\} ,$$

with

$$\mathcal{E}\{\delta[y_1 - \underset{\sim}{y}_1]\ \delta[y_2 - \underset{\sim}{y}_2] \qquad (5)$$

$$= f_{\underset{\sim}{y}_1, \underset{\sim}{y}_2}(\underset{\sim}{y}_1 = y_1,\ \underset{\sim}{y}_2 = y_2) = \frac{1}{2\pi\sigma_1\sigma_2\sqrt{1-r^2}}$$

$$\cdot \exp\left\{-\frac{1}{2(1-r^2)}\left[\frac{y_1^2}{\sigma_1^2} - \frac{2r y_1 y_2}{\sigma_1\sigma_2} + \frac{y_2^2}{\sigma_2^2}\right]\right\} ,$$

in which $\sigma_1^2 = 2\beta\tau_1$, $\sigma_2^2 = 2\beta\tau_2$, and, for a Wiener-Levy process (integral of white noise, consistent with taking the large-time approximation for σ), the correlation coefficient is given by (e.g., see Papoulis 1965)

$$r^2 = \begin{cases} \tau_1/\tau_2 , & \tau_1 \le \tau_2 \\ \tau_2/\tau_1 , & \tau_2 \le \tau_1 \end{cases} . \qquad (6)$$

It is possible to perform the integrations in Equation (4), but a simpler method is to work with a double Fourier transform of Equation (4) and use the characteristic function for the joint normal:

$$\Phi(k_1,k_2) = \exp\{-\tfrac{1}{2}[\sigma_1^2 k_1^2 + 2r\sigma_1\sigma_2 k_1 k_2 + \sigma_2^2 k_2^2]\} .$$

By either route, the result (evaluated at the same y and t) is

$$\mathcal{E}\{\underset{\sim}{c}^2(y,t)\} = \frac{g_o^2}{2\sqrt{2}\ell_o\beta} \exp\left\{-\left[\frac{2\ell_o y^2}{\beta}\right]^{1/2}\right\} . \qquad (7)$$

Consequently, the square of the normalized standard deviation (or "coefficient of deviation"), one measure of the concentration fluctuations, is

$$f_c^2 = \frac{\sigma_c^2}{\mathcal{E}^2\{\underset{\sim}{c}\}} = \frac{[\mathcal{E}\{\underset{\sim}{c}^2\} - \mathcal{E}^2\{\underset{\sim}{c}\}]}{[\mathcal{E}\{\underset{\sim}{c}\}]^2} \qquad (8)$$

$$= -1 + \sqrt{2} \exp\left\{(\sqrt{2}-1)\sqrt{\frac{2\ell_o y^2}{\beta}}\right\} .$$

For the case of more practical interest, with three dimensions, diffusivities α, β, and γ, and with both a mean wind and loss, algebra leads to

$$\mathcal{E}\{\underset{\sim}{c}(\vec{r},t)\ c(\vec{r},t)\} = \frac{g_o^2}{(4\pi)^3} \frac{e^{\frac{x u_o}{2\alpha}}}{\alpha\beta\gamma} \left[\int_0^\infty d\tau_1\right.$$

$$\cdot \left\{\exp\left(-\ell_o + \frac{u_o^2}{4\alpha}\right)\tau_1\right\} \int_0^{t_1} \frac{d\tau_2 e^{-\ell_o\tau_2}}{[\tau_2(\tau_1 - \tau_2)]^{3/2}}$$

$$\cdot \exp\left\{-\frac{1}{4\tau_2} r'^2\right\} + \left.\int_0^\infty \frac{d\tau_1}{\tau_1^{3/2}} \exp\left\{-\ell_o\tau_1 - \frac{r'^2}{4\tau_1}\right\}\right.$$

$$\cdot \left.\int_{\tau_1}^\infty \frac{d\tau_2}{[\tau_2 - \tau_1]^{3/2}} \exp\left\{-\left(\ell_o + \frac{u_o^2}{4\alpha}\right)\tau_2\right\}\right] ,$$

with $(r')^2 = x^2/\alpha + y^2/\beta + (z \pm h)^2/\gamma$. Unfortunately, though, these integrals do not converge. The root problem is the incorrect use of $\sigma^2 \sim \tau$ for small time. However, a more reasonable time dependence of σ leads to analytically intractable integrals. Consequently, there appears to be no alternative but to proceed numerically, a task left for future studies. In the meantime, the plots of Equation (8) in Figure 1, inconsistently comparing Equation (8) with data collected during cases when the fluids (air and water) had mean motion, nevertheless suggest that the theory does contain the major feature demonstrated by the data: an increase in the coefficient

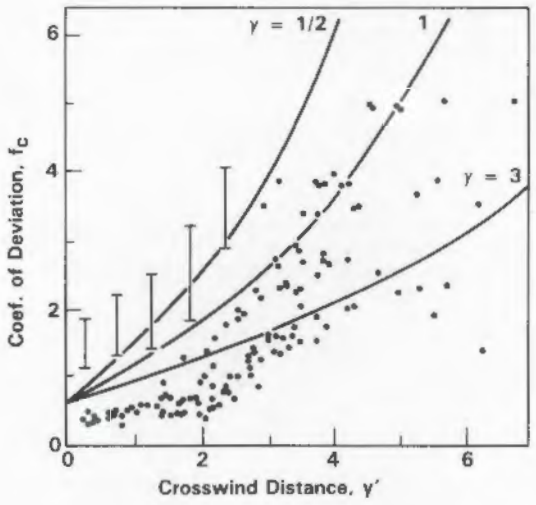

FIGURE 1. Plots of Equation (8), with Normalized "Crosswind" Distance $y' = (\gamma \ell_o/\beta)^{1/2} y$. Data for concentration fluctuations for plumes in the atmosphere (I) from Ramsdell and Hinds (1971) and in a lake (•) from Murthy and Csanady (1971).

of deviation with increasing distance from the plume centerline.

Along-Wind Diffusion plus Stochastic Gain

The complexities of the integrals encountered in the previous subsection, in the evaluation of second moments, force retreat to another relatively simple case (one-dimensional along-wind diffusion plus a stochastic gain-term), which nevertheless is of practical interest. For this case, the mean value is the same as the result given in Equation (20) of the article "Some Practical Consequences of the Randomness of Precipitation Scavenging" (Slinn 1988c). This result was derived using $\sigma_x^2 = 2K\tau$, for $\tau \gg T_L$, and for the present case, take $\lambda_p = 0$, leaving a deterministic loss rate ℓ_o. For the second moment, we assume a stochastic gain term, with

$$\mathcal{E}\{\dot{g}(t_1 - \tau_1)\, \dot{g}(t_2 - \tau_2)\} = \sigma_g^2 \exp\{-\gamma|\tau_1 - \tau_2|\} , \qquad (9)$$

and a jointly normal pdf for ξ_1 and ξ_2, similar to Equation (5), but with mean values $u_o\tau$. Thus, the double Fourier transform of the pdf is

$$\Phi_{\xi_1,\xi_2}(k_1,k_2) = \exp\{iu_o[k_1\tau_1 + k_2\tau_2]\} \cdot \exp\{-\tfrac{1}{2}[\sigma_{x_1}^2 k_1^2 + 2r\sigma_{x_1}\sigma_{x_2}k_1k_2 + \sigma_{x_2}^2 k_2^2]\} , \qquad (10)$$

with σ_x as before and the correlation coefficient, r, as in Equation (6).

The evaluation of Equation (4), even for this case of only x-diffusion, is rather tedious: using Fourier transforms, there are eight poles (within the contour integration) at which residues must be found. For $x \geq 0$, $x_1 = x_2 = x$, and $t_1 = t_2$, the result is

$$\frac{\mathcal{E}\{\underset{\sim}{c}^2\}}{(g_o/u_o)^2} = \frac{2}{[(1+\epsilon)(1+2\epsilon)]^{1/2}} \cdot \exp\{-x'[(1+2\epsilon)^{1/2} - 1]\} \cdot \left[1 + \left(\frac{\sigma_g}{g_o}\right)^2 \left\{\frac{1+\epsilon}{1+\epsilon+\epsilon'}\right\}^{1/2}\right] , \qquad (11)$$

in which

$$\epsilon = \frac{4\ell_o K}{u_o^2} = 4\left(\frac{\sigma_u}{u_o}\right)^2 \frac{T_L}{T_r} , \quad \epsilon' = \frac{4\gamma K}{u_o^2} , \quad x' = \frac{u_o x}{2K} , \qquad (12)$$

where $T_r = \ell_o^{-1}$ is a measure of the material's residence time in the atmosphere. In contrast, Equation (20) (Slinn 1988c) yields for the square of the mean [for $x > 0$]:

$$\frac{\mathcal{E}^2\{\underset{\sim}{c}\}}{(g_o/u_o)^2} = \frac{1}{(1+\epsilon)} \cdot \exp\{-2x'[(1+\epsilon)^{1/2} - 1]\} . \qquad (13)$$

There are several interesting features of these results.

A. For $\sigma_g = 0$ (see Figure 2).

A.1 No Loss.

Even without loss (viz., $\ell_o = 0 = \epsilon$), there is a steady-state solution (if there is a ventilating wind):

$$\langle c \rangle^2 \equiv \mathcal{E}^2\{\underset{\sim}{c}\}/[g_o/u_o]^2 = 1 \qquad (14a)$$

$$\langle c^2 \rangle \equiv \mathcal{E}\{\underset{\sim}{c}^2\}/[g_o/u_o]^2 = 2 \qquad (14b)$$

$$f = \sigma/\langle c \rangle = [\langle c \rangle - \langle \underset{\sim}{c}^2 \rangle]^{1/2}/\langle c \rangle^{1/2} = 1 \qquad (14c)$$

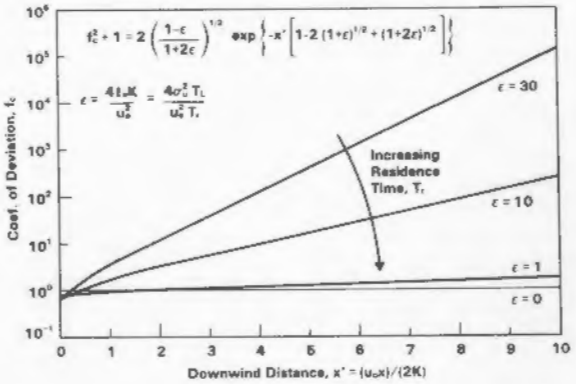

FIGURE 2. Plots of the Coefficient of Deviation, Derived from Equations (11) and (12), as a Function of Downwind Distance, for Different Residence Times, Tr, and for $\sigma_g = 0$.

The result [Equation (14c)] predicts that, for all $x > 0$, there are large fluctuations when there is no loss term: the standard deviation is equal to the mean value.

A.2 Large Loss

If $\epsilon \to \infty$, both the first and second moments decrease exponentially with increasing distance,

$$\langle \underset{\sim}{c} \rangle \to \epsilon^{2} \exp\{-2\sqrt{\epsilon}\, x'\} \qquad (15a)$$

$$\langle \underset{\sim}{c}^2 \rangle \to \sqrt{2}\, \epsilon^{-1} \exp\{-\sqrt{2\epsilon}\, x'\} , \qquad (15b)$$

but the coefficient of deviation, f, increases with x:

$$1 + f_c^2 = \langle \underset{\sim}{c}^2 \rangle / \langle \underset{\sim}{c} \rangle^2 \qquad (15c)$$

$$\to \sqrt{2} \exp\{2 - \sqrt{2})\, \sqrt{\epsilon}\, x'\} ,$$

in essence because the mean concentration falls more rapidly with x than does $\langle \underset{\sim}{c}^2 \rangle$. Because of this sensitivity of f^2 on $\langle \underset{\sim}{c} \rangle$, which is not easy to obtain accurately (either experimentally or theoretically), it is hoped that future experimental studies would report not only f^2 (e.g., Deardorff and Willis 1984), but also $\langle \underset{\sim}{c}^2 \rangle$.

A.3 No Wind

With $u_o \to 0$, it can be seen that Equation (11), with $\sigma_g = 0$, reduces to Equation (7).

B. $\sigma_g \neq 0$

For variations in the source strength and for ϵ and ϵ' small, then

$$f_c \to \left[\frac{\sigma_g}{g_o}\right]^2 = f_g^2 , \qquad (16)$$

essentially independent of x. As a practical application of Equation (16), suppose that this theory were describing modeling uncertainties (rather than natural variabilities) and that σ_g was a measure of uncertainties in specifying source strengths. Then Equation (16) gives, for example, that if $(\sigma_g/g_o) = 50\%$, then with little loss from a well-mixed layer, with no cross-wind variations, and with major fluctuations caused by x-diffusion, $f_c = (0.5)^2 = 0.25$. More realistically, if emissions were known to within 10%, then this first measure of the uncertainty in the calculated concentration gives $f_c \sim 1\%$, which certainly is negligible compared with other uncertainties in the "acid-rain issue."

References

Deardorff, J. W., and G. E. Willis. 1984. "Groundlevel Concentration Fluctuations from a Buoyant and a Non-Buoyant Source Within a Laboratory Convectively Mixed Layer." Atmos. Environ. 18:1297-1309.

Murthy, C. R., and G. T. Csanady. 1971. J. Phys. Oceanog. 1:17. Data from G. T. Csanady. 1973. Turbulent Diffusion in the Environment. D. Reidel Pub. Co., Boston, Massachusetts.

Papoulis, A. 1965. Probability, Random Variables, and Stochastic Processes. McGraw-Hill, New York.

Ramsdell, J. V., and W. T. Hinds. 1971. "Concentration Fluctuations and Peak-to-Mean Concentration Ratios in Plumes from a Ground-Level Continuous Point Source." Atmos. Environ. 5:483-495.

Slinn, W. G. N. 1988a. "Concentration Statistics for Dispersive Media." Tellus 40B (in press).

Slinn, W. G. N. 1988b. "Foundations for an Integral Description of Concentration Fluctuations." In this annual report.

Slinn, W. G. N. 1988c. "Some Practical Consequences of the Randomness of Precipitation." In this annual report.

AIRBORNE RADIOACTIVITY MEASUREMENTS FROM THE CHERNOBYL PLUME

E. A. Lepel, W. K. Hensley, J. F. Boatman(a), K. M. Busness, W. E. Davis, D. E. Robertson, and W. G. N. Slinn

The accident at the 3200-MWt RBMK Reactor #4 near Chernobyl, in the USSR, resulted in the forceful release of 3 to 5% of the reactor core (Goldman et al. 1987). It was estimated that 3 to 5 x 10^7 Ci were released from the fuel during the accident, excluding the activities of Xe and Kr. Greater than 90% of the radioactive noble gases were released as well as 10 to 40% of the volatile radionuclides (including 40 to 50 MCi of ^{131}I and 2 to 3 MCi of ^{137}Cs), and 3 to 5% of the nonvolatile radionuclides (including the uranium fuel).

The accident occurred on April 26, 1986, at 1:23 a.m. Chernobyl time. Twenty-five percent of all the material was released on the first day. The rest of the material continued to be released at varying intensities over the next nine days until, on May 5, 1986, the core was smothered with boron carbide, dolomite, clay/sand, and lead. In response to concerns about where, when, and at what activity level this radioactive material would reach the United States, and in anticipation of unique opportunities to study the fate of radionuclides released to the atmosphere, DOE directed PNL to mobilize a team to sample the Chernobyl plume as it entered the western coast of North America.

PNL initiated a comprehensive field program to detect and monitor the Chernobyl plume as it reached the western coast of North America (Slinn et al. 1987). This program consisted of monitoring the air, ground deposition, and precipitation when present. Two research aircraft were used in the studies reported here: PNL's DC-3 and a King Air operated by the National Oceanic and Atmospheric Administration (NOAA). We also conducted sampling aboard a U-2 stationed at Ames, California, and a Sabreliner operated by the National Center for Atmospheric Research (NCAR). The present report will discuss the airborne sampling and measurements principally obtained using PNL's DC-3.

The DC-3 aircraft has been outfitted as an instrumented platform to perform gas analyses using a variety of instruments, to collect samples of air particulates using a high-volume air sampling system, and to measure all relevant meteorological variables (including winds, cloud liquid-water content, droplet sizes, etc.). For the Chernobyl plume studies, the capability to measure gamma-emitting radioactive materials by high-resolution gamma-ray spectroscopy was added.

The program's initial goals were to determine the width to which the radioactive plume had diffused by the time it reached the North American continent, the radioactive isotopes present, and the concentration of each radioisotope. These goals were to be accomplished by collecting airborne particulates (aerosol particles) with the high-volume air filter system and by counting the filters with the high-resolution gamma-ray spectrometers while the plane was in flight and still sampling. In this way, a near real-time measurement of the air mass through which the airplane was passing would be obtained. During these studies, it was found that the gamma-ray detectors were sensitive enough to measure ^{131}I and ^{137}Cs directly in the detector environment. The detector environment was the aircraft cabin, which was ventilated with exterior air, and the surrounding sphere of air outside the aircraft. Other goals of the program were to define the wet and dry removal of the radionuclides and their venting to higher altitudes by convective storms (Slinn et al. 1987).

Data Acquisition

Aboard the DC-3, aerosol particles were collected using a high-volume air pump operated at 1.13 m^3/min (40 cfm). Upstream of the filter assembly, a cyclone pre-separator removed raindrops as well as particles greater than about 10 μm. The particles were collected on IPC filter paper (Stafford and Ettinger 1970).

The DC-3 aircraft was also equipped with two gamma-ray analysis systems (an intrinsic germanium (IG) and a lithium-drifted germanium [Ge(Li)] detector), which were shock-mounted as much as possible. The two side-looking detectors in their standard 30 L Dewar flasks were mounted in the main cabin of the DC-3. The typical effective volume of each detector was about 110 cm^3 with a relative efficiency of 25% for the measurement of the 1332.5 keV gamma ray of ^{60}Co. The electronics for each detector consisted of bias supply, integrator/amplifier and ADCAM system and data acquisition memory. The data acquisition electronics for the two detectors fit into one NIM bin, which supplied power to the individual modules and was controlled with a portable computer (see Figure 1). The result was an effective and powerful computer-based data acquisition/reduction system, which provided the capability to immediately analyze the gamma-ray spectra

(a) Air Quality Group, Environmental Sciences Laboratory, National Oceanic and Atmospheric Administration, Boulder, Colorado.

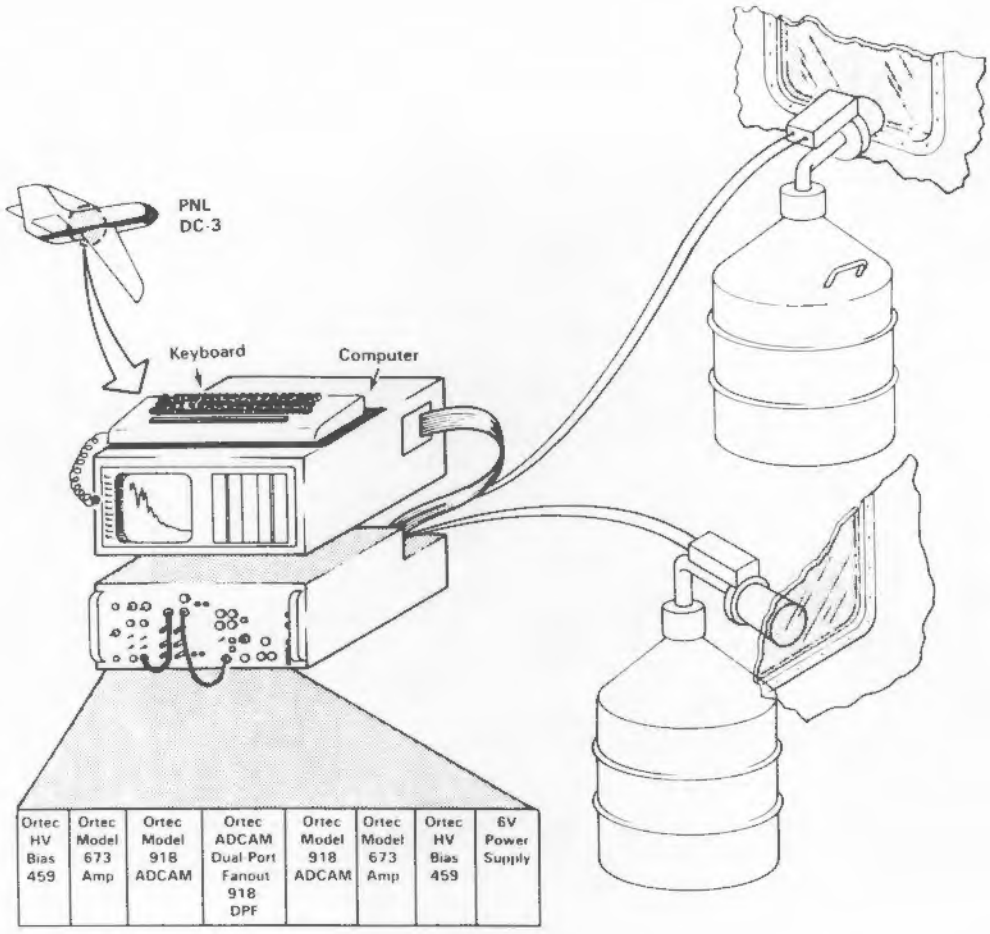

FIGURE 1. Schematic of Computer-Controlled Data Acquisition System for Gamma-Ray Analysis on the DC-3 Aircraft.

collected aboard the aircraft, whether the spectrum was from a collected filter or an in situ measurement.

After collection, the air filters were sealed in polyethylene bags, sent by air to PNL in Richland, Washington, and counted as soon as possible in an around-the-clock operation. The analyses were performed using a coincidence-noncoincidence counting system (Laul 1979, Wogman et al. 1977); the advantage of these systems is that they minimize the mid-to-low energy Compton continuum, which increases the sensitivity for the noncoincident gamma rays compared to a normal spectrum.

The flight paths of the DC-3 and King Air were guided by real-time calculations of the trajectories of the leading edge of the Chernobyl plume (Slinn et al. 1987). Calculations of these trajectories were difficult because of complications from transport through storms and from the general trajectory endpoint uncertainty that increases with time. Compounding difficulties were caused by the continuing release of radioactivity from the source, the lack of data reports over Siberia, and the likelihood that the reported sitings of radioactivity over Japan were from the tapping by precipitation and/or mixing downward of the radioactivity at 5 km. The King Air was initially stationed at Juneau, Alaska, where it was poised to sample above the Alaskan Panhandle. It was stationed at Juneau because of the aforementioned complications and uncertainties, and because it is relatively easier for the aircraft to travel (at speeds of approximately ten times the wind speed) downwind to the vicinity of a ground-station siting (e.g., at our real-time sampling station at Richland) rather than travel upwind to where there was no real-time sampling. The DC-3 was stationed at Seattle, Washington, ready to sample along the west coasts of Oregon, Washington, and British Columbia (the

latter with permission from the Atmospheric Environment Service of Canada).

Results and Discussion

The flight paths of the DC-3 are listed in Table 1. The flights on May 5, 6, and 7 were apparently before the leading edge of the low-altitude radioactive plume reached North America. On May 7, the DC-3 flew from Seattle to Ketchikan, Alaska, passing through a weather front (which might have separated the contaminated air from the uncontaminated air mass) and then back to Seattle without detecting any in situ ^{131}I. On May 8, the DC-3 detected ^{131}I in situ on the flights from Seattle to Ketchikan and Ketchikan to Juneau. Iodine-131 was detected each succeeding day as the plane returned from Juneau to Pasco, Washington, and then traveled south to Reno, Nevada. Flights were made on two additional days (May 14 and 15) during which the plane flew as far east as Duluth, Minnesota. Iodine-131 was detected in the air mass all the way from Pasco to Duluth, but not on the last leg from Duluth to Minneapolis, Minnesota. At the time of sampling, Minneapolis was east of a cold front separating the contaminated northern air mass from uncontaminated air from the Gulf of Mexico (Slinn et al. 1987).

During the flights, the high-resolution gamma-ray spectrometers were initially to be used to count the gamma-ray-emitting particles collected on the filters. The gamma-ray detector systems were turned on once the planes were in flight and background spectra were collected. Beginning on the May 8 flight of the DC-3, direct measurement of ^{131}I was obtained in the "background" spectra. The gamma-ray detectors in the aircraft were essentially measuring the radionuclide concentrations in the air mass through which the aircraft was flying. Although the detector was pointed to the exterior of the plane, the environment both inside and outside of the airplane was being measured. Thus, the gamma-ray detectors were used to qualitatively determine if we were sampling the radioactive plume. Because of the presence of ^{131}I and due to the difficulty of obtaining power while the plane was on the ground, the air filters were not measured using the gamma-ray detectors on the DC-3. The air filters were returned to PNL for quantitative analysis.

The air filters were counted to determine the radionuclide concentrations associated with the collected particles. The detected radionuclides are listed in Table 2 and consisted of ^{95}Zr, ^{99}Mo, ^{103}Ru, ^{125}Sb, ^{131}I, ^{132}Te, ^{134}Cs, ^{137}Cs, and ^{140}Ba. Table 2 lists the date and time (PST) of the air filter collection, volume of air sampled, and the concentration of the radionuclides present (in MBq/m^3). The presence of ^{131}I as well as ^{103}Ru, ^{132}Te, ^{134}Cs, ^{137}Cs, and ^{140}Ba were observed on the filters collected May 7. The

TABLE 1. Flight Paths for the Battelle DC-3

Date	Flight	Path				
05/05/86	1	Pasco, WA	→	Red Bluff, CA		
	2	Red Bluff, CA	→	Seattle, WA		
05/06/86	3	Seattle, WA	→	Astoria, OR	→	Seattle, WA
05/07/86	4	Seattle, WA	→	Ketchikan, AK		
	4A	Ketchikan, AK	→	Seattle, WA		
05/08/86	5	Seattle, WA	→	Ketchikan, AK		
	5A	Ketchikan, AK	→	Juneau, AK		
05/09/86	6	Juneau, AK	→	Ketchikan, AK		
	6A	Ketchikan, AK	→	Seattle, WA		
	7	Seattle, WA	→	Pasco, WA		
05/10/86	8	Pasco, WA	→	Seattle, WA		
	9	Seattle, WA	→	Reno, NV		
05/11/86	10	Reno, NV	→	Pasco, WA		
05/14/86	11	Pasco, WA	→	Billings, MT		
	12	Billings, MT	→	Fargo, ND		
05/15/86	13	Fargo, ND	→	Duluth, MN	→	Minneapolis, MN

TABLE 2. Radionuclide Concentrations Measured on DC-3 Air Filters

					(Concentration as indicated)									
Day	On	Off	Vol., m^3	Units	^{95}Zr	^{99}Mo	^{103}Ru	^{125}Sb	^{131}I	^{132}Te	^{134}Cs	^{137}Cs	^{140}Ba	COMMENTS
5/6/86	1510	1645	108	mBq/m^3	<1	<0.5	<0.4	<3	0.33 ± 0.11	<0.2	<2	<0.2	<3	
5/7/86	0848	1015	94.1	mBq/m^3	<3	<7	3.6 ± 1.1	<10	14.7 ± 1.8	<1	<7	<2	<10	
5/7/86	1022	1156	102	mBq/m^3	<0.7	<7	2.0 ± 0.3	<3	23.5 ± 0.9	2.0 ± 0.3	2.3 ± 0.2	4.62 ± 0.37	1.2 ± 0.3	
5/7/86	1705	1825	86.3	mBq/m^3	<1	—	0.7	<3	2.2 ± 0.4	—	<3	<0.6	<5	
5/7/86	—Blank—		—	mBq	<1500	—	<100	<550	<200	—	<400	<70	<700	
5/8/86	1308	1643	247	mBq/m^3	<2	2.3 ± 0.3	43.7 ± 1.5	<7	127 ± 10	28 ± 4	19.6 ± 0.7	36.6 ± 1.5	15.5 ± 1.1	
5/8/86	1845	1945	67.2	mBq/m^3	<3	—	<2	<9	15.3 ± 1.5	—	<6	2.7 ± 0.7	<10	
5/8/86	—Blank—		—	mBq	<100	<800	<70	<300	<200	<70	<200	<40	<500	
5/9/86	1219	1319	67.8	mBq/m^3	<2	2.5 ± 0.3	40.7 ± 1.5	<8	238 ± 26	26.3 ± 2.6	30.7 ± 0.7	62.2 ± 1.8	16.6 ± 1.1	
5/9/86	1450	1750	196	mBq/m^3	0.15 ± 0.07	0.30 ± 0.13	3.23 ± 0.12	<1	19.8 ± 0.6	2.6 ± 0.3	2.8 ± 0.2	5.48 ± 0.18	2.00 ± 0.15	Clouds
5/9/86	1917	1957	47.2	mBq/m^3	<2	<12	<2	<6	1.9 ± 0.7	1.3 ± 0.8	<4	<1	<8	Clouds/
5/9/86	—Blank—		—	mBq	<100	—	<70	<300	<150	—	<200	<40	<400	rain
5/10/86	1437	1520	45.5	mBq/m^3	<5	2.6 ± 0.7	38.8 ± 2.6	<20	167 ± 11	25 ± 4	39.6 ± 2.2	74.4 ± 4.1	<20	Clouds
5/10/86	1641	1741	68.4	mBq/m^3	<2	<1	6.9 ± 0.6	<6	20.4 ± 0.9	2.8 ± 0.4	<4	8.36 ± 0.78	<7	Clouds
5/10/86	1746	1836	55.2	mBq/m^3	<4	<4	22.6 ± 2.0	<15	93.6 ± 7.0	11.5 ± 2.7	13.4 ± 1.9	32.1 ± 2.7	<20	Clouds
5/10/86	1842	2000	87.2	mBq/m^3	<3	<10	32.9 ± 2.5	<20	130 ± 11	11.7 ± 1.8	11.1 ± 1.8	24.2 ± 2.4	16.3 ± 5.6	Clouds
5/10/86	—Blank—		—	mBq	<200	<400	<150	<500	<300	<70	<400	<70	<700	
5/11/86	1117	1209	57.5	mBq/m^3	<6	1.2 ± 0.5	55.5 ± 3.7	<20	289 ± 28	19.8 ± 1.4	20.1 ± 3.8	45.1 ± 3.3	14.9 ± 3.9	
5/11/86	1219	1354	108	mBq/m^3	<0.4	<0.7	2.1 ± 0.1	<1	7.92 ± 0.44	<4	1.3 ± 0.1	2.8 ± 0.2	1.1 ± 0.3	
5/14/86	1002	1205	134	mBq/m^3	<0.7	<2	1.6 ± 0.2	<3	5.62 ± 0.41	<0.4	0.92 ± 0.15	1.6 ± 0.3	<3	Clouds
5/15/86	1247	1330	47.5	mBq/m^3	<1	<5	4.4 ± 0.4	<5	12.6 ± 0.7	<0.7	1.8 ± 0.3	3.7 ± 0.5	3.4 ± 1.1	Clouds
5/15/86	1352	1433	45.8	mBq/m^3	<2	<5	10.4 ± 1.1	<8	14.1 ± 1.0	2.2 ± 0.6	3.4 ± 0.6	9.51 ± 1.0	<9	Clouds
5/15/86	—Blank—		—	mBq	<70	<300	<40	<200	<70	<300	<200	<30	<300	

same nuclides were observed on all of the filters collected on subsequent flights. The positive ^{131}I concentration observed on the air filter collected between Seattle and Portland, Oregon, on May 6 indicates that the Chernobyl plume was just arriving. The concentration of particulate ^{131}I ranged from a low of 0.33 MBq/m^3 to a high of 289 MBq/m^3 observed on May 11. Meteorological reasons for these variations will be suggested in later papers from our group.

The observed concentration of ^{137}Cs was derived from both fresh fission products (Chernobyl) as well as previous atmospheric testing (bomb debris). However, the average airborne fallout ^{137}Cs concentration from January 15 through April 15 was 0.00067 ± 0.00033 MBq/m^3, which is 3 to 5 orders of magnitude below the levels determined on the air filters containing the Chernobyl debris.(a) The observed nuclides that are clear indicators of fresh fission products are ^{99}Mo, ^{131}I, ^{132}Te, and ^{140}Ba.

In Table 3, the normalized airborne concentrations (relative to ^{137}Cs) determined from the air-filter measurements are compared with reported Soviet data (Goldman et al. 1987, USSR 1986). The airborne air-filter measurements reflect the concentrations decay-corrected to the end of the filter collection period. Thus, these samples reflect the normalized concentration values (relative to ^{137}Cs) as observed between May 5 and May 15 while the Soviet data have been corrected for decay to May 6. The airborne air-filter data for particulate ^{131}I ranged from 1.5 to 6.4 (average of 3.7 ± 1.4) or 2.8 to 12 (average of 7.0 ± 2.7) for the total ^{131}I.(a) In contrast, the core relative composition value on May 6 was 4.5 and the Soviet reported discharge value was 7.3. The airborne air-filter average value (total ^{131}I of 7.0 ±2.7) agrees with the Soviet reported discharge value and falls within the range of the other values listed in Table 3.

The nonvolatile radioisotopes ^{103}Ru and ^{140}Ba on the air filters show values relative to ^{137}Cs of 0.44 to 1.4 and 0.26 to 0.90, respectively. These values are lower than either the core relative composition or the Soviet reported discharge values (Table 3). The ^{103}Ru values are also lower than the "Other" values listed in Table 3. The ^{140}Ba values fall within the range of values observed in

(a) Unpublished data from C. W. Thomas (1987) at PNL.

(a) The total ^{131}I was calculated assuming 53% particulates and 47% gaseous ^{131}I as determined by PNL from surface-level measurements. However, the ratio of particulate to gaseous ^{131}I might be significantly different at the altitude of the airborne sampling, typically 10,000 ft.

TABLE 3. Comparison of In-Situ and Airborne Air Filter Measurements with Soviet Data

(All values are relative to ^{137}Cs)

	Date	Time (PST) ON	Time (PST) OFF	^{103}Ru	^{131}I[b]	^{132}Te	^{134}Cs	^{140}Ba
Airborne Air Filter[a]	5/7/86	0848	1015	—	—	—	—	—
		1022	1156	0.44	5.1(9.6)	0.43	0.50	0.26
		1705	1825	—	—	—	—	—
	5/8/86	1308	1643	1.2	3.5(6.6)	0.77	0.54	0.42
		1845	1945	—	5/7(11)	—	—	—
	5/9/86	1219	1319	0.65	3.8(7.2)	0.42	0.49	0.27
		1450	1750	0.59	3.6(6.8)	0.47	0.52	0.36
		1917	1957	—	—	—	—	—
	5/10/86	1437	1520	0.52	2.2(4.2)	0.34	0.53	—
		1641	1741	0.83	2.4(4.5)	0.34	—	—
		1746	1836	0.71	2.9(5.5)	0.36	0.42	—
		1842	2000	1.4	5.4(10)	0.48	0.46	0.67
	5/11/86	1117	1209	1.2	6.4(12)	0.44	0.45	0.33
		1219	1354	1.2	2.8(5.3)	—	0.47	0.41
	5/14/86	1002	1205	0.98	3.4(6.4)	—	0.57	—
	5/15/86	1247	1330	1.2	3.4(6.4)	—	0.49	0.90
		1352	1433	1.1	1.5(2.8)	0.23	0.35	—
Soviet Data								
Core Relative Composition[c]	5/6/86			14	4.5	1.1	0.66	10
Soviet Reported Discharge[c]	5/6/86			3.2	7.3	1.3	0.50	4.3
Other Values (Range)[d]	5/6-10/86			2.3-3.7	3.9-19	1.4-85	0.40-0.56	0.40-3.0

(a) Ratios of the concentrations which are in mBq/m3.
(b) ^{131}I values are particulate ^{131}I. The values in ( ) are calculated total ^{131}I assuming a gaseous I fraction of 47% and a particulate fraction of 53%, although these relative fractions were likely different at different altitudes and different distances from the release point.
(c) Data from USSR decay corrected to May 6, 1986.
(d) Data from Goldman et al.

Hungary, Greece, Finland, and Germany that make up the "Other" values. Shifts in these ratios, caused by differing particle size-distributions and by atmospheric removal rates that depend on particle size, are not unexpected.

The volatile radioisotope ^{132}Te has a range of 0.23 to 0.77 for the air filter data in contrast to a core relative composition value of 1.1 and a Soviet reported discharge value of 1.3. The values are slightly below the range observed for the "Other" values. The volatile radioisotope ^{134}Cs shows a range of 0.42 to 0.57 (average of 0.48 ± 0.06), which agrees well with the Soviet reported discharge value.

A calibration of the in situ gamma-ray measurement systems with the air filter data was attempted. Although a correlation between the in situ and the air filter data for ^{131}I was expected, it was not observed in the data. The explanation is not obvious because some very complex physical and chemical processes (e.g., wet and dry removal processes) were

occurring. For example, PNL[a] has determined that for ^{131}I, 53% of the ^{131}I was in the form of particulates and 47% was in the gaseous state (24% was organic and 23% as inorganic iodine species) at least for surface-level air.

Conclusions

Using two research aircraft, the radioactive cloud from the Chernobyl accident was detected as it passed over the western coast of North America. Measurements were made from Anchorage, Alaska, to Reno, Nevada. The cloud was first detected using gamma-ray spectrometers on May 8, 1986. Subsequent analysis of air filters showed that the leading edge of the cloud was just reaching the west coast on May 6, 1986, in relatively good agreement with forecasts from our trajectory calculations. A comparison of the reported Soviet discharge concentrations relative to ^{137}Cs showed agreement for the volatile radionuclides ^{131}I and ^{134}Cs collected on the airborne air filters. Agreement was also observed for the nonvolatile ^{140}Ba.

A calibration of the high-resolution gamma-ray detector systems was attempted with the concurrently taken particle samples. Unfortunately, no correlation was observed in the data to allow a calibration factor to be determined. A possible cause is that the real-time system sampled all the ^{131}I, including the iodine captured by cloud water, whereas the cyclone preseparator in front of the filter removed the iodine that had become attached to the cloud water. This and other potential causes are under investigation. Meanwhile, we note that just the real-time in situ measurement of ^{131}I in the aircraft is a unique observation. This capability could be extended to the placement of high-resolution gamma-ray detectors on an aircraft (e.g., a helicopter) that could be used to monitor radioactivities near nuclear facilities. In the event of an accident, an in situ measurement could then be obtained in near real-time.

Acknowledgments

We sincerely thank the approximately 30 scientists and technicians from PNL and NOAA (and, for other parts of the study, from NASA, NCAR, and the University of Maryland) who responded rapidly and worked effectively to conduct these studies. We also gratefully acknowledge the administrative leadership of R. W. Perkins (PNL), D. H. Slade (DOE), and P. E. Merilees (Atmospheric Environment Service of Canada).

(a) Unpublished data from J. A. Young (1987) at PNL.

References

Goldman, M., et al. 1987. Health and Environmental Consequences of the Chernobyl Nuclear Power Plant Accident. DOE/ER-0332, U.S. Department of Energy, Washington, D.C.

Laul, J. C. 1979. At. Energ. Rev. 17:603.

Slinn, W. G. N., et al. 1987. "Field Studies of the Atmospheric Processing of Radionuclides Released at Chernobyl." In Pacific Northwest Laboratory Annual Report for 1986 to the DOE Office of Energy Research, Part 3 - Atmospheric Sciences. PNL-6100 Pt. 3, Pacific Northwest Laboratory, Richland, Washington.

Stafford, R. G., and H. J. Ettinger. 1970. Efficiency of IPC-1478 Filter Paper Against Polystyrene Latex and Dioctyl Phthalate Aerosols. LA-4356, Los Alamos National Laboratory, Los Alamos, New Mexico.

USSR. 1986. The Accident at Chernobyl Nuclear Power Plant and Its Consequences. Information compiled by the USSR State on the Utilization of Atomic Energy for the IAEA Experts' Meeting, August 25-29, 1986 (IAEA Translation), Vienna, Austria.

Wogman, N. A., H. G. Rieck, J. C. Laul and K. W. MacMurdo. 1977. Instrum. Meth. 539.

MODELED AIR CONCENTRATIONS, DEPOSITIONS, AND DOSES FOR THE CHERNOBYL REACTOR ACCIDENT USING THE MLAM MODEL

W. E. Davis, A. R. Olsen, J. K. Soldat, B. T. Didier, B. A. Napier, and R. A. Peloquin

Numerous measurements of air concentration and deposition of radioactive materials were made after the Chernobyl reactor accident in April and May 1986. In some countries the observations may be sufficient for determining general air concentration and deposition patterns. However, there are large areas in Europe for which such measurements are not available, and for these areas modeling predictions can provide additional aid in determining the impact of the accident. The spatial and temporal patterns of air concentrations and depositions that resulted from the Chernobyl reactor accident are predicted for Europe by a multilayer, three-dimensional, meso-alpha scale atmospheric transport model, MLAM. The air concentrations and the wet and dry deposition can then be used to calculate the resultant radiation doses from the deposited radionuclides. Information is provided here on the atmospheric transport of the effluent plume

from the damaged reactor, the surface air concentrations, and the wet and dry deposition to the ground calculated by MLAM, and on the resultant radiation doses from the deposited radionuclides.

Model Calculations

Characterization of the radionuclide releases from the Chernobyl accident depends on specifying the reactor core inventory at the time of the accident, the amount of the core inventory released over time, and the height of release over time. The core inventory was estimated by an ORIGIN computer code simulation of an RBMK reactor. For ^{133}Xe, ^{137}Cs, and ^{131}I, 168, 6.2, and 82 MCi, respectively, are estimated to be in the reactor core at the time of the accident. Based on a review of available information, two distinct release periods were assumed for the time distribution of release. The initial release occurred during the first hour after the accident (April 26, at 00Z) and the second release extended for the next 10 days, ending on May 5, at 23Z GMT. During the initial release, 11% of the ^{133}Xe core inventory (18.5 MCi) was released, the remaining 89% (149.5 MCi) was released at the rate of 0.63 MCi per hour during the second release period. Two release height distributions were used, one for each release period. A uniform release from the reactor to a height of 2500 m was used for the initial release period and a uniform release from the reactor to a height of 500 m was used for the second release period.

Upper-air radiosonde data were layer-averaged and interpolated to a regular three-dimensional grid (0.5 NMC) to provide the necessary winds, humidity and potential temperatures used to drive MLAM. Observed 24-h precipitation data were interpolated to a smaller, finer mesh grid (0.1 NMC) to provide the mechanism for wet removal within MLAM. The finer mesh grid covers Europe and the eastern USSR (Figure 1). Using the meteorological data and the release characterization as input, MLAM produces daily wet and dry deposition and surface air concentration estimates for each radionuclide at each grid node of the finer mesh grid.

The calculated air concentrations and deposition were compared with available measured data. The comparison indicates that the patterns from the calculated values generally reproduce the patterns from the measured data. Wet deposition based on 24-h precipitation data appears to be underestimated in regions where significant precipitation occurred. The use of 24-h precipitation data and inadequate spatial coverage for precipitation occurrence are known limitations in calculating

FIGURE 1. Polar Stereographic Projection of Europe and Area of Model Coverage.

deposition (see Davis and Eadie 1979). Analysis of the spatial pattern of deposition associated with the first few hours after the accident indicates that the observational wind data interpolated to a grid inadequately represents the complicated meteorological conditions the plume encountered in Sweden and Finland. Indications by other researchers are that mass-balanced wind fields would give better representation of the flow and result in better estimates of deposition in both western Europe and the western USSR. When high-quality hourly precipitation data for the study area become available, we recommend that the study be redone using mass-balanced wind fields.

Results

Spatial patterns determined from modeled deposition for ^{137}Cs and ^{131}I provided information on the extent of the Chernobyl reactor accident's impact. Of the 806 kCi of ^{137}Cs and 16.4 MCi of ^{131}I released between April 26 and May 5, 60% is deposited within Europe. Approximately 70% of the total deposition of ^{137}Cs and 50% of the ^{131}I take place in wet deposition.

On May 15, 1986, the regional impact of total (wet and dry) deposition of ^{137}Cs is calculated to be greater than 100 Bq/m^2 (2700 pCi/m^2) for all of Europe east of central France, extending to the Mediterranean Sea and Turkey to the south, and northern Scandinavia and the USSR

to the north (see Figure 2). The same region is also calculated to have greater than 100 Bq/m^2 for total deposition of ^{131}I (Figure 3). The maximum calculated deposition of ^{137}Cs is approximately 50,000 Bq/m^2, immediately northwest of Chernobyl. Total deposition of ^{137}Cs greater than 1,000 Bq/m^2 extend from central Finland to southern Turkey and from Czechoslovakia to east of Moscow with local peaks of over 15,000 Bq/m^2 southeast of Moscow. Near the Ob River a local maximum of 35,000 Bq/m^2 for ^{131}I is calculated to occur. Total deposition of ^{131}I greater than 100,000 Bq/m^2 is calculated to occur immediately northwest of Chernobyl and along the initial transport path between Minsk and the eastern border of Poland. The maximum calculated deposition of ^{131}I is approximately 650,000 Bq/m^2 immediately northwest of Chernobyl.

Surface deposition calculated by MLAM was used in the PABLM model to calculate lifetime (70-year) radiation doses to individuals and population groups. The model is designed to calculate accumulated doses from chronic ingestion of contaminated food products and from external exposure to radionuclides in the environment. The maximum estimated lifetime radiation dose category assuming a

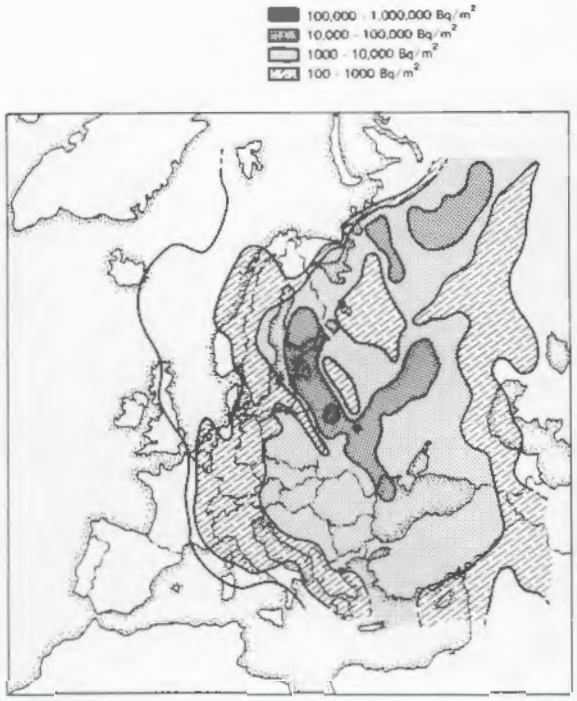

FIGURE 3. Iodine-131 Total Deposition (Bq/m^2), Cumulative to May 16, 1986.

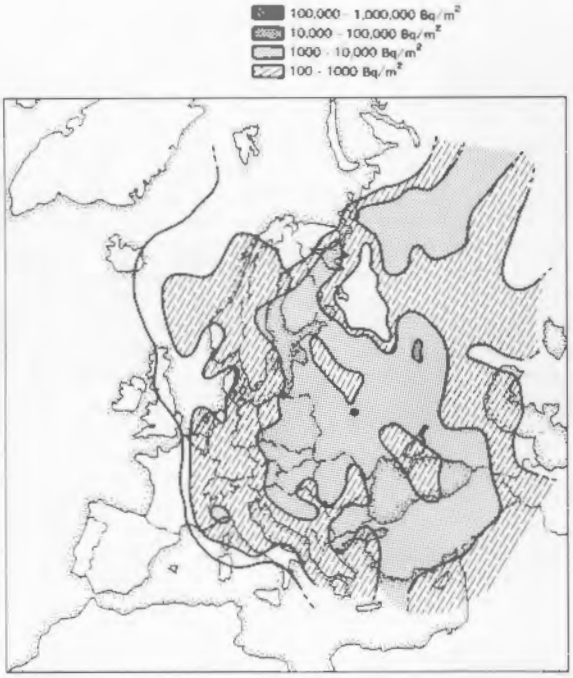

FIGURE 2. Cesium-137 Total Deposition (Bq/m^2), Cumulative to May 15, 1986.

70-year exposure period is 10 to 100 mSv (1 to 10 rem). This category encloses a three-pronged region that extends from Chernobyl northwest toward Finland, south to the Black Sea, and northeast toward Moscow (Figure 4). Dose estimates for western Europe are less than 0.10 mSv (10 mrem). Most of eastern Europe and north-central USSR have estimated doses greater than 0.10 mSv, with the eastern portion generally exceeding 1.0 mSv. The calculated lifetime collective radiation dose for Europe is 540,000 person-sieverts (excluding dose from inhalation and ingestion of initially contaminated food). For the portion of the USSR included in the study area, the total collective dose is 340,000 person-sieverts. This collective dose translates to an average per person dose of 3.1 mSv (0.31 rem). Within the USSR, the calculated collective radiation dose is 260,000 person-sieverts (5.2 mSv average per person dose) for the Ukraine and is 16,000 person-sieverts (1.7 mSv average per person dose) for Byelorussia.

Conclusion and Recomendations

The MLAM calculations of the release of radioactivity during the Chernobyl accident compare favorably with observed air concentrations and

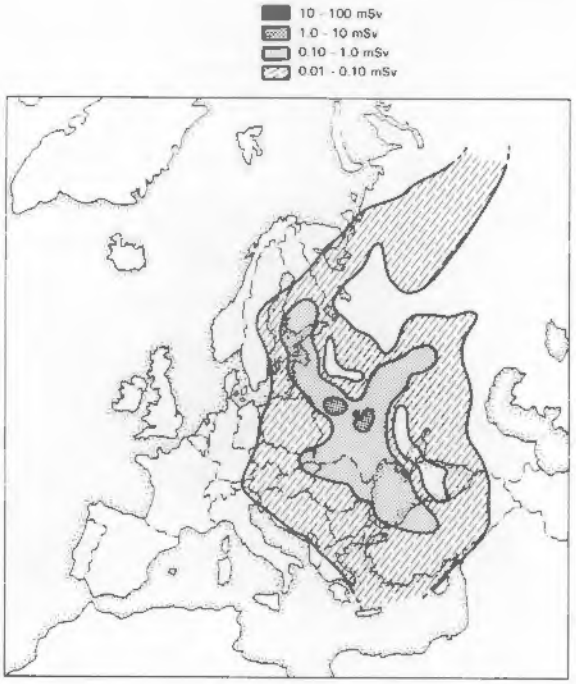

FIGURE 4. Lifetime Radiation Doses to Individuals from 1-yr Exposure to Residual Contamination on the Ground and in Food (mSv).

deposition patterns. Problems occurred in the transporting the material near Sweden due to complexitities in meteorology when using observed wind fields and 24-h precipitation. The model should be rerun with a mass-conserving wind field and hourly precipitation; rerun model results can then be compared with the observed values and model performance can be reevaluated.

References

Croff, A. G. 1980. ORIGIN2-A Revised and Updated Version of the Oak Ridge Isotope Generation and Depletion Code. ORNL-5621, Oak Ridge National Laboratory, Oak Ridge, Tennessee.

Napier, B. A., W. E. Kennedy, Jr. and J. K. Soldat. 1980. PABLM-A Computer Program to Calculate Accumulated Radiation Doses from Radionuclides in the Environment. PNL-3209, Pacific Northwest Laboratory, Richland, Washington.

Acknowledgments

This work could not have been performed without the mutual support of OHER and the National Security Technology Office at PNL. In particular, James Davidson III and Richard Kleinknecht provided the initial direction and administrative encouragement to carry out the project.

AIRBORNE MEASUREMENT OF A PERFLUOROCARBON TRACER DURING THE ANATEX STUDY

R. N. Lee, K. M. Busness, J. Hubbe, and L. Harrison

The Across North America Tracer Experiment (ANATEX) was conducted over a 3-month period (January through March) during the winter of 1987. This study, which featured the release of different perfluorocarbon tracers (PFT) from sites in Montana and Minnesota, was conducted to obtain data for assessing the performance of long-range atmospheric transport models. The resulting data base was acquired over a total of 33 separate experiments conducted under a variety of meteorological conditions. Simultaneous tracer releases were performed at 2-1/2-day intervals from Glasgow, Montana, and St. Cloud, Minnesota. A single tracer gas was employed at the Montana site while a single or, in the case of nighttime experiments, dual tracer release was carried out at the St. Cloud site. Properties of ANATEX tracers and characteristics of their release during this study are summarized in Table 1.

After a tracer was released to the atmosphere, its downwind transport was defined by collecting sequential samples at surface sites (up to 3000 km from the point of release), at a limited number of tall towers, and during airborne sampling operations at near-source distances. All samples were collected by pulling ambient air through a solid adsorbent trap. With the exception of real-time airborne measurements, such as those reported here, samples were returned for laboratory analysis. An overview of the ANATEX study and a preliminary summary of the meteorological setting for each experiment has been prepared by R. Draxler et al. (1987).(a)

Airborne sampling near the Montana release site was conducted using two small aircraft stationed at Miles City, Montana. These aircraft, operated under the direction of PNL, were equipped with sequential sampling devices especially constructed by the Electronics/Engineering Division of the

(a) Draxler, et al., Across North America Tracer Experiment (ANATEX), Preliminary Report prepared for the ANATEX Model Evaluation Study (AMES), October 20, 1987.

TABLE 1. Properties and Release Characteristics of Perfluoro- Tracers During the ANATEX Program

	Methylcyclohexane	ortho-dimethylcyclohexane	trimethylcyclohexane
Abbreviation	PMCH	o-PDCH	PTCH
Release site	St. Cloud, Minnesota (nighttime releases only) 45.56° N/94.17° W	St. Cloud, Minnesota 45.56° N/94.17° W	Glasgow, Montana 48.40° N/106.51° W
Release times	1700-2000 GMT - daytime release 0500-0800 GMT - nighttime release		
Elevation, m MSL	311	311	831
Background conc., fL/L	3.9	<0.15	<0.06
Release rate, g/s	4.6	10.7	7.9

National Weather Service for airborne sampling during the ANATEX study. In addition to this device, the lead aircraft was equipped with the PNL two-trap analyzer for real-time detection of the tracer plume. While available meteorological data were used to define aircraft sampling tracks, in-flight measurements served to pinpoint plume location and provide input for modifying flight tracks. This report describes PNL aircraft operations during the ANATEX field program and presents tracer concentration data obtained with the on-board analyzer for missions conducted on March 4, 1987.

PNL Aircraft Sampling Operations

Airborne sampling was performed to obtain data on the vertical distribution of the tracer, locate the plume centerline, and measure near-source dispersion. For each tracer release, meteorologists at NOAA's Air Resources Laboratory suggested an initial flight path, which was based on regional meteorological conditions, observations at the release site, and rawinsonde soundings at the Glasgow, Montana, National Weather Service station. The decision to conduct a sampling mission was dependent on current and anticipated conditions at both the projected sampling location and Wiley Field in Miles City. In this regard, aircraft safety required sampling to be conducted in clear air. Aircraft missions were generally initiated with the lead aircraft at, or below, 1000 ft AGL. The second (shadow) aircraft was positioned 500 to 1000 ft above and slightly ahead of the lead aircraft to maintain visual contact. After plume encounter, flight tracks were modified in accordance with observed real-time tracer data. Radio contact was maintained throughout the flight to assist in maintaining the aircraft at a safe distance of separation and to communicate directions for sequential sampler operation.

In-flight detection of the tracer plume provided essential information for positioning the aircraft and setting sample collection times. The PNL two-trap analyzer consequently served as a vital component of the airborne sampling program. Its utilization provided confirmation of plume encounter and enabled the on-board scientist to establish flight patterns to maximize in-plume sampling time.

The two-trap analyzer consists of an adsorption trap module, with two adsorption traps, interfaced with a gas chromatograph to sequentially collect and measure perfluorocarbon tracers in ambient air. Its characteristics and operational features have been described previously (Allwine et al. 1986). Under conditions employed during the ANATEX study, samples were collected and analyzed over a 12-minute operational cycle. Material collected on one of the traps during the first half of the cycle was measured following thermal desorption and injection into the carrier gas stream of the gas chromatograph while the second trap was engaged in sample collection.

In addition to the sequential sampler and two-trap analyzer, systems on the lead aircraft included a Loran-C navigation system, dewpoint hygrometer, temperature sensor, and pressure transducer to provide meteorological and aircraft position data. These devices were interfaced with a data acquisition system consisting of a PNL-designed data logger coupled to a microcomputer. Raw data and event signals

from the two-trap analyzer and NOAA sampler were recorded on micro floppy disk for post-flight data reduction. The pilot of the shadow aircraft hand-recorded sampler on/off times and the corresponding position data. This aircraft was also equipped with a Loran-C navigation system.

A special gas mixture, prepared for ANATEX participants, was used to perform in-flight calibration of the two-trap analyzer during ANATEX sampling missions. Calibrations were performed at the end of a sampling mission when the aircraft was out of the tracer plume and returning to the aircraft base. A Tedlar bag, filled to approximately one-half of its capacity to avoid rupture at airborne sampling pressures, was employed for in-flight calibrations. They were conducted by the introduction of a measured volume of the standard gas mixture at the "sample-in" port of the analyzer. A typical calibration curve for PTCH, obtained by plotting chromatogram peak area versus tracer volume, corrected to STP, is displayed in Figure 1.

Tracer Release #24, March 4, 1987

Meteorological data on the afternoon of March 3 indicated easterly transport of the tracer plume from Glasgow following nighttime release (0500 to 0800 GMT). Models used to predict transport winds suggested flows of 7 to 8 m/s. At the time of release, surface winds at the Glasgow NWS station were reported to be 220° at 4 m/s with flow above the 200-m inversion layer measured at 7 to 11 m/s. Under these conditions, a flight track along the 104°30' longitude was expected to be at the leading edge of the plume at 0300 MST (5 h after the start of tracer release).

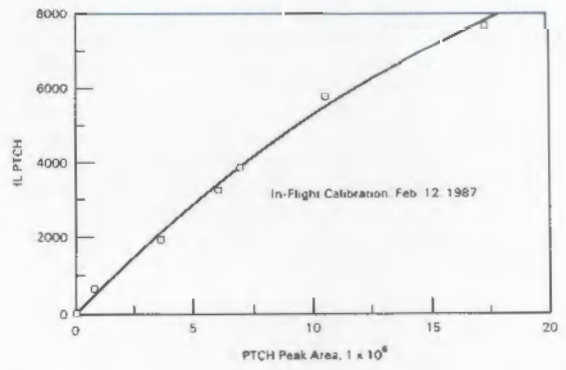

FIGURE 1. In-Flight Calibration Curve for the Tracer PTCH.

Flight tracks for the sampling mission of March 4 are identified in Figure 2. The early morning sortie, flown between way points A and B, was conducted with "real-time" tracer measurement at 3600 and 3000 ft MSL. The plume was centered at about 48°30'N with concentrations at 3000 ft exceeding those at 3600 ft by more than an order of magnitude. Integrated tracer concentrations plotted with respect to the aircraft position at the midpoint of the sampling period are displayed in Figure 3 for five plume traverses along the A-B flight track.

Following a refueling stop in Williston, North Dakota, sampling was resumed along the 103°W longitude (way points A' and B'). After locating the plume and measuring tracer concentrations at 3000 and 2500 ft MSL (Figure 4), the

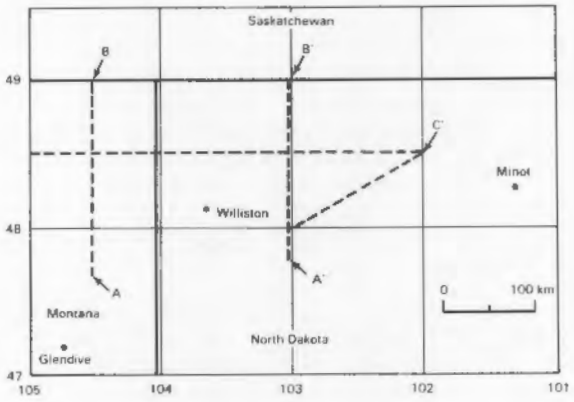

FIGURE 2. Aircraft Flight Tracks, March 4, 1987.

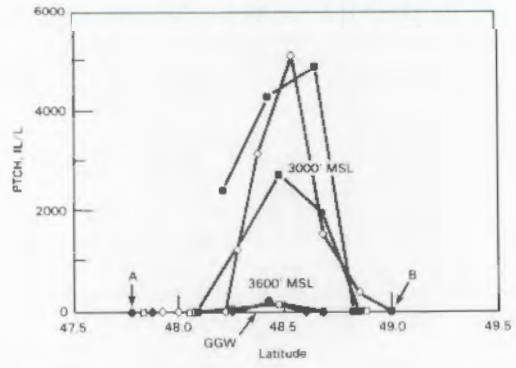

FIGURE 3. Tracer Quantity Versus Position at MidPoint in Sampling Interval, Sortie #1 Along 104° 30 'W Longitude (0430-0736 MST).

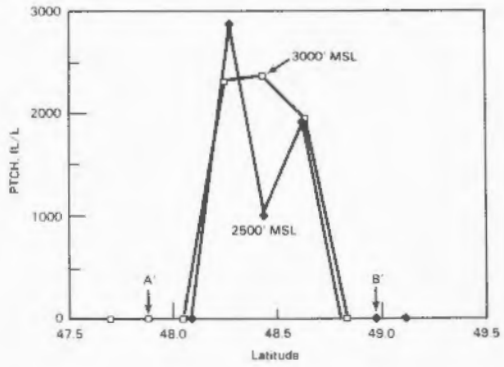

FIGURE 4. Tracer Quantity Versus Position at MidPoint in Sampling Interval, Sortie #2 Along 103°00'W Longitude (1026-1132 MST).

lead aircraft moved farther downwind (way point C') to measure the east-west extension of the tracer cloud. These measurements, conducted at 2800 ft, found the leading edge of the plume at about 102°20'W (approximately 12 h after the start of tracer release) with the trailing edge located at about 104°30'W. Sampling along the east-west flight track was performed while the shadow aircraft continued to make crosswind traverses between way points A' and B'.

Summary

Results from the ANATEX series provide a clear illustration of the contribution of an in-field measurement capability to the performance of long-range tracer experiments. Plume detection was often only marginally successful when sampling aircraft were positioned, at even short transport distances, on the basis of available meteorological information. With "real-time" data, flight tracks were altered when no tracer was detected. When the tracer cloud was observed, the region of interest was easily defined and sampling operations devoted to measuring both its vertical and horizontal distribution. Consequently, in-plume flight time was maximized while adjusting aircraft flight tracks to yield information on plume structure.

References

Allwine, K. J., R. N. Lee and M. M. Orgill. 1985. "Real-Time Measurement of Multiple Perfluorocarbon Tracers During the 1984 ASCOT Experiments." In Pacific Northwest Laboratory Annual Report for 1984 to the DOE Office of Energy Research, Part 3, Atmospheric Sciences, pp. 10-13, PNL-5500 PT3, Pacific Northwest Laboratory, Richland, Washington.

Measurement and Analysis Techniques

MEASUREMENT AND ANALYSIS TECHNIQUES

The development and deployment of new measurement and analysis systems for both surface-based and airborne operations are continually being addressed by PNL in the Multi-State Air Pollution and Power Production Study/Precipitation Chemistry Network (MAP3S/PCN) and the Research Aircraft Operations project. PNL's internally funded exploratory research also contributes to these advancements. Measurements in air, clouds, and precipitation began more than a decade ago on a multi-state basis to identify and characterize energy-related pollutants, chemical species resulting from their transformation, and other involved atmospheric constituents through the MAP3S network and our instrumented DC-3 aircraft. As new understanding of important processes and reactions has progressed, measurement and analytical capabilities have been advanced to ensure that regional air and surface chemistry distributions and their changes can be characterized sufficiently to anticipate new and growing threats to the environment. Our close association through the MAP3S/PCN network with scientists at universities and other federal laboratories and our detailed analysis of precipitation samples from their measurement sites have created a valuable data base serving a host of related investigations on atmospheric chemistry and environmental cycling at their sites and across the network.

In the future, atmospheric chemistry measurements by surface networks will capitalize on recent studies of trace metals in precipitation. The relationship of chemical inputs at the sampling site environments to outputs from specific source areas may be identified by various combinations of trace metals. Apportionment of other associated pollutants from these source areas will be studied across the precipitation chemistry network. Trace metal exchange and accumulation at remote sampling locations will also be investigated. Advanced measurement and analytical capabilities will permit more detailed characterization of organic species in air and precipitation as well. Increased emphasis will be placed on their role in contaminant processing and as biogenic inputs to the atmosphere.

Aircraft measurement efforts will focus on the production and distribution of oxidants throughout the atmosphere and their crucial role in cloud processing and removal of anthropogenic sulfur. Where insufficient oxidants are present, the high altitude venting from clouds and subsequent long-range transport of contaminants will be characterized. A Gulfstream-1 turboprop aircraft, recently acquired by Battelle for the more demanding requirements of future aircraft operations, will be equipped to probe the outflow as well as inflow regions of clouds and measure more diverse and complex chemical processes over expanded spacial scales of interest. Concurrent aircraft measurements, remote and in situ, of cloud physics and radiative transfer processes will characterize the response of energy budgets to pollution-induced changes in aerosol and cloud properties. The studies described in the following articles were supported by:

- **MAP3S/PCN**
- **Research Aircraft Operations**
- **Exploratory Research**

THE MAP3S PRECIPITATION CHEMISTRY NETWORK IN 1987

W. R. Barchet

Hales et al. (1986) identify four important functions of research deposition measuring networks that are critical to increasing our quantitative understanding of atmospheric deposition. These functions are:

1. Serve as pilot facilities for the development and testing of measurement methods.
2. Discover and flag, through a wider range of measurements, important chemical constituents not observed by the regular monitoring networks.
3. Provide detailed and precise measurements that can be a basis for intercomparison, calibration, and quality control for routine monitoring networks.
4. Enable mechanistically informative examination of atmospheric and deposition processes through the use of the detailed and temporally resolved measurements of the research network.

These functions well describe the objectives of the Multi-State Atmospheric Power Production Pollution Study/Precipitation Chemistry Network (MAP3S/PCN). PNL's role within MAP3S/PCN is to:

- manage operations at a network of separately funded precipitation collection sites
- conduct quality assurance audits of site operations
- perform chemical analysis of event precipitation samples received from the field sites
- report on a regular basis the results of the chemical analyses.

History of MAP3S/PCN

In 1976, PNL researchers, in support of DOE's Multi-State Air Pollution and Power Production Study (MAP3S), organized a network of four sites in the eastern United States to investigate the acidity that develops in rain when pollutants are removed from the atmosphere by precipitation. By 1981 the network had expanded to nine sites. Figure 1 shows the location of these sites and Table 1 lists the dates on which each site began operation.

Several of MAP3S/PCN sites are co-located with other federally funded acid deposition measuring programs. National Trends Network (NTN) sites are co-located with MAP3S/PCN sites at:

- Whiteface Mountain, Wilmington, New York
- Pennsylvania State University, State College, Pennsylvania
- University of Virginia, Charlottesville, Virginia
- University of Illinois, Bondville, Illinois
- Miami University, Oxford, Ohio
- Oak Ridge National Laboratory, Oak Ridge, Tennessee.

National Dry Deposition Network (NDDN) sites are co-located with MAP3S/PCN sites at Whiteface Mountain; Ithaca, New York; Pennsylvania State University; and Miami University. A Canadian Acid Precipitation Monitoring Network (CAPMoN) site for comparing sampling and analysis protocols is co-located at the Pennsylvania State University site.

FIGURE 1. Locations of the MAP3S Precipitation Chemistry Network Sites.

TABLE 1. Network Site Details

Site Number	Name	Location		Elevation (m, msl)	Date of First Sample Collected
		Longitude	Latitude		
1	Whiteface	73° 51′	44° 23′	605	October 11, 1976
2	Ithaca	76° 43′	42° 23′	503	October 26, 1976
3	Penn State	77° 57′	40° 47′	396	September 22, 1976
4	Virginia	78° 32′	38° 2′	171	December 12, 1976
5	Illinois	88° 22′	40° 3′	213	November 20, 1977
6	Brookhaven	72° 53′	40° 52′	24	February 9, 1978
7	Lewes	75° 0′	38° 46′	0	March 1, 1978
8	Oxford	84° 44′	39° 32′	283	October 1, 1978
9	Oak Ridge	84° 17′	35° 58′	330	January 7, 1981

Funding of MAP3S/PCN

Over its history, funding for the management of the MAP3S/PCN has shifted between DOE and the U.S. Environmental Protection Agency (EPA). Initial funding was from DOE as part of MAP3S. During this time research programs at the field sites and at network management and chemical analysis at PNL were funded by DOE. When MAP3S evolved into a precipitation scavenging project, the EPA began to fund network management and chemical analyses while DOE continued to fund the field sites. In FY 1984, EPA funding of network management was separated from the precipitation scavenging project; this arrangement continued through FY 1986. In FY 1987, DOE resumed the funding of network management and chemical analysis and continued to fund separately the research programs at the nine field sites.

Site Management and Supply in 1987

Site supply involves the preparation of sample collection and shipping containers. Inventory records kept at PNL and at the sites control the shipment of scrupulously cleaned sample buckets and shipping bottles and other supplies to the sites.

Network management includes updating site operator manuals for any changes in sample collection protocol, recording the arrival of samples from the sites, and conducting site audits. The site audits are used to certify that site operators follow the protocol set forth in the operator's manual. Table 2 gives the dates on which site audits were conducted in FY 1987. Not all sites were audited during the fiscal year.

TABLE 2. Site Audits Conducted During FY 1987

Site	Location	Date of Audit
1	Whiteface	9/23/87
2	Ithaca	9/22/87
3	Penn State	9/21/87
4	Virginia	9/17/87
6	Brookhaven	9/25/87
7	Lewes	9/28/87

Chemical Analyses in 1987

Chemical analyses of precipitation samples are carried out using the methods indicated in Table 3. Detailed procedures for all aspects of laboratory operation and analyses are given in quality control descriptors (Dana 1988).

The MAP3S/PCN analytical laboratory participates in an external QA program administered by the U.S. Geological Survey (1985). Standard solutions of known concentrations of the major ions, sent by the USGS to the site operators, are transferred to sample bottles, given fictitious sample identification, and shipped to PNL for analysis as normal samples. Blind samples are later identified at the time quarterly data reports are prepared and the results of the analyses reported to the USGS. Figure 2 illustrates the performance of the PCL for sulfate analyses. Table 4

TABLE 3. Chemical Species and Analysis Details

Species	Method[a]	Instrument	Minimum Detection Limit (μM)[b]	Quantitative Detection Limit (μM)[c]	Estimated Error[d]
H^+ (free)	Electrode	Corning® Model 135 pH/Ion Meter	—	—	± 0.05 pH units[e]
Conductivity	Bridge	Markson Electromark®	1.20	—	± 20%
$SO_3^=$	AWC	Alpkem® Auto Analyzer	0.10	0.20	± GO(QDL or 10%)
$SO_4^=$	IC	Dionex™ System 2000i (Anion)	0.03	0.20	± GO(QDL or 10%)
NO_3^-	IC	Dionex™ System 2000i (Anion)	0.05	0.20	± GO(QDL or 10%)
Cl^-	IC	Dionex™ System 2000i (Anion)	0.50	2.00	± GO(QDL or 10%)
PO_4^{3-}	IC	Dionex™ System 2000i (Anion)	0.05	0.20	± GO(QDL or 10%)
NH_4^+	IC	Alpkem® Auto Analyzer	0.10	0.50	± GO(QDL or 10%)
Na^+	ICAP	Leeman Labs Plasma-Spec®. ICP 2.5	0.10	0.40	± GO(QDL or 10%)
K^+	ICAP	Leeman Labs Plasma-Spec®. ICP 2.5	0.20	0.50	± GO(QDL or 10%)
Ca^{++}	ICAP	Leeman Labs Plasma-Spec®. ICP 2.5	0.05	0.20	± GO(QDL or 10%)
Mg^{++}	ICAP	Leeman Labs Plasma-Spec®. ICP 2.5	0.08	0.20	± GO(QDL or 10%)

(a) AWC = Automated Wet Chemistry; IC = Ion Chromatography; ICAP = Inductively Argon Coupled Plasma.
(b) Concentrations are expressed in molar units: μM = μmol/ℓ.
(c) Best obtained—Some analysis sessions result in higher maximum detection limits. These are noted, where relevant, in the Appendix.
(d) GO = Greater Of; QDL = Quantitative Detection Limit.
(e) At pH = 4.

Corning® is a registered tradename of Corning Glass Works, Medfield, Massachusetts.
Markson Electromark® is a registered tradename of Markson Science, Inc., Del Mar, California.
Alpkem® is a registered tradename of the Alpkem Corporation, Clackamas, Oregon.
Dionex™ System 2000i is a registered trademark of the Dionex Corporation, Sunnyvale, California.
Leeman Labs Plasma-Spec®. is a registered tradename of Leeman Labs, Inc., Lowell, Massachusetts.

indicates the accuracy and bias of the PNL analyses for the six ions evaluated in the blind sample audit. More detail is given by Dana (1988).

Data Reporting

Three forms of data reporting make MAP3S/PCN data available to external users. Quarterly data reports of individual sample analyte concentrations and hourly precipitation amounts are sent to all sites (and a limited number of other recipients); Table 5 lists the data reports released in FY 1987. In FY 1987 and earlier years, annual summary reports listed all data for the year and gave annual summary statistics (for example, Rothert and Dana 1984 and Dana 1987). In FY 1988, the annual report for 1985 (Dana 1988) will contain monthly and annual data summaries and QA/QC statistics but the detailed data listing will be omitted. Analyte concentrations and precipitation amounts for each event are transferred to the Acid Deposition System national computerized data base for wet deposition maintained for the EPA by PNL.

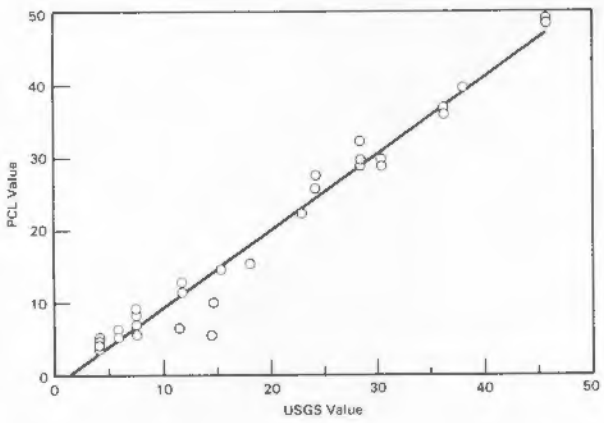

FIGURE 2. Comparison of USGS and PCL Concentrations of Sulfate in Blind QA Samples for 1985. The solid line is a least-squares fit ($R_2 = 0.97$).

TABLE 4. Summary of External Blind QA Sample Results for 1985

Species	Accuracy, %	Bias, %
SO_4	6.2	-1.5
Na	8.4	2.0
Mg	7.8	0.0
K	29	5.0
Cl	12	-9.4
Ca	11	-0.9

TABLE 5. Quarterly Data Reports Issued in FY 1987

Volume	No.	From	To
19	4	October 1, 1986	December 31, 1986
20	1	January 1, 1987	March 31, 1987
20	2	April 1, 1987	June 30, 1987

Summary of Results

Precipitation-weighted annual mean concentrations (C) are calculated as follows:

$$C = \frac{\sum_{i=1}^{n} c_i p_i}{\sum_{i=1}^{n} p_i}$$

where c_i and p_i are the concentration and precipitation amount, respectively, of the ith event and n is the number of events (samples) in the period. Mean concentrations for 1985 and for all available years, 1977 through 1985, are presented for sulfur (includes sulfate and dissolved SO_2), nitrate, ammonium and hydrogen ion by Dana (1987). Figure 3 shows the relationship between hydrogen ion concentration in 1985 compared with all available years; Figure 4 shows the same for sulfur. For most sites the 1985 mean concentrations were slightly, but not significantly, lower than for all available years.

The period of record at some MAP3S sites is sufficient to evaluate temporal trends. Dana and Easter (1987) reported that for the period 1976 through 1983, ionic concentrations decreased for sulfur, nitrate, and hydrogen ion at most sites but the rate of decrease was not statistically significant.

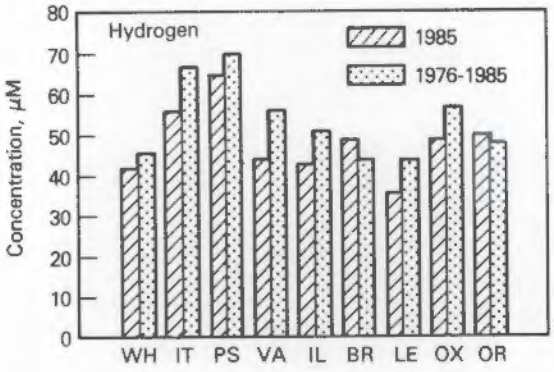

FIGURE 3. Precipitation-Weighted Hydrogen Ion Concentration for 1985 and for All Available Years, 1976 Through 1985, at MAP3S Sites.

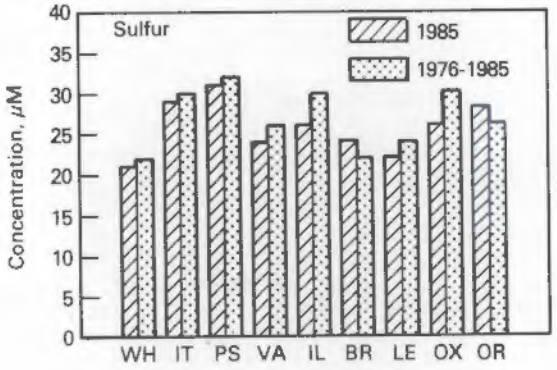

FIGURE 4. Precipitation-Weighted Sulfur (Sulfate Plus Dissolved SO_2) Concentration for 1985 and for All Available Years, 1976 Through 1985, at MAP3S Sites.

The distribution of event concentrations was reported by Dana and Easter (1987). Figure 5 illustrates the wide range of event concentrations with data from the Ithaca site. Lowest concentrations were below the level of detection. The distribution of concentration by event is approximately log-normal.

The distribution for the deposition of ions (defined as the concentration times the precipitation amount) indicates for the combined sites of the MAP3S network that a large fraction of annual deposition is produced by a relatively small fraction of events (Dana and Slinn 1987). About 55% of the annual deposition of sulfur and 40% of the annual precipitation amount are produced by 20% of the events.

Cooperation with Other Research Programs

Since the start of the National Acid Precipitation Assessment Program, the MAP3S network has been part of a nationwide effort to describe the chemical climate of precipitation. Of the federal networks, MAP3S has proven most useful for the investigation of the processes by which pollutants are transformed and removed by precipitation because of its event sampling protocol. The ongoing PRECP project has frequently used the MAP3S network as the basis for detailed field studies.

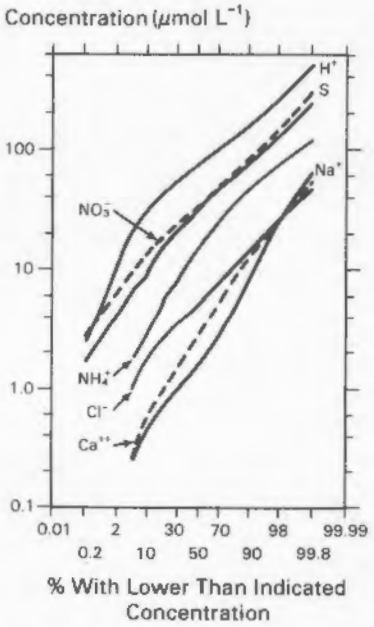

FIGURE 5. The Distribution of Ionic Concentrations by Event at Ithaca, New York for 1976 Through 1983 (Dana and Easter 1987).

References

Dana, M. T. 1987. The MAP3S Precipitation Chemistry Network: Eight Periodic Summary Report (1984). PNL-6055, Pacific Northwest Laboratory, Richland, Washington.

Dana, M. T. 1988. The MAP3S Network Data and Quality Control Summary for 1985. PNL-6461, Pacific Northwest Laboratory, Richland, Washington.

Dana, M. T., and R. C. Easter. 1987. "Statistical Summary and Analyses of Event Precipitation Chemistry from the MAP3S Network, 1976-1983." Atmos. Environ. 21(1):113-128.

Dana, M. T., and W. G. N. Slinn. 1987. "Acidic Deposition Distribution and Episode Statistics from the MAP3S Network Data Base." Submitted to Atmos. Environ.

Hales, J. M., B. B. Hicks and J. M. Miller. 1987. "The Role of Research Measurement Networks as Contributors to Federal Assessments of Acid Deposition." Bull. Am. Meteor. Soc. 86(3):216-225.

Rothert, J. E., and M. T. Dana. 1984. The MAP3S Precipitation Chemistry Network: Seventh Periodic Summary Report (1983). PNL-5298, Pacific Northwest Laboratory, Richland, Washington.

PNL RESEARCH AIRCRAFT ACTIVITIES

K. M. Busness and J. M. Hales

During September of 1987, Battelle purchased a Grumman Gulfstream 1 (G-1) aircraft, which is intended for long-term DOE atmospheric sciences research at PNL. The G-1, shown in Figure 1, is a twin-engine turboprop; it will eventually replace the Battelle DC-3 that is currently in research use. Performance features of the G-1 and DC-3 are summarized in Table 1.

The decision to purchase the G-1 was based on present and future scientific needs, particularly within the scope of DOE's storm-research and global-change activities. Precipitation-scavenging research, for example, is currently at a state where measurements in the upper regions of storm systems are badly needed. Past in-storm measurements at lower altitudes with the DC-3 have been invaluable in advancing scientific understanding of such systems; but this advancement has brought knowledge to the point where higher-altitude measurements are needed. The G-1's 30,000-ft ceiling

FIGURE 1. The Grumman Gulfstream 1 (G-1) Aircraft.

TABLE 1. Aircraft Performance Features

	G-1	DC-3
Airspeed (normal cruise), kt	275	140
Ceiling altitude, ft	30,000	19,000
Range, mi	1,650	850
Engine lifetime, h	4,300	1,200

capability will contribute significantly to the removal of this constraint. The G-1 will also enhance DOE's global-change research capability significantly, since it provides the opportunity for measurements in oceanic, arctic, and other remote regions of the globe.

Currently the G-1 is at PNL, where it is being reconfigured for scientific application; trace-gas and fine-particle probes, electrical distribution systems, instrument racks and work-station systems, air-mover devices, and the data acquisition unit are being designed and installed. Essentially all pumping for the system will be performed by air ejectors that are driven by the aircraft engines.

The electrical-distribution, sampling-probe and instrument work-station systems are being designed specifically for the G-1. The data-acquisition unit, however, will be the existing HP-200-based system currently operating in the DC-3. Future developments of the G-1 will include provisions for cloud-chemistry and cloud-physics measurements, as well as adaptation for a variety of remote-sensing activities.

The first research flights of the G-1 are scheduled in Illinois for May of 1988, in conjunction with the 3CPO/PRECP VI field study.

SNOW CRYSTAL RESIDUAL AEROSOL

D. J. Luecken and G. L. Laws

In this study we have measured the aerosol residue left from individual snow crystals that were collected during a snow storm above Boonville, New York. Many different types of crystals were collected during the experiment, and the types of crystals varied widely with event. A method developed to analyze snow crystals is applied here, in detail, to two single crystals. The amount of aerosol collected by these two crystals is compared

to theory, to previous investigations reported in the literature, and with other very limited auxiliary measurements that were also made during the storm.

Collection and Analysis Methods

The individual snowflakes were collected during specific PRECP-III events by exposing clean sheets of 0.4 μm Nucleopore™ filter to the snowfall. The crystal was then photographed using a camera with a telephoto lens and tungsten film to record the crystal type and location before sublimation. The water from the crystal was sublimated in a cold desiccator with a small vacuum pulled on it. The filters were put in clean plastic Petri dishes and stored in tightly sealed plastic bags after sublimation to avoid contamination.

In addition to the snow photographs that were taken of the crystals used for the aerosol residue study, many other photographs were taken of representative samples of the snowfall. These photographs were taken approximately every half hour to record any changes in the types of crystals produced by the storm as the storm evolved.

Examination of the aerosols was done using a scanning electron microscope (SEM) located at PNL. The sample surface was coated with gold in a vacuum. Because the magnification needed to see the submicron particles was so high, and the particles were sparse at this magnification, it was often difficult to locate the exact position on the filter of the snow crystal prior to sublimation. Previous studies (i.e., Magono et al. 1979) have used both optical and electron microscopes but have found that they give very different size distributions. In this study, we have tried to resolve the size distribution into one continuous spectrum by using the electron microscope at several different magnifications. A low magnification was used to initially locate the entire crystal in one screen, followed by observations of different segments of the crystal at higher magnifications to count the various sizes of crystals. The data were classified by size of each of the two major axes and by particle shape.

Results and Discussion

The size distributions for crystals 1 and 2, taken at 0920 and 1127 EST on January 27, 1986, are shown in Figures 1 and 2. The majority of the aerosols are found in the submicron range. The particle size distributions found for these crystals have been compared with those reported by Murakami and Magono (1984), for aerosol residue from cloud droplets, and with the aerosol size distributions measured by the NOAA King Air at 7000 ft, taken several hours after the storm at Boonville. The size distribution of the snow crystal residual aerosols tends to match the size distribution of the cloud residue much better than it does the aerosol count in the air. This situation suggests that the majority of the aerosol in the snow crystal

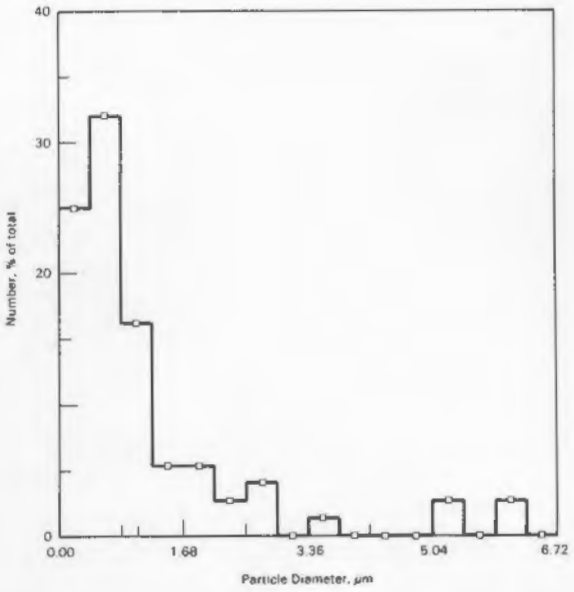

FIGURE 1. Particle Size Distribution for Snow Crystal 1.

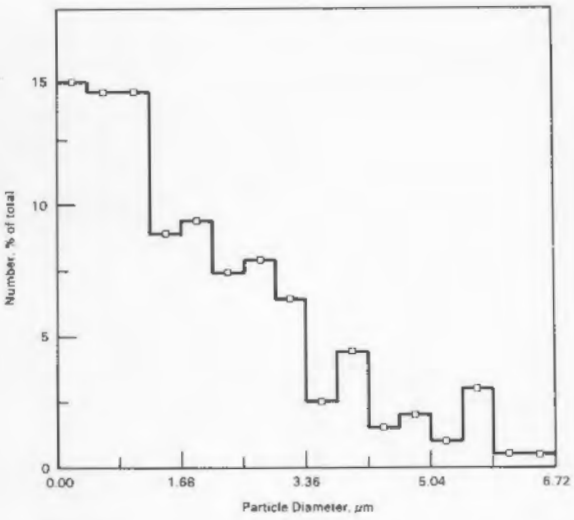

FIGURE 2. Particle Size Distribution for Snow Crystal 2.

™Nuclepore Corp., Pleasanton, California.

originates from riming of cloud droplets, as Murakami et al. (1981) found in many of their measurements, although measurements of cloud droplet residue at the Boonville site would be necessary to confirm this.

A total of 984 particles was calculated to have been captured by crystal 1. These total numbers are similar to those reported by Magono et al. (1979). It is hard to compare total number of aerosols counted because aerosol collection by snowflakes is extremely sensitive to many factors such as pollutant loading in the sampling location, storm type, etc. In addition, many of the previous studies were done in experimental chambers with artificially generated aerosols. Although many different particle shapes were found, the very thin, sheetlike particle was very common.

There is not enough certainty in the exact crystal location and orientation before sublimation to determine, quantitatively, which section of the original crystal contained the most particles. However, the densest areas of the filter corresponded to areas that should have been located near the outer edges of the crystal. This is especially evident in several crescent-shaped areas of the filter that seemed to outline the crystal area.

This work shows that aerosol counting of particles from sublimated crystals is a feasible though time-consuming project. The method we have demonstrated is reasonable, and along with suggestions we have compiled for improvements in future work, provides a basis for further analysis and evaluation.

References

Magono, C., T. Endoh, F. Ueno, S. Kubota and M. Itasaka. 1979. "Direct Observations of Aerosols Attached to Falling Snow Crystals." Tellus 31:102-114.

Murakami, M., and C. Magono. 1984. "Relationship Between the Size of Cloud Droplets and Their Residual Particles." J. Met. Soc. Japan 62:696-701.

Murakami, M., C. Hiramatsu and C. Magono. 1981. "Observation of Aerosol Scavenging by Falling Snow Crystals at Two Sites of Different Heights." J. Met. Soc. Japan 59:763-771.

ANALYSIS OF ATMOSPHERIC ORGANICS: ASSESSMENT OF NEW ANALYTICAL TECHNIQUES

E. G. Chapman and N. S. Laulainen

This ER program has assessed the potential application of new analytical techniques under development at PNL to the analysis of organic compounds in the atmosphere. Two techniques were investigated in FY 1987: supercritical fluid extraction with conventional gas chromatographic analysis (SFE/GC) and capillary zone electrophoresis with mass spectrometry detection (CZE/MS).

Experiments conducted on aerosol filter samples and blanks indicated that SFE can extract more material in a shorter time period than conventional Soxhlet extraction. Results suggested that pretreatment of filters or use of a fractionation process during analysis may be desirable for quantitative determination of certain organic compounds, such as polycyclic aromatic hydrocarbons (PAHs). Analyses using SFE/GC of National Bureau of Standards urban aerosol further demonstrated the potential usefulness of this technique. Experiments using CZE/MS with laboratory solutions of ions important in precipitation chemistry led to what we believe to be the first mass spectra of hydroxymethane sulfonate (HMSA), a S(IV) compound of increasing interest to atmospheric scientists. Circumstantial evidence suggests that this SO_2-HCHO adduct should exist in certain rainwater samples; however, definitive identification of the compound had never been performed because of the difficulties of introducing the ion into a mass spectrometer.

In FY 1988, field samples will be analyzed to demonstrate the potential importance of SFE/GC and CZE/MS in atmospheric measurement problems. Pretreatment and SFE/GC analysis of aerosol filters will be performed in conjunction with the May 1988 PRECP field experiment. Analysis of additional precipitation anions (e.g., sulfate, nitrate, organic acids) will be attempted with CZE/MS, and detection limits and operating conditions likely to influence these limits assessed using laboratory solutions. Analysis of actual precipitation samples, including identification and quantitation of HMSA, will also be attempted.

DEVELOPMENT OF PARTICLE-INDUCED X-RAY EMISSION (PIXE) AND OTHER ION BEAM ANALYSIS TECHNIQUES

A. C. D. Leslie and D. R. Baer

Exploratory research (ER) funding during FY 1987 enabled the development of ion beam analysis techniques in conjunction with the PNL accelerator. A primary objective was the completion of a quantified PIXE system. This article describes the work that was undertaken in fulfillment of these aims.

PIXE Method

PIXE is an elemental analysis method that is sensitive at trace levels; it yields fractional mass sensitivities in the parts per million range. PIXE has the advantages of being sensitive to a wide range of elements (to all elements with atomic number (Z) of 11 or greater), of having a sensitivity that varies smoothly from element to element, of being rapid (several minutes analysis time is typical), of being multi-element (all elements are measured at the same time), and of being nondestructive.

The basic principle of the energy-dispersive PIXE technique is as follows:

- Incoming energetic ions (here protons from a Van der Graaff accelerator) are allowed to bombard the sample of interest and produce vacancies in the inner shells of atoms in the target sample.
- The resultant vacancies are then filled by transitions of electrons from higher-energy orbitals resulting in the emission of characteristic x-rays.
- Subsequent measurement of the intensities and energies of these x-rays (as K, L or M lines) using a Si(Li) detector provides a quantitative assessment of the detected elements within the sample.

Work Carried Out

During FY 1987 major progress was made in establishing PIXE as a quantitative low-cost analysis method. Tasks that were thereby completed included the adaptation of an x-ray spectra analysis computer code ("HEXB"), obtained from Florida State University; the automated quantitative analysis of thin targets; procuring and analyzing more than 40 elemental standards to build up a data base or library of x-ray line intensities needed during quantitative sample analysis; modification of a experimental bombardment chamber built in the previous year and of the beam line from the accelerator to allow for better accuracy and analytical speed; and the extension of the analysis code to elements with high atomic numbers. During 1987 absolute accuracy was obtained to within 8% and relative accuracy to better than 4% for detection of elements from sodium (Z=11) to curium (Z=96) for amounts of material in a nanogram through microgram range. Fluorine (Z=9) was also measured, but outside of the above accuracy limits.

Several other activities were undertaken as part of the development of the ion beam facility. Rutherford backscattering (RBS) measurements were made on nitrogen-implanted silicon as part of work with the University of Washington; copper-implanted aluminum with Washington State University; oxide scales containing thorium as part of a seed/ER microchemistry scale program; and on thin carbon foils. Other work carried out within the ion beam facility included the preparation of specimens as part of an ER dosimetry program.

Outcome

The work carried out in FY 1987 has allowed PIXE and RBS to become integral parts of several ongoing and new programs: analysis of PRECP aerosol filters, analysis of filtered gel from defense-waste leached glass, analysis of aerosol filters from animal toxicology studies, and characterization of ultra-thin carbon foils.

Future Developments

Additional developments planned beyond FY 1987 include reduction in absolute accuracy of PIXE to $\leq$5%, increase in sample analysis rate, analysis of quantitative thick targets, and addition of a microbeam PIXE/RBS capability.

Air-Surface Interaction

AIR-SURFACE INTERACTION

PNL has contributed over the years to research in air-surface exchange processes through dry deposition and resuspension studies. Evidence of this foundation is given through two international conferences co-chaired and contributed to strongly by PNL scientists. In 1983, the state-of-the-science for air-surface exchange of contaminants was represented by the results of these conferences in the book, *Air-Sea Exchange of Gases and Particles*, edited by P. S. Liss (U.K.) and W. G. N. Slinn, and the two-volume proceedings *Precipitation Scavenging, Dry Deposition, and Resuspension,* coordinated by H. R. Pruppacher (UCLA), R. G. Semonin (ISWS), and W. G. N. Slinn.

The importance of understanding multi-media and interactive environmental exchange processes in the integrated geosphere-biosphere system has received growing international recognition in recent years. At the 1985 meeting of the International Council of Scientific Unions (ICSU), endorsement was given to a 2-year study to draw up plans for an International Geosphere-Biosphere program (IGBP), which would encompass studies of the global climate, the biosphere, and biogeochemical cycling of a host of natural and man-made chemicals. The goal of the IGBP is to understand how the Earth's environment functions as an integrated whole. As of July 1987, 25 nations [including the Peoples Republic of China (PRC) and the USSR] have committed themselves to involvement in the IGBP.

The IGBP is described by *Science* (226:33-35) as "the largest cooperative endeavor in the history of science." At the July 16-19, 1987, Paris meeting of the ICSU Special Committee for the IGBP, four research areas were chosen for initial emphasis in the IGBP:

1. Terrestrial Biosphere-Atmospheric Chemistry Interactions
2. Marine Biosphere-Atmosphere Interactions
3. Biospheric Aspects of the Hydrological Cycle
4. Effects of Climate Change on Terrestrial Ecosystems.

The specific interests of PNL in air-surface exchange processes and the needs of DOE in understanding contaminant transfer are clearly aligned with these four areas of emphasis.

More fundamental approaches to air-surface exchange research are active at PNL, replacing the prior dry deposition and resuspension research projects. New directions in atmospheric cleansing processes being defined within the PRECP program as its emphasis is reoriented from the specific needs of NAPAP. A gradual transition from studies attempting to solve regional-scale acidic deposition problems to studies of more general geosphere-biosphere problems, at spatial scales from regional to global, is anticipated. The goal of this transition is to prepare for significant DOE contributions to the U.S. Global Change Program, which is the proposed U.S. component of the IGBP.

Exploratory research at PNL consists of small projects of a creative and exploratory character having potential for stimulating new directions of research consistent with the Laboratory's Institutional Plan. This internal program also includes new research efforts related to global change and geosphere-biosphere concerns. Future annual reports will provide specific scientific findings from these efforts, as in the case of the two contributions included here, as well as state-of-the-science summaries for various elements of the scientific framework being defined for PNL's future geosphere-biosphere research.

COMPARISONS BETWEEN THEORY AND DATA FOR PARTICLE DEPOSITION TO VEGETATIVE CANOPIES

W. G. N. Slinn

Particles are removed from the atmosphere by precipitation scavenging (wet deposition) and dry deposition. This dry deposition of aerosol particles depends on many variables, including the state of the atmosphere (e.g., wind speed, stability, turbulence intensity, and humidity), properties of the particles (e.g., size distribution, morphology, hygroscopicity), and characteristics of the surface (e.g., smoothness, dampness, and many relevant characteristics of any vegetative cover). The purpose of this article is to compare theoretical and experimental results for the particle-size dependence of particle deposition to vegetation.

Measurement Methods

Three general methods have been used to try to measure dry deposition of particles (and, also, the air-surface exchange of gases), and each method has substantial difficulties. These three methods and some of their limitations are listed below.

1) Actual Deposition Measurements

For particle deposition, the major difficulty with measurements of the quantity of material deposited is to determine the particle size dependence of the deposition. To date, all studies of this type appear to have used polydisperse aerosols (viz., multiple particle sizes), and therefore, the measurements (of the mass, radioactivity, or other tag on the particles deposited) are actually particle-average results, from which it is difficult to infer information about the dependence of the deposition on particle size. It appears that studies that count the actual number of particles deposited, as a function of their size, have not yet been performed--at least not for submicron particles, where the particle size dependence appears to be most important.

2) Concentration Change Measurements

Interpretations of measured changes (temporal, vertical, or horizontal) in airborne concentrations, caused by dry deposition, are complicated by the many different causes of these changes, such as chemical transformations, variations in mixing-layer height, and horizontal and vertical diffusion. Nocturnal changes of concentrations in the atmosphere have been revealing for ozone, but not (as far as the author is aware) for any other gas or any particles: at a particular measurement site, the number of aerosol particles in the 0.1 to 1.0 μm size range can actually be larger than the daytime values (Slinn et al. 1979), possibly caused by water vapor condensation on smaller particles or by less atmospheric dilution of local sources. Dry deposition's influence on horizontal variations in particle concentrations has been examined in a number of studies (e.g., Slinn et al. 1983), but none has unambiguously identified the contributions to the changes caused by variations in the mixing-layer height or by horizontal diffusion. Vertical variations in concentrations (the "gradient method") are revealing for chemicals that deposit sufficiently rapidly, but questions arise about the contribution to the gradients from chemical reactions of gases, changes in particle sizes (e.g., from water-vapor condensation in a nonuniform humidity profile), and the contribution to the gradient resulting from incomplete diffusion from upwind sources. Yet, to obtain relative rates of deposition of a host of chemicals to forest, it would be valuable to obtain vertical profiles of their air concentrations within and above the canopy; e.g., for sulfate particles in various size classes.

3) Vertical Flux Measurements

The various ways to measure or infer the flux of pollution above a surface, and then to relate the measured flux to the surface flux, are plagued with problems similar to the case of concentration measurements. Particle growth by water vapor condensation (especially in eddies moving from moist surfaces), gas reactions at heights between the sampler and the surface (especially between NO, NO_2, and O_3), and meteorological contributions to the fluxes (e.g., caused by vertical diffusion of the pollutant from a nearby source or caused by changes in mixing-layer height) have plagued many of the reported studies. In addition, compromises with desired instrument specificity have been made to meet the need for short response times and for statistically significant results. The unavailability of fast-response, high-flow rate, size-specific detectors to measure aerosol particles has caused inadequacies in many of the particle flux measurements illustrated below.

Theory Versus Data

In spite of many experimental (and theoretical) difficulties, understanding of particle deposition to pubescent vegetation is fairly consistent with available data. This statement is illustrated with Figure 1. The two theoretical curves in Figure 1 are for two indicated values for the parameter γ in the (assumed) exponential decrease of mean wind speed with depth into the canopy. In the formula at the bottom of Figure 1 (from Slinn 1982 and 1989), the other terms have the following definitions:

v_d = the dry deposition velocity, which is the dry deposition flux divided by the particle concentration at a convenient reference height above the canopy

u_r = mean wind speed at this same reference height

u_h = wind speed at the top of the canopy

v_g = gravitational settling velocity of the particles

β = a parameter with value near 2.0

R = the rebound term, functionally describing that some supermicron particles rebound from collisions with elements of the vegetation

LAI = double-sided Leaf Area Index

u^* = friction velocity, assumed to be constant within the canopy

C_H = coefficient of heat transfer (related to the drag coefficient for the canopy and to the Richardson number)

ε = the total collection efficiency, given as a sum of the indicated contributions from Brownian diffusion (B), interception (IN), and impaction (IM)

Sc = Schmidt number = ν/D, in which ν is the kinematic viscosity of air and D is the Brownian diffusivity for each particle size (particle radius, a)

St = Stokes number, the ratio of the particle stopping time ($=v_g/g$) to the characteristic time scale ($=L/V$) for the fluid flowing with speed V about vegetative elements of size L.

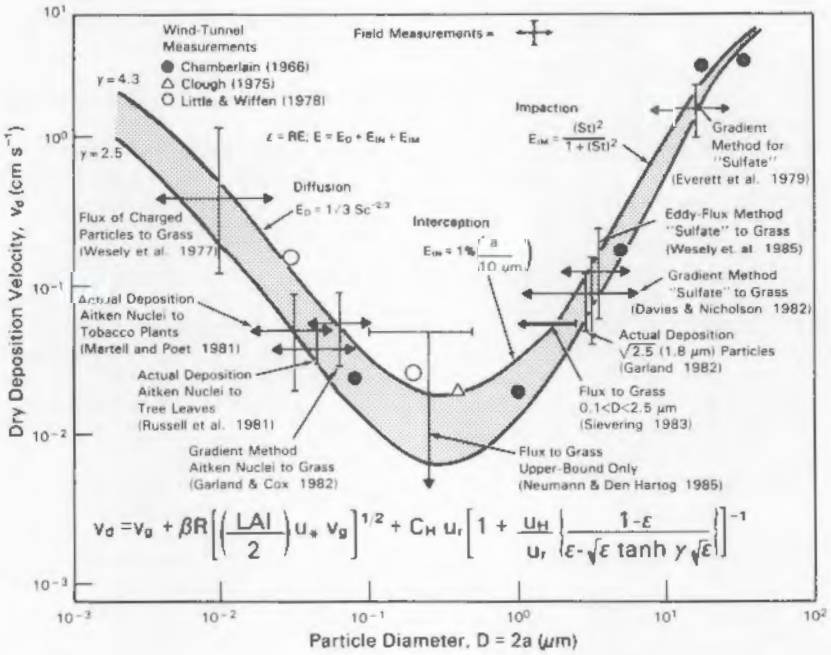

FIGURE 1. Comparisons Between Theory (equation shown at bottom of figure) and Data for the Dependence of Particle Dry Deposition Velocities on Particle Size and Other Variables (defined in the text).

For the theoretical results shown in Figure 1, the following illustrative values were chosen: $u_r = 5\ ms^{-1}$, $h = 10$ cm, and for $\gamma = 2.5$, $z_o = 1.73$ cm, $C_H = C_D(5m) = 4.9 \times 10^{-3}$, $u_h/u_r = 0.35$, $u_* = 35\ cm\ s^{-1}$, and for $\gamma = 4.3$, $z_o = 3.94$ cm, $C_D(5m) = 7.2 \times 10^{-3}$, $u_h/u_r = 0.24$, $u_* = 42\ cm\ s^{-1}$ (Slinn 1989).

The data plotted in Figure 1 include results from wind tunnel studies and from all three types of field methods listed in the previous section. Generally there is agreement between the wind-tunnel, field, and theoretical results, but this agreement is not without its difficulties and limitations. One of the limitations is that parameters in the theory have been adjusted to fit some of the wind tunnel data (Slinn 1982). A more significant problem is related to the horizontal "two-headed arrows" associated with most of the data "points" from field studies. In essence, these arrows mean that the data are for dry deposition of particles of unknown size, and the corresponding data "point" could be put at any of many horizontal locations on the graph. The location of these "points" (with vertical spread given by the spread in measured values) was chosen at what seems to be the most reasonable deposition-mean (not mass-mean) diameters of the particles for the particular site at which the experiments were conducted. The results will be site-specific because the particle size distribution can change with location. In spite of these uncertainties in some of the data "points," however, the general impression can be gained that our understanding of particle dry deposition to vegetation is becoming fairly realistic.

References

Chamberlain, A. C. 1966. "Transport of Gases to and from Grass and Grass-like Surfaces." Proc. Roy. Soc. London 290A:236-265.

Clough, W. S. 1975. "The Deposition of Particles on Moss and Grass Surfaces." Atmos. Environ. 9:1113-1119.

Davies, T. D., and K. W. Nicholson. 1982. "Dry Deposition Velocities of Aerosol Sulfate in Rural England." In Deposition of Atmospheric Pollutants, eds. H.-W. Georgii, and J. Pankrath, pp. 31-42. D. Reidel, Boston.

Everett, R. G., et al. 1979. "An Analysis of Particulate Sulfur and Lead Gradient Data Collected at Argonne National Laboratory." Atmos. Environ. 13:931-934.

Garland, J. A., and L. C. Cox. 1982. "Deposition of Small Particles to Grass." Atmos. Environ. 16:2699-2702.

Garland, J. A. 1982. "Field Measurements of the Dry Deposition of Small Particles to Grass." In Deposition of Atmospheric Pollutants, eds H.-W. Georgii, and J. Pankrath, pp. 9-16. D. Reidel, Boston.

Little, P., and R. D. Wiffin. 1978. "Emission and Deposition of Lead from Motor Exhausts - II. Airborne Concentration, Particle Size, and Deposition of Lead Near Motorways." Atmos. Environ. 12:1331-1341.

Martell, E. A., and S. E. Poet. 1981. Radon Progeny on Biological Surfaces and Their Effects. Report available from the National Center for Atmospheric Research, P.O. Box 3000, Boulder, Colorado.

Neumann, H. H., and G. den Hartog. 1985. "Eddy Correlation Measurements of Atmospheric Fluxes of Ozone, Sulfur, and Particles During the Champaign Intercomparison Study." J. Geophys. Res. 90:2097-2110.

Russell, I. J., et al. 1981. "Forest Vegetation as a Sink for Atmospheric Particulates: Quantitative Studies in Rain and Dry Deposition." J. Geophys. Res. 86:5347-5363.

Sievering, H. 1983. "Eddy Flux and Profile Measurements of Small Particle Dry Deposition Velocity at the Boulder Atmospheric Observatory (BAO)." In Precipitation Scavenging, Dry Deposition, and Resuspension, Vol. 2, coords. H. R. Pruppacher, et al., pp. 963-978. Elsevier, New York.

Slinn, W. G. N. 1982. "Predictions for Particle Deposition to Vegetative Canopies." Atmos. Environ. 16:1785-1794.

Slinn, W. G. N. 1989. "Particle Dry Deposition to Vegetation." In Proc. Conf. on Biometeorology, ed. D. E. Aylor, 17-19 October 1988, New Haven, Connecticut. To be published as a special issue of Agric. and Forest Meteor.

Slinn, W. G. N., et al. 1979. Wet and Dry Deposition and Resuspension of AFCT/TFCT Fuel Processing Radionuclides. Final Report. SR-0980-10, September 1979. Air Resources Center, Oregon State University, Corvallis, Oregon. Available from NTIS, Springfield, Virginia.

Slinn, W. G. N., et al. 1983. "Inland Transport, Mixing, and Dry Deposition of Sea-Salt Particles." In Precipitation Scavenging, Dry Deposition, and Resuspension, Vol. 2, coords. H. R. Pruppacher, et al., pp. 1037-1046. Elsevier, New York.

Wesely, M. L., et al. 1977. "An Eddy-Correlation Measurement of Particulate Deposition from the Atmosphere." Atmos. Environ. 11:561-563.

Wesely, M. L., et al. 1985. "Measurements and Parameterization of Particulate Sulfur Dry Deposition Over Grass." J. Geophys. Res. 90:2131-2143.

TRANSPIRATION'S INHIBITION OF AIR POLLUTION FLUXES TO SUBSTOMATAL CAVITIES

W. G. N. Slinn

The purpose of this article is to present an estimate for the resistance to the dry transport of air pollutants through stomatal openings, accounting for the counterflowing flux of water vapor associated with transpiration. Estimates for the stomatal resistance, ignoring the influence of transpiration, are given, for example by Bennett et al. (1973) and O'Dell et al. (1977). In Figure 1, after O'Dell et al., the sum of the aerodynamic and canopy resistances has been identified as r_{ata}. The specific goal of this article is to estimate the influence of transpiration on the stomatal resistance, r_{sto}. O'Dell et al. have estimated the substomatal and mesophyll resistances r_{asc} and r_{aes}. It might be expected that any influence of the water-vapor flux on pollutant transport would be a maximum at the stomatal opening since, at the constricted area of the stoma, the water flux is a maximum.

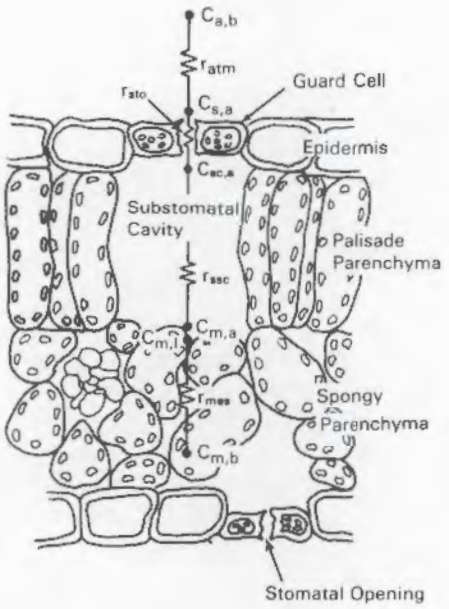

FIGURE 1. Schematic Cross-Section of a Dicotyledonous Leaf, Indicating Resistances Identified in the Text (after O'Dell et al. 1977).

Stomatal Resistance and Stefan Flow

It is of interest to examine stomatal resistance for both particles and gases. For particles, the influence of stomatal resistance on atmospheric cleansing is no doubt ignorable (because the total stomatal area is typically only a few percent of the total area of the vegetation), but if the stomatal resistance to particle transfer is large, it may be important to plant health (if, for example, submicron sulfuric acid droplets are thereby inhibited from entering the substomatal cavity). For many gases (e.g., SO_2, O_3, NO_2, PAN, and, of course, CO_2), it appears that usually the dominant gas-exchange route is via the stomata (except, for some gases, when the plant is wet); therefore, it is important to understand the stomatal resistance for many gases, including gases used in agricultural activities. Since the theory to be developed in this article is applicable both for particles and gases, the word "particle" will be used for both cases.

Airborne particles and gases in the presence of water flux (or other vapor flux) experience Stefan flow (and/or diffusiophoresis; see, e.g., Waldmann and Schmitt 1966). Here, the term Stefan flow is used to designate the mean drift of "particles" swept along by the flux of water vapor from each stoma. The fluxes of CO_2 and O_2 are typically about two orders of magnitude smaller than the water flux and therefore produce negligible Stefan flow. Also, in the present case, the concentration gradients, even in the absence of a net drift of the gases, produce negligible diffusiophoretic drift. Further, since the dominant route for the heat needed to evaporate the water is from the air and soil through the rest of the plant, then thermophoresis (viz., particle drift caused by heat flow) is negligible. Consequently, the focus in this article will be only on the Stefan flow associated with transpiration.

A first estimate of the magnitude of the resulting drift velocity of "particles" is found by setting this Stefan drift velocity, v_{Sd}, equal to the mean velocity of the mixture of air (subscript "a") and water vapor (subscript "v"). Thus, with ρ symbolizing mass density, a first-order estimate of the Stefan drift velocity is

$$v_{Sd} \doteq \frac{\rho_a v_a + \rho_v v_v}{\rho_a + \rho_v} \doteq \frac{\rho_v v_v}{\rho_a} = \frac{T}{\rho_a} . \qquad (1)$$

To obtain the second approximate equality in Equation (1), it was assumed that the air is essentially stationary within the stomatal opening, $v_a \triangleq 0$, and that $\rho_v \ll \rho_a$. In Equation (1), $\overline{T} = \rho_v v_v$ is the flux of water vapor from the plant (i.e., the transpiration rate).

Preliminary numerical values in Equation (1) might suggest that Stefan drift is negligible. Thus, with $\overline{T} = 0.36$ mm $h^{-1} = 10^{-5}$ (g H_2O) cm^{-2} s^{-1} (typical values are in the range 0.1 to 1 mm h^{-1}) and $\rho_a \approx 10^{-3}$ g cm^{-3}, then $v_{Sd} = 10^{-2}$ cm s^{-1}, which is quite small (e.g., compared to the numerical values in Figure 1 of the previous article in this annual report). However, this estimate uses whole-plant-average values (identified in the above formulation with overbars) and ignores the fact that the water is evaporated only through stomata, whose area is typically only a few percent of the plant's total area. Stated differently, the Stefan drift velocity at each stoma is one to two orders of magnitude larger than the value just estimated (depending on the leaf area index and the transpiration rate); i.e., v_{Sd} is likely to be in the range from 0.1 to 1.0 cm s^{-1}. Consequently, it appears likely that Stefan flow can significantly inhibit the flux of air pollution through stomatal openings.

In the next section, this inhibition will be examined more closely, using a simple one-dimensional model. To emphasize the importance of accounting only for the area of the stomata, Equation (1) is written as

$$v_{Sd} = \overline{T}/[\rho_a(LAI)(A_s/A_p)] \qquad (2)$$

in which (LAI) is the one-or two-sided leaf area index (depending on the distribution of stomata), A_s/A_p is the total stomatal area per unit area of the plant (typically 1 to 3 percent), and $\overline{T}$ is the plant-average water-vapor flux (viz., the familiar transpiration rate). Calculations will be made with v_{Sd} = 0.1, 0.5, and 2.0 cm s^{-1}.

One-Dimensional Model

It is instructive to examine a simple one-dimensional model of "particle" diffusion (plus gravitational settling) in the presence of Stefan flow, even though the model has some obvious limitations. In this simple model (e.g., of particle motion within a vertical cylinder of height h and with no flux to the cylinder's walls), it is assumed that the "pollutant's" concentration, C, near the stomatal opening (top of the cylinder) is held constant at the value C_o and that the concentration at the top of the substomatal cavity (bottom of the cylinder) is zero (perfect sink). This boundary condition at the top of the substomatal cavity is not realistic, but it permits substantial simplifications into these "scoping" studies; namely, it permits a formulation in terms of transfer resistances. Later studies should account for particle motion through the leaf's boundary layer (above the cylinder), within the substomatal cavity (below the cylinder), and deposition on the cylinder's walls.

For this simple model, steady conditions, and no sources or sinks of the pollutant within the air, then the advection-diffusion equation simplifies to

$$\nabla \cdot \overrightarrow{Flux} = 0 \rightarrow \frac{\partial F_z}{\partial z} = 0 \rightarrow F_z = -K \; ; \qquad (3)$$

i.e., the vertical component of the flux is a constant, K. If positive z is taken to be away from the leaf's interior (on either side of the leaf's surface), then K will be positive for the case of deposition.

For the flux, account is taken only for Brownian or molecular diffusion (diffusivity D), gravitational settling (speed v_g; negative at the top of the leaf; positive, below), and Stefan drift velocity (v_{Sd}, given by Equation (2); positive for transpiration). Thus,

$$F_z = -D \frac{dC}{dz} + (v_{Sd} \mp v_g) C \; , \qquad (4)$$

with the minus or plus sign depending on whether the stomata are at the top or bottom of the leaf, respectively.

If Equation (4) is used in Equation (3) and the resulting equation is integrated and subjected to the boundary conditions (at z = 0, C = 0; at z = h, C = C_o, where h is the thickness of the stomatal opening), then the result for the concentration profile is

$$C/C_o = [\exp(kz') - 1]/[\exp(k) - 1] \; , \qquad (5)$$

in which z' = z/h is the nondimensional height and

$$k = (v_{Sd} \mp v_g)/(D/h) \qquad (6)$$

is the ratio of the two relevant speeds: the drift speed to the "diffusion speed" D/h. Notice from (5) that for $k \rightarrow 0$ (e.g., a gas molecule with $v_g \triangleq 0$ and $v_{Sd} = 0$), then expansion of the two exponentials in (5) leads to $C/C_o \rightarrow z/h$, which is a desired result (viz., with only diffusion, there should be a linear profile for the pollutant's concentration). Figure 2 gives plots of Equation (5) for other k values, including negative values (i.e., for particles with $v_g > v_{Sd}$ and stomata on the upper side of the leaf).

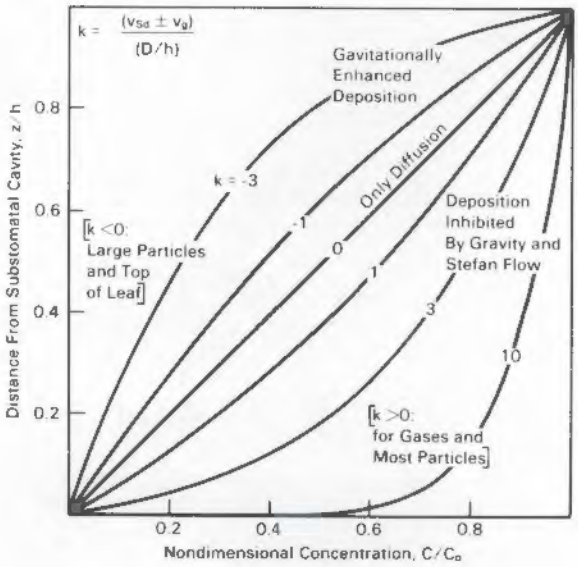

FIGURE 2. Concentration Profiles Within a Modeled Stoma as a Function of the Speed Ratio: Stefan Drift Speed (minus or plus gravitational settling at top or bottom of the leaf, respectively) to Diffusion Speed D/h.

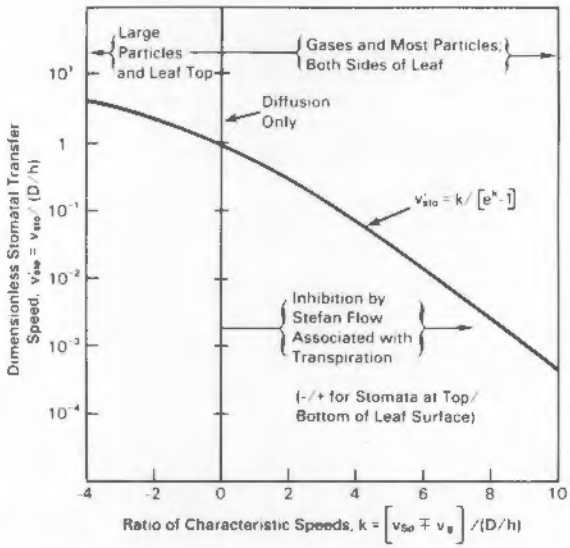

FIGURE 3. Transfer Velocity Through the "Stomatal" Opening as a Function of the Speed Ratio, k. This transfer velocity is enhanced over the value D/h if gravitational settling is larger than the Stefan drift speed (upper left); otherwise, the transfer velocity is substantially inhibited by transpiration (lower right).

The stomatal transfer velocity, v_{sto}, can now be obtained by dividing the magnitude of the flux, K, by C_o. The flux can be obtained by substituting Equation (5) into Equation (4). The result for v_{sto}, nondimensionalized with the diffusion speed D/h, is

$$v'_{sto} = v_{sto}/(D/h) = k/[\exp(k) - 1] \quad (7)$$

and is plotted in Figure 3 as a function of k. This result shows the potentially dramatic decrease in the stomatal transfer velocity (viz., dramatic increase in stomatal resistance) that can be caused by Stefan flow. For example, for $k \geq 4$ (i.e., Stefan drift velocity $v_{sd} \geq 4\ D/h$), then the stomatal resistance exceeds the value of the diffusion-only resistance of h/D by more than an order of magnitude.

It might be useful to comment here on the consequences of the assumption that the concentration at the top of the substomatal cavity (or equivalently, at the bottom of the cylinder), $C_{sc,a} \equiv C_b$, is zero. If this assumption were abandoned, then the transfer velocity would have been

$$[(C_o - C_b e^k)/(C_o - C_b)]\ k/[\exp(k) - 1] \ . \quad (8)$$

Since this (more realistic) result demonstrates that the flux is not related linearly to the concentration difference across the stoma, it reveals the failure of resistance models when there is a mean drift velocity (such as gravity) and when the perfect sink assumption is abandoned. However, because the resulting formulation is not so appealing and because the entire analysis here contains many approximations, the assumption that $C_b = 0$ will be maintained--until the entire problem is examined more rigorously.

Thus, with the results from the simple model, the ingredients are now available to estimate the overall resistance to (or deposition velocity for) "particle" transport to the substomatal cavity. Using the notation of Figure 2, $r_{atm} = r_a + r_c$ is the resistance to particle transport to the stomatal opening, and therefore, r_{atm} is the inverse of the "whole plant, perfect sink" deposition velocity (Slinn 1982), labeled now as $v_{d,1}$. Consequently, the overall resistance from the bulk atmosphere to the substomatal cavity, $(v_{d,ssc})^{-1}$, can be found by summing the resistances r_{atm} and the stomatal resistance given by the inverse of the transfer velocity v_{sto} in Equation (7):

$$v_{d,ssc}^{-1} = r_{atm} + v_{sto}^{-1} = v_{d,1}^{-1} + v_{sto}^{-1} \ . \quad (9)$$

Equation (9) is plotted in Figure 4 for two different wind speeds (Slinn 1982), three transpiration rates (viz., the three Stefan

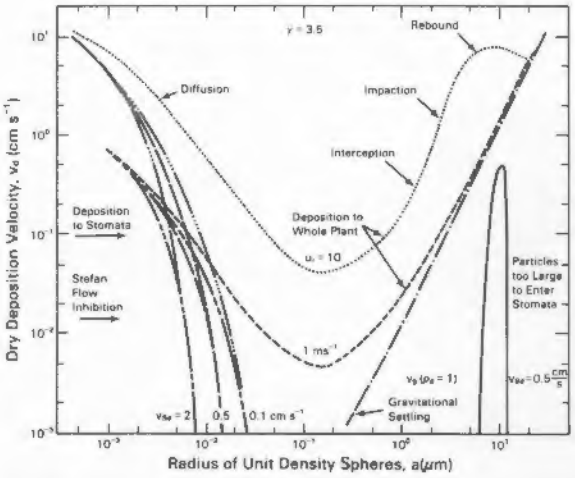

FIGURE 1. Comparisons Between Results for the Distance Dependence of the Normalized Concentration Predicted by the Current Theory, Equation (9) with Results for a Gaussian Plume, Equation (16). The comparison reveals that the show-down signularity of the Gaussian plume model is eliminated by including x-diffusion.

velocities of 0.1, 0.5, and 2.0 cm s^{-1}), and using h = 10 μm. For the Stefan velocity of 0.5 cm s^{-1}, a single curve is also shown for the case when gravitational settling overcomes Stefan drift (on the upper side of the leaf): see the "blip" near the particle radius of 10 μm. However, the resulting potential for particle transfer to the substomatal cavity is small, since the particle size needed to overcome the Stefan flow is comparable to or larger than the stomatal opening itself.

Conclusions

From Figure 4 and the fact that there are few particles in the atmosphere smaller than about 0.01 μm (because of rapid interparticle coagulation of such small particles; see Slinn 1983b), it can be concluded that essentially no aerosol particles enter the substomatal cavities of transpiring plants, unless the transpiration rate is low (and the stomata are open, e.g., when the relative humidity is high). Similarly, high-molecular-weight gases (diffusivity $D < hv_{sd}/4 \sim 10^{-4}$ cm^2 s^{-1}) are substantially inhibited from stomatal entry by the counterflowing water vapor. The suggestion in Figure 4 that even small-molecular-weight gases may be inhibited from passage through stomata at high wind speeds should not be considered too seriously until a more rigorous analysis of the whole problem is performed. Many opportunities for improvements to the analysis are clear, but it is expected that the major results of this scoping study are sound.

Stefan flow therefore appears to have survival value for plants. That is, Stefan flow associated with transpiration apparently inhibits entrance to the substomatal cavity of, for example, submicron sulfuric acid droplets (derived from natural and anthropogenic emissions of reduced sulfur compounds such as H_2S and SO_2), and yet this Stefan flow negligibly influences CO_2 exchange. Similarly, bacteria and high-molecular-weight gases (e.g., used in agricultural practices) are inhibited from entering the substomatal cavity by Stefan flow: trying to pass such material through a transpiring stoma is like a parachutist trying to jump down the throat of a large industrial cooling tower! However, transpiration through stomata appears to insignificantly inhibit the passage of relatively small molecules (e.g., SO_2, O_3, HNO_3, PAN, etc.) through the stomata, and therefore, by entering the substomatal cavity, such pollutants have greater potential for threatening plant survival, if their concentrations are excessive.

References

Bennett, J. H. , A. C. Hill and D. M. Gates. 1973. "A Model for Gaseous Pollutant Sorption by Leaves." J. Air Pol. Cont. Assoc. 23:957-962.

Horst, T. W., and W. G. N. Slinn. 1984. "Estimates for Pollution Profiles Above Finite Area-Sources." Atmos. Env. 18:1339-1346.

O'Dell, R. A., M. Taheri and R. L. Kabel. 1977. "A Model for Uptake of Pollutants by Vegetation." J. Air Pol. Cont. Assoc. 27:1104-1109.

Slinn, W. G. N. 1982. "Predictions for Particle Deposition to Vegetative Canopies." Atmos. Env. 16:1785-1794.

Slinn, W. G. N. 1983a. "Air-to-Sea Transfer of Particles." In Air-Sea Exchange of Particles and Gases, eds. P. S. Liss and W. G. N. Slinn, pp. 299-405 (see esp. pp. 391-393). Reidel, Boston.

Slinn, W. G. N. 1983b. "Sources and Surface-Area Distributions of Atmospheric Particles." Atmos. Env. 17:2263-2264.

Waldmann, L., and K. H. Schmitt. 1966. "Thermophoresis and Diffusiophoresis of Aerosols." Chapter VI of Aerosol Science, ed., C. N. Davies, pp. 137-162. Academic Press, New York.

Publications and Presentations

PUBLICATIONS

Bader, D. C., T. B. McKee and G. J. Tripoli. 1987. "Mesoscale Boundary Layer Evolution Over Complex Terrain. Part 1. Numerical Simulation of the Diurnal Cycle." J. Atmos. Sci. (in press).

Ballinger, M. Y., J. Defferding, E. G. Chapman, M. D. Bettinson and C. S. Glantz. 1987. User's Guide to a Data Base of Current Environmental Monitoring Projects in the U.S.-Canadian Transboundary Region. PNL-6377, Pacific Northwest Laboratory, Richland, Washington.

Ballinger, M. Y., P. C. Owczarski, J. W. Buck and J. E. Ayer. 1987. Methods for Describing Airborne Fractions of Free Fall Spills of Powders and Liquids. NUREG/CR-4997, PNL-6300, U.S. Nuclear Regulatory Commission, Washington, D.C.

Buck, J. W., and J. G. Droppo. 1987. "Characterization of the Atmospheric Pathway at Hazardous Waste Sites." In SUPERFUND '87 Hazardous Materials Control Research Institute 8th National Conference and Exhibition, November 16-18, 1987, Washington, D.C. (in press).

Chapman, E. G., D. J. Luecken, M. T. Dana, R. C. Easter, J. M. Hales, N. S. Laulainen and J. M. Thorp. 1987. "Inter-Storm Comparisons from the OSCAR High Density Network Experiment." Atmos. Environ. 21(3):531-549.

Chapman, E. G., D. J. Luecken and C. D. Whiteman. 1987. Application and Sensitivity Studies of the Reactive Storm Model MCCP PLUVIUS. PNL-6292, Pacific Northwest Laboratory, Richland, Washington.

Chapman, E. G., and D. S. Sklarew. 1987. "Introduction of Formate and Acetate Ions into Precipitation: Assessment of Possible Pathways." In Symposium on the Chemistry of Acid Rain: I. Sources & Atmospheric Processes, eds. R. W. Johnson and G. E. Gordon, Chapter 19, pp. 219-220. American Chemical Society, Washington, D.C.

Dana, M. T. 1987. The MAP3S Precipitation Chemistry Network: Eighth Periodic Summary Report (1984). PNL-6055, Pacific Northwest Laboratory, Richland, Washington.

Dana, M. T., and R. C. Easter. 1987. "Statistical Summary and Analyses of Event Precipitation Chemistry from the MAP3S Network, 1976-1983." Atmos. Environ. 21(1):113-128.

Dana, M. T., and W. G. N. Slinn. "Acidic Deposition Distribution and Episode Statistics from the MAP3S Network Data Base." Atmos. Environ., in press.

Dickerson, R. R., G. J. Huffman, W. T. Luke, L. J. Nunnermacker, K. E. Pickering, A. C. D. Leslie, C. G. Lindsey, W. G. N. Slinn, T. J. Kelly, P. H. Daum, A. C. Delany, J. P. Greenberg, P. R. Zimmerman, J. F. Boatman, J. D. Ray and D. H. Stedman. 1987. "Thunderstorms: An Important Mechanism in the Transport of Air Pollutants." Science 235:460-465.

Doran, J. C. 1987. "Sensitivity Studies Using Pielke's Model for Øresund Wind Simulation." In The Øresund Experiment - Proceedings from Workshop II, pp. 39-42, October 13-14, 1987, Uppsala, Sweden.

Doran, J. C., and S.-E. Gryning. 1987. "Wind and Temperature Structure Over a Land-Water-Land Area." J. Climate Appl. Meteor. 26(8):973-979.

Doran, J. C., T. W. Horst and C. D. Whiteman. 1987. "Wind and Temperature Structure on the Slopes of a Mountain Valley." In Extended Abstracts of the Fourth Conference on Mountain Meteorology, American Meteorological Society, Boston, Massachusetts, August 25-28, 1987, Seattle, Washington (in press).

Droppo, J. G., and R. M. Ecker. 1987. "Development of a Gaussian Puff Model for Over-Ocean Incineration Applications." In Proceedings of SUPERFUND '87 Hazardous Materials Control Research Institute 8th National Conference and Exhibition, November 16-18, 1987, Washington, D.C.

Hales, J. M., C. M. Berkowitz and R. C. Easter. 1987. "Wet Scavenging Processes." In Preprints of the NATO-CCMS 16th International Technical Meeting on Air Pollution Modeling, pp. 85-102. Plenum Publishing Corp., New York, New York, April 6-10, 1987, Lindau, Federal Republic of Germany.

Hales, J. M., B. B. Hicks and J. M. Miller. 1987. "The Role of Research Measurement Networks as Contributors to Federal Assessments of Acid Deposition." Bull. Amer. Meteor. Soc. 68(3):216-225.

Horst, T. W., K. J. Allwine and C. D. Whiteman. 1987. "A Thermal Energy Budget for Nocturnal Drainage Flow in a Simple Valley." In Extended Abstracts of the Fourth Conference on Mountain Meteorology, American Meteorological Society, Boston, Massachusetts, August 25-28, 1987, Seattle, Washington (in press).

Horst, T. W., and J. C. Doran. 1987. "The Turbulence Structure of Nocturnal Slope Flow." Accepted for publication in J. Atmos. Sci.

Hubbe, J. M., C. D. Whiteman, H. P. Foote and L. G. McWethy. 1987. "Applications of Digital Image Processing in Ongoing Research to Complex Terrain Meteorology." In Proceedings of SPIE's 1987 Cambridge Symposium on Digital Image Processing and Visual Communications Technologies in Meteorology, October 25-30, 1987, Cambridge, Massachusetts.

Laulainen, N. S., and E. G. Chapman. 1987. Precipitation Scavenging Module Development Quarterly Progress Report: April - June 1987. PNL-4647-19, Pacific Northwest Laboratory, Richland, Washington.

Laulainen, N. S., D. J. Luecken and J. M. Hales. 1987. "Model Investigations of Atmospheric Ammonia Scavenging." In Proceedings of International Symposium on Ammonia and Acidification, pp. 149-173. National Institute of Public Health, and Environmental Hygiene, Bilthoven, The Netherlands, April 14, 1987, Bilthoven, The Netherlands.

Lee, R. N., K. J. Allwine and M. M. Orgill. 1987. "Real-Time Measurement of Multiple Perfluorocarbon Tracers." Submitted to J. Atmospheric Oceanic Technology.

Lepel, E. A., et al. "In-Situ Gamma-Ray Measurements in the Chernobyl Plume." J. Rad. & Nuclear Chem., in press.

Lindsey, C. G. 1988. "Interpreting National Weather Service Rawinsonde Wind Profiles: A Note of Caution for Pollutant Transport Studies." Submitted to J. Climate Appl. Meteor.

Mueller, H., and C. D. Whiteman. 1987. "Buildup of a Nocturnal Temperature Inversion in the Dischma Valley During DISKUS." Accepted for publication in J. Climate Appl. Meteor.

Pielke, R. A., M. Garstang, C. G. Lindsey and J. Gusdorf. 1987. "Use of a Synoptic Classification Scheme to Define Seasons." Theor. and Appl. Climo. (in press).

Ramsdell, J. V. 1987. Atmospheric Diffusion for Control Room Habitability Assessments. NUREG/CR-5055, PNL-6391, U.S. Nuclear Regulatory Commission, Washington, D.C.

Ramsdell, J. V., G. F. Athey, T. J. Bander, R. I. Scherpelz. 1987. The MESORAD Dose Assessment Model, Volume 2: Computer Code. NUREG/CR-4000, PNL-5219, Vol. 2, U.S. Nuclear Regulatory Commission, Washington, D.C.

Scherpelz, R. I., T. J. Bander, G. F. Athey and J. V. Ramsdell. 1987. "The MESORAD Dose Assessment Model." In Proceedings of the American Nuclear Society Topical Meeting - Radiological Accidents: Perspectives and Emergency Preparedness, pp. 237-240. American Nuclear Society, La Grange Park, Illinois, September 15-17, 1986, Bethesda, Maryland.

Scott, B. C. 1987. User's Manual for the Cloud and Scavenging Module Version 1.2. PNL-6192, Pacific Northwest Laboratory, Richland, Washington.

Slinn, W. G. N. "Concentration Statistics for Dispersive Media." Tellus-B, in press.

Slinn, W. G. N. "On Junge's Relationship Between Concentration Fluctuations and Residence Times for Tropospheric Trace Gases." Tellus-B, in press.

Slinn, W. G. N. 1987. "Transpiration's Inhibition of Air Pollution Fluxes to Substomatal Cavities." In Proceedings of Eighth Conference on Biometeorology, pp. 277-280, American Meteorological Society, Boston, Massachusetts.

Vergeiner, I., E. Dreiseitl and C. D. Whiteman. 1987. "Dynamics of Katabatic Winds in Colorado's Brush Creek Valley." J. Atmos. Sci. 44:148-157.

Whiteman, C. D., K. J. Allwine, J. M. Hubbe, H. P. Foote, M. M. Orgill and L. J. Fritschen. 1987. "Radiation and Surface Energy Budgets for a Colorado Valley." In Extended Abstracts of the Fourth Conference on Mountain Meteorology, American Meteorological Society, Boston, Massachusetts, August 25-28, 1987, Seattle, Washington (in press).

Whiteman, C. D., R. Lambeth and K. J. Allwine. 1987. Major Vegetation Types, Climatological Data and Solar Radiation Calculations for Colorado's Brush Creek Valley. PNL-6209/ASCOT-87-1, Pacific Northwest Laboratory, Richland, Washington.

PRESENTATIONS

Bader, D. C. 1987. "Valley Mass and Energy Budgets Computed From Model Simulations." Preprints, Fourth Conference on Mountain Meteorology, August 25-28, 1987, Seattle, Washington. American Meteorological Society, Boston, Massachusetts, pp. 149-150.

Baer, D. R. 1986. "XPS, AES, RBS, NRA and Laser Raman Studies of Oxidation." Invited paper presented at the Norman L. Peterson Memorial Symposium of Oxidation of Metals, Fall Meeting of the Metals Society of the AIME, October 1986, Orlando, Florida.

Baer, D. R., A. C. D. Leslie, M. H. Englehard and M. E. Middendorf. 1987. "Analysis of Materials and Contaminants Using PIXE." Paper presented at the Fall Meeting of the Metals Society, October 1987, Cincinnati, Ohio.

Ballinger, M. Y., and P. C. Owczarski. 1987. "Radioactive Aerosols from Burning Contaminated Combustible Liquids." Paper presented at the 18th Annual Meeting of the Fine Particle Society, August 3-7, 1987, Boston, Massachusetts.

Barchet, W. R., A. R. Olsen, D. S. Daly and D. B. Carr. 1987. "Temporal Changes in Wet Deposition for Eastern North America from 1980 to 1984." Paper presented at the EMEP Workshop on Data Analysis and Presentation, June 15-17, 1987, Cologne, Federal Republic of Germany, The Netherlands.

Barchet, W. R., A. R. Olsen and D. W. Engel. 1987. "Spatial Patterns in Wet Deposition for Eastern North America: A 1980-1984 Composite." Paper presented at the EMEP Workshop on Data Analysis and Presentation, June 15-17, 1987, Cologne, Federal Republic of Germany, The Netherlands.

Berkowitz, C. M., and R. R. LaBarge. 1987. "Regional Acid Deposition Model (RADM) Scavenging Module Code Package." Paper presented at the U.S. Environmental Protection Agency Tutorial Audit, August 3-5, 1987, Raleigh, North Carolina.

Berkowitz, C. M., and D. J. Luecken. 1987. "Sensitivity Studies from Two Scavenging Models." Paper presented at the ACID-MODES Workshop, August 4-7, 1987, Raleigh, North Carolina.

Donley, M. S., D. R. Baer and T. G. Stoebe. 1987. "Nitrogen 1s Charge Referencing for Si_3N_4 and Related Compounds." Paper presented at the Applied Surface Analysis Symposium, June 1987, Dayton, Ohio.

Doran, J. C., T. W. Horst and C. D. Whiteman. 1987. "Wind and Temperature Structure on the Slopes of a Mountain Valley." Preprints, Fourth Conference on Mountain Meteorology, August 25-28, 1987, Seattle, Washington. American Meteorological Society, Boston, Massachusetts, pp. 48-51.

Horst, T. W., K. J. Allwine and C. D. Whiteman. 1987. "A Thermal Energy Budget for Nocturnal Drainage Flow in a Simple Valley." Preprints, Fourth Conference on Mountain Meteorology, August 25-28, 1987, Seattle, Washington. American Meteorological Society, Boston, Massachusetts, pp. 15-19.

Hubbe, J. M., C. D. Whiteman, H. P. Foote and L. G. McWethy. 1987. "Applications of Digital Image Processing in Ongoing Research in Complex Terrain Meteorology." SPIE's 1987 Cambridge Symposium on Digital Image Processing and Visual Communications Technologies in Meteorology, October 25-30, 1987, Cambridge, Massachusetts.

Slinn, W. G. N. 1987. "Concepts for Anticipating Global Change." Paper presented at the DOE Global Change Meeting, June 8-12, 1987, Chicago, Illinois.

Slinn, W. G. N. 1987. "Outlines for a General Environmental Chemistry Model." Paper presented at the DOE Global Change Meeting, March 16-17, 1987, Boulder, Colorado.

Slinn, W. G. N. 1987. "Outlines of a New Initiative: Anticipating Global Changes." Paper presented to the Director of DOE's Office of Health & Environmental Research, August 5, 1987, Germantown, Maryland.

Slinn, W. G. N. 1987. "Transpiration's Inhibition of Air Pollution Fluxes to Substomatal Cavities." Paper presented at the Eighth Conference on Biometeorology & Aerobiology of the AMS, September 14-18, 1987, Lafayette, Indiana.

Whiteman, C. D., K. J. Allwine, J. M. Hubbe, H. P. Foote, M. M. Orgill and L. J. Fritschen. 1987. "Radiation and Surface Energy Budgets for a Colorado Valley." Preprints, Fourth Conference on Mountain Meteorology, August 25-28, 1987, Seattle, Washington. American Meteorological Society, Boston, Massachusetts, pp. 11-14.

Author Index

AUTHOR INDEX

Distribution

DISTRIBUTION

No. of Copies

OFFSITE

10 DOE/Office of Scientific and Technical Information

R. E. Alexander
ORPBR, NL
Nuclear Regulatory Commission
Washington, DC 20545

E. L. Alpen
Donner Laboratory
University of California
Berkeley, CA 94720

D. Anderson
ENVIROTEST
1108 N.E. 200th St.
Seattle, WA 98155

J. A. Auxier
IT/Radiological Sciences Laboratory
1550 Bear Creek Road
Box 549
Oak Ridge, TN 37831

F. Badgley
13749 41st Street, N.E.
Seattle, WA 98125

R. E. Baker
820 Ivy League Lane
Rockville, MD 20850

R. W. Barber
EH-133, GTN
Department of Energy
Washington, DC 20545

A. D. Barker
Battelle, Columbus Laboratories
505 King Avenue
Columbus, OH 43201

J. R. Barker
Office of Environmental Audit and Compliance
Department of Energy
Washington, DC 20545

No. of Copies

H. M. Barnes
ASRL (MD-57)
U.S. Environmental Protection Agency
Research Triangle Park, NC 27711

N. F. Barr
ER-73, GTN
Department of Energy
Washington, DC 20545

S. Barr
Environmental Studies Group
MS-D466
Los Alamos National Laboratory
P.O. Box 1663
Los Alamos, NM 87544

J. A. Bibb
DOE - Oak Ridge Operations Office
P.O. Box E
Oak Ridge, TN 38730

J. F. Boatman
NOAA/ERL/AQC
325 Broadway
Boulder, CO 80303

L. C. Brazley, Jr.
NE-22, GTN
Department of Energy
Washington, DC 20545

J. C. Brown
Environmental Studies Group
MS-A114
Los Alamos National Laboratory
P.O. Box 1663
Los Alamos, NM 87545

P. Buhl
FE-34, GTN
Department of Energy
Washington, DC 20545

R. J. Bull
Associate Professor of Pharmacology/Toxicology
College of Pharmacy
Pullman, WA 99164-6510

No. of Copies

D. Bunch
Assistant Secretary for Safety, Health and Quality Assurance
EH-30, GTN
Washington, DC 20545

G. Burley
Office of Radiation Programs (ANR-458)
U.S. Environmental Protection Agency
Washington, DC 20460

W. W. Burr
Oak Ridge Associated Universities
P.O. Box E
Oak Ridge, TN 37830

L. K. Bustad
College of Veterinary Medicine
Washington State University
Pullman, WA 99163

R. Catlin
Electric Power Research Institute
3412 Hillview Avenue
Palo Alto, CA 94304

J. Chang
Atmospheric Sciences Research Center
State University of New York at Albany
100 Fuller Road
Albany, NY 80307

R. J. Charlson
Department of Atmospheric Sciences
University of Washington
Seattle, WA 98195

J. A. Coleman
NE-24, GTN
Department of Energy
Washington, DC 20545

Council on Environmental Quality
72 Jackson Place, NW
Washington, DC 20006

No. of Copies

T. V. Crawford
E. I. Du Pont de Nemours and Co.
Atomic Energy Division
Savannah River Laboratory
Aiken, SC 29808

J. B. Cunning
NOAA/ERL
325 Broadway
Boulder, CO 80303

P. H. Daum
Brookhaven National Laboratory
Upton, Long Island, NY 11973

J. Decker
ER-1, FORS
Department of Energy
Washington, DC 20585

K. Demerjian
Atmospheric Sciences Research Center
State University of New York at Albany
100 Fuller Road
Albany, NY 80307

R. L. Dennis
ASRL (MD-80)
U.S. Environmental Protection Agency
Research Triangle Park, NC 27711

G. DePlanque
13 Bowdoin Street
Maplewood, NJ 07040

M. H. Dickerson
L-262
P.O. Box 808
Livermore, CA 94550

R. R. Dickerson
Department of Meteorology
University of Maryland
College Park, MD 20742

H. Drucker
Argonne National Laboratory
9700 South Cass Avenue
Argonne, IL 60439

A. P. Duhamel
ER-74, GTN
Department of Energy
Washington, DC 20545

No. of Copies

J. L. Durham
ASRL (MD-59)
U.S. Environmental Protection Agency
Research Triangle Park, NC 27711

W. H. Ellett
Project Director
National Academy of Sciences, JH-554
2101 Constitution Avenue, NW
Washington, DC 20418

R. J. Engelmann
11701 Karen
Potomac, MD 20854

Environmental Measurements Laboratory
Department of Energy
375 Hudson Street
New York, NY 10014

B. M. Erickson
DOE - Schenectady Naval Reactors Office
P.O. Box 1069
Schenectady, NY 12301

G. J. Foley, Director
EMSL (MD-75)
U.S. Environmental Protection Agency
Research Triangle Park, NC 27711

R. D. Gilmore, President
Environmental Health Sciences, Inc.
Nine Lake Bellevue Building
Suite 104
Bellevue, WA 98005

G. H. Gronhovd
Grand Forks Energy Research Center
Department of Energy
Box 8213, University Station
Grand Forks, ND 58202

J. W. Healy
51 Grand Canyon Drive
White Rock, NM 87544

No. of Copies

B. Hicks
National Oceanic and Atmospheric Administration
Atmospheric Turbulence and Diffusion Laboratory
P.O. Box 2456
Oak Ridge, TN 37830

F. Hutchinson
Department of Molecular Biophysics and Biochemistry
Yale University
P.O. Box 6666
260 Whitney Ave.
New Haven, CT 06511

H. Ishikawa
General Manager
Nuclear Safety Research Association
P.O. Box 1307
Falls Church, VA 22041

A. Johnson
Vice President for Academic Affairs
San Diego State University
San Diego, CA 92128

L. J. Johnson
EG&G Idaho
P.O. Box 1625
Idaho Falls, ID 83415

G. Y. Jordy
ER-30, GTN
Department of Energy
Washington, DC 20545

F. Koomonoff
ER-12, GTN
Department of Energy
Washington, DC 20545

R. Kornasiewicz
Mail Stop 1130-55, ONRR
Nuclear Regulatory Commission
Washington, DC 20555

R. T. Kratzke
EH-131, GTN
Department of Energy
Washington, DC 20545

No. of Copies

D. Lal
Geological Research Division A-020
Scripps Institute of Oceanography
La Jolla, CA 92093

T. V. Larsen
Department of Civil Engineering
University of Washington
Seattle, WA 98195

W. Lauder
Office of Health and Environmental Research
Office of Energy Research
Department of Energy
Washington, DC 20545

L. Levin
Electric Power Research Institute
3412 Hillview Ave.
Palo Alto, CA 94303

Librarian
Brookhaven National Laboratory
Research Library, Reference
Upton, Long Island, NY 11973

Librarian
Colorado State University
Serials Section
Ft. Collins, CO 80521

Librarian
Electric Power Research Institute
P.O. Box 10412
Palo Alto, CA 94303

Librarian
Atmospheric Sciences Library, AK-50
University of Washington
Seattle, WA 98195

Librarian
Health Sciences Library, SB-55
University of Washington
Seattle, WA 98195

No. of Copies

Librarian
Lawrence Livermore National Laboratory
University of California
Technical Information Dept., L-3
P.O. Box 808
Livermore, CA 94550

Librarian
Los Alamos National Laboratory
P.O. Box 1663
Los Alamos, NM 87545

Librarian
Tri-Cities University Center
100 Sprout Road
Richland, WA 99352

I. R. Linger
ER-63, GTN
Department of Energy
Washington, DC 20545

D. L. Lundgren
Lovelace - ITRI
P.O. Box 5890
Albuquerque, NM 87185

O. R. Lunt
Laboratory of Nuclear Medicine and Radiation Biology
University of California
900 Veteran Avenue
West Los Angeles, CA 90024

D. P. MacDonald
10830 S.W. Canterbury Lane
Apt. 66
Tigard, OR 97224

J. N. Maddox
ER-73, GTN
Department of Energy
Washington, DC 20545

W. J. Madia, Director
Battelle Columbus Laboratory
505 King Avenue
Columbus, OH 43201

J. R. Maher
ER-65, GTN
Department of Energy
Washington, DC 20545

No. of Copies

J. Mahoney
National Acid Precipitation Assessment Program
722 Jackson St.
Washington, DC 20006

B. Manowitz
Energy and Environment Division
Brookhaven National Laboratory
Upton, Long Island, NY 11973

S. Marks
8024 47th Place West
Mukilteo, WA 98275

D. D. Mayhew
ER-63, GTN
Department of Energy
Washington, DC 20545

H. M. McCammon
ER-75, GTN
Department of Energy
Washington, DC 20545

R. O. McClellan
Inhalation Toxicology Research Institute
Lovelace Foundation for Medical Education and Research
P.O. Box 5890
Albuquerque, NM 87115

T. F. McCraw
EH-132, GTN
Department of Energy
Washington, DC 20545

C. B. Meinhold
Safety and Environmental Protection Division
Brookhaven National Laboratory
Upton, Long Island, NY 11973

M. L. Mendelsohn
Biomedical and Environmental Research Program
Lawrence Livermore National Laboratory, L-523
University of California
P.O. Box 808
Livermore, CA 94550

No. of Copies

P. Michael
Brookhaven National Laboratory
Upton, NY 11973

C. Miller
P.O. Box 180
Watermill, NY 11976

M. L. Minthorn, Jr.
ER-72, GTN
Department of Energy
Washington, DC 20545

V. Mohnen
State University of New York at Albany
100 Fuller Road
Albany, NY 80307

D. R. Monti
ER-14, GTN
Department of Energy
Washington, DC 20545

B. Morgan
Environmental Division
DOE - Savannah River Operations Office
P.O. Box A
Aiken, SC 29801

H. Moses
ER-74, GTN
Department of Energy
Washington, DC 20545

W. E. Mott
EH-12, GTN
Department of Energy
Washington, DC 20545

P. Mueller
EPRI, Environmental Science Division
P.O. Box 10412
Palo Alto, CA 94303

R. Nathan
Battelle Project Management Division
505 King Avenue
Columbus, OH 43201

W. Neff
Wave Propogation Lab, NOAA
325 Broadway
Boulder, CO 80303

No. of Copies

N. Nelson
Environmental Protection Agency
Washington, DC 20460

L. Newman
Brookhaven National Laboratory
Upton, Long Island, NY 11973

W. R. Ney, Executive Director
National Council on Radiation Protection and Measurements
7910 Woodmont Avenue
Suite 1016
Bethesda, MD 20B14

Nuclear Regulatory Commission
Advisory Committee on Reactor Safeguards
Washington, DC 20555

M. J. O'Brien
Radiation Safety Office
University of Washington, GS-05
Seattle, WA 98105

G. Oertel
Deputy Assistant Secretary for Safety, Health and Quality Assurance
Department of Energy
Washington, DC 20545

A. A. Patrinos
ER-74, GTN
Department of Energy
Washington, DC 20545

R. Pawr
EMSL (MD-44)
U.S. Environmental Protection Agency
Research Triangle Park, NC 27711

A. A. Pitrolo
Morgantown Energy Research Center
Department of Energy
P.O. Box 880
Morgantown, WV 26505

No. of Copies

R. G. Rader
ER-33, GTN
Department of Energy
Washington, DC 20545

D. P. Rall, Director
NIEHS
P.O. Box 12233
Research Triangle Park, NC 27709

C. R. Richmond
Oak Ridge National Laboratory
P.O. Box X
Oak Ridge, TN 37830

J. S. Robertson
ER-73, GTN
Department of Energy
Washington, DC 20545

J. M. Rusin
404 W. Halladay
Seattle, WA 98119

L. Sagan
Electric Power Research Institute
3412 Hillview Avenue
P.O. Box 10412
Palo Alto, CA 94304

P. Samson
Atmospheric and Oceanic Sciences
University of Michigan
Ann Arbor, MI 48109

R. A. Scarano
Nuclear Regulatory Commission
Mill Licensing Section
Washington, DC 20545

F. A. Schiermeier
U.S. Environmental Protection Agency
Environmental Sciences Research Laboratory (MD-80)
Research Triangle Park, NC 27711

M. Schulman
ER-70, GTN
Department of Energy
Washington, DC 20545

No. of Copies

R. Setlow
Brookhaven National Laboratory
Upton, NY 11973

R. Shikiar
Battelle - Seattle
4000 NE 41st Street
Seattle, WA 98105

P. Silverman
Donner Laboratory
University of California
Berkeley, CA 94720

J. Simmons
Bioeffects Analysis Branch
U.S. Environmental Protection Agency
401 M Street, S.W.
Washington, DC 20460

W. K. Sinclair, President
National Council on Radiation Protection and Measurements
7910 Woodmont Avenue
Suite 1016
Bethesda, MD 20814

D. H. Slade
ER-74, GTN
Department of Energy
Washington, DC 20545

J. Snow
ER-6, FORS
Department of Energy
Washington, DC 20585

C. Spicer
Battelle Columbus Laboratory
505 King Avenue
Columbus, OH 43201

J. N. Stannard
17441 Plaza Animado #132
San Diego, CA 92128

R. W. Starostecki
NE-40, GTN
Department of Energy
Washington, DC 20545

R. J. Stern
EH-10, FORS
Department of Energy
Washington, DC 20585

No. of Copies

J. F. Stevens
Dayton Area Office
DOE - Albuquerque Operations Office
P.O. Box 66
Miamisburg, OH 45342

E. T. Still
Kerr-McGee Corporation
P.O. Box 25861
Oklahoma City, OK 73125

G. Sverdrup
Battelle Columbus Laboratory
505 King Avenue
Columbus, OH 43201

J. Swinebroad
EH-12, GTN
Department of Energy
Washington, DC 20545

Technical Information Service
Savannah River Laboratory
Room 773A
E. I. du Pont de Nemours & Company
Aiken, SC 29801

R. G. Thomas
ER-72, GTN
Department of Energy
Washington, DC 20545

C. Tiller
RG-30, FORS
Department of Energy
Washington, DC 20585

U.S. Department of Energy
Environment, Safety and Health Division
P.O. Box 5400
Albuquerque, NM 87115

E. J. Vallario
EH-13, GTN
Department of Energy
Washington, DC 20545

C. R. Vest
Battelle Memorial Institute
Washington Operations
2030 M Street, NW
Washington, DC 20036

No. of Copies

G. J. Vodapivc
DOE - Schenectady Naval Reactors Office
P.O. Box 1069
Schenectady, NY 12301

G. L. Voelz
Los Alamos National Laboratory
P.O. Box 1663
Los Alamos, NM 87545

B. W. Wachholz
Low Level Radiation Effects Branch
National Cancer Institute
Landow Bldg., Room 8C09
Rockville Pike
Bethesda, MD 20205

M. L. Walker
EH-1, FORS
Department of Energy
Washington, DC 20585

R. A. Walters
Los Alamos National Laboratory
Assistant to the Associate Director
P.O. Box 1663
MS-A114
Los Alamos, NM 87545

M. E. Walsh
Battelle - Seattle
4000 NE 41st Street
Seattle, WA 98105

C. G. Welty, Jr.
EH-123, GTN
Department of Energy
Washington, DC 20545

I. Wender
Department of Chemical Engineering
1249 Benedum Hall
University of Pittsburgh
Pittsburgh, PA 15261

M. L. Wesely
Argonne National Laboratory
Building 181, ER
Argonne, IL 60439

W. W. Weyzen
Electric Power Research Institute
3412 Hillview Avenue
Palo Alto, CA 92665

No. of Copies

M. M. Williamson
DOE - Idaho Operations Commission
550 Second Street
Idaho Falls, ID 83401

F. J. Wobber
14 Goshen Court
Gaithersburg, MD 20879-4403

M. T. Wood
Battelle - Seattle
4000 NE 41st Street
Seattle, WA 98105

R. W. Wood
ER-74, GTN
Department of Energy
Washington, DC 20545

FOREIGN

W. A. Asman
Laboratory for Air Research
RIVM
P.O. Box 1
NL-3720 BA Bilthoven
THE NETHERLANDS

D. C. Aumann
Institut für Physikalische Chemie
Der Universität Bonn
Abt. Nuklearchemie
WegelerstraBe 12
5300 Bonn 1
FEDERAL REPUBLIC OF GERMANY

J. K. Basson
Raad Op Atomic
Atoomkrag Energy Board
Privaatsk X 256
Pretoria 0001
REPUBLIC OF SOUTH AFRICA

A. M. Beau, Librarian
Commissariat à l'Energie Atomique
Départment de Protection Sanitaire
BP No. 6
F-92260 Fontenay-aux-Roses
FRANCE

No. of Copies

G. Bengtsson
Director-General
Statens Stralskyddsinstitut
Box 60204
S-104 01 Stockholm
SWEDEN

D. J. Beninson
Gerencia de Protection Radiologica y Seguridad
Comision Nacional de Energia Atomica
Avenida del Libertador 8250
1429 Buenos Aires
ARGENTINA

R. Berkowicz
Air Pollution Laboratory
National Agency for Environmental Protection
Risø National Laboratory
DK-4000 Roskilde
DENMARK

A. Brink
SASOL-One Limited
P.O. Box 1
Sasolburg 9570
REPUBLIC OF SOUTH AFRICA

N. Busch
Risø National Laboratory
DK-4000 Roskilde
DENMARK

Cao Shu-yuan, Deputy Head
Laboratory of Radiation Medicine
North China Institute of Radiation Protection
Tai-yuan, Shan-xi
THE PEOPLE'S REPUBLIC OF CHINA

M. Carpentier
Commission of the E.C.
200 Rue de la Loi
J-70 6/16
B-1049 Brussels
BELGIUM

CEC
DG XII Library
SDM8 R1
200 Rue de la Loi
B-1049 Brussels
BELGIUM

No. of Copies

Chen Xing-an, M.D.
Laboratory of Industrial Hygiene
Ministry of Public Health
2 Xinkang Street
Deshangmanwai, Beijing
THE PEOPLE'S REPUBLIC OF CHINA

G. H. Clark
Australian Nuclear Science and Technology Organization
Environmental Science Division
Private Mail Bag 1
Menai NSW 2234
AUSTRALIA

R. Clarke
National Radiological Protection Board
Harwell, Didcot
Oxon OX11 ORQ
ENGLAND

P. Crutzen, Director
Atmospheric Chemistry
Max-Planck-Institut für Chemie
Postfach 3060
D-6500 Mainz
FEDERAL REPUBLIC OF GERMANY

H. T. Daw, Director
International Atomic Energy Agency
Kaerntner ring 11
A-1010 Vienna 1
AUSTRIA

Deng Zhicheng
North China Institute of Radiation Protection
Tai-yuan, Shan-xi
THE PEOPLE'S REPUBLIC OF CHINA

Director
Commissariat à l'Energie Atomique
Centre d'Etudes Nucléaires
Fontenay-aux-Roses (Seine)
FRANCE

Director
Commonwealth Scientific and Industrial Research Organization
Aspendal, Victoria
AUSTRALIA

No. of Copies

Director
Laboratorio di
Radiobiologia Animale
Centro di Studi Nucleari
Della Casaccia
Comitate Nazionale per
l'Energia Nucleare
Casella Postale 2400
00100 Roma
ITALY

D. Djuric
Institute of Occupational
and Radiological Health
11000 Beograd
Deligradoka 29
YUGOSLAVIA

H. Dovland
Director
Norwegian Institute for
Air Research
Elvegaten 52
N-2001 Lillestryom
NORWAY

H. J. Ounster
National Radiological
Protection Board
Harwell, Didcot
Oxon OX11 ORQ
ENGLAND

C. Edington
Radiation Effects Research
Foundation
S-2 Hijiyama Park
Minami-Ward
Hiroshima 732
JAPAN

L. Feinendegen, Director
Institut für Medezin
Kernsforschungsanlage
Jülich
Postfach 1913
D-5170 Jülich
FEDERAL REPUBLIC
OF GERMANY

R. M. Fry
Office of the Supervising
Scientist for the
Alligator Rivers Region
P.O. Box 387
Bondi Junction NSW 2022
AUSTRALIA

No. of Copies

G. B. Gerber
Radiobiology Department
Commission of European
Communities
Rue de la Loi
Brussels
BELGIUM

A. R. Gopal-Ayengar
73-Mysore Colony
Mahul Road, Chembur
Bombay-400 074
INDIA

P. Grennfelt
Swedish Water and Air
Pollution Research
Institute (IVL)
Dagjämningsgatan 1
P.O. Box 47086
S-402 58 Göteberg
SWEDEN

S. E. Gryning
Physics and Meteorology
Risø National Laboratory
DK-4000 Roskilde
DENMARK

G. F. Gualdrini
C.N.E.N.
V. Mazzini 2
40138 Bologna
ITALY

O. Hov
Norwegian Institute for
Air Research
Elvegaten 52
N-2001 Lillestryom
NORWAY

D. Irwin
Librarian
Supervising Scientist
for the Alligator
Rivers Region
P.O. Box 387
Bondi Junction 2022
AUSTRALIA

K. E. Lennart Johansson
National Defense Research
Institute
FOA 45 1
S-901 82 Umea
SWEDEN

No. of Copies

V. A. Kamath
Scientific Information
Officer
Library & Information
Service
Atomic Energy
Establishment, Trombay
Apollo Pier Road
Bombay-1
INDIA

Dr. rer. nat. Hans-Joachim
Klimisch
BASF Aktiengesellschaft
Abteilung Toxikologie
D-6700 Ludwigshafen
FEDERAL REPUBLIC
OF GERMANY

L. Kristensen
Physics and Meteorology
Risø National Laboratory
DK-4000 Roskilde
DENMARK

T. Kumatori, Director
National Institute of
Radiological Sciences
9-1, 4-Chome, Anagawa
Chiba-shi, Chiba 260
JAPAN

A. Lacser
Israel Institute of
Biological Research
Department of Mathematics
P.O. Box 19
704 50
Ness-Ziona
ISRAEL

J. R. A. Lakey
Director
Department of Nuclear
Sciences & Technology
Royal Naval College
Greenwich, London
SE10 9NN
ENGLAND

S. E. Larsen
Physics and Meteorology
Risø National Laboratory
DK-4000 Roskilde
DENMARK

No. of Copies

H. P. Leenmouts
National Institute of Public Health and Environmental Hygiene
P.O. Box 1, 3720 BA
Bilthoven
THE NETHERLANDS

Li De-ping
Professor and Director of North China Institute of Radiation Protection, NMI
Tai-yuan, Shan-xi
THE PEOPLE'S REPUBLIC OF CHINA

Librarian
Atomic Energy Research Establishment
Building 465
Harwell, Didcot
Oxon OX11 ORD
ENGLAND

Librarian
Australian Atomic Energy Commission
Riverina Laboratory
P.O. Box 226
Deniliquin, New South Wales 2710
AUSTRALIA

Librarian
Centre d'Etudes Nucléaires de Saclay
P.O. Box 2, Saclay
Fig-sur-Yvette (S&O)
FRANCE

Librarian
Commonwealth Scientific and Industrial Research Organization
314 Albert Street
P.O. Box 89
East Melbourne, Victoria
AUSTRALIA

Librarian
Commonwealth Scientific and Industrial Research Organization
Div. of Atmospheric Research
Station Street
Aspendale, Vic. 3195
AUSTRALIA

No. of Copies

Librarian
Commonwealth Scientific and Industrial Research Organization
Rangelands Research Centre
Private Mail Bag, P.O.,
Deniliquin, New South Wales 2710
AUSTRALIA

Librarian
ECN
3 Westerdiunweg
NL-1755 ZG Petten
THE NETHERLANDS

Librarian
ENEA (OECD) Health and Safety Office
38, Blvd. Suchet
Paris
FRANCE

Librarian
HCS/EHE
World Health Organization
CH-1211 Geneva 27
SWITZERLAND

Librarian
Kernforschungzentrum Karlsruhe
Institut für Strahlenbiologie
D-75 Karlsruhe 1
Postfach 3640
FEDERAL REPUBLIC OF GERMANY

Librarian
Max-Planck-Institut für Biophysics
Forstkasstrasse
D-6000 Frankfurt/Main
FEDERAL REPUBLIC OF GERMANY

Librarian
Ministry of Agriculture, Fisheries and Food
Fisheries Laboratory
Lowestoft, Suffolk NR33 OHT
ENGLAND

Library
Risø National Laboratory
DK-4000 Roskilde
DENMARK

No. of Copies

Library, Periodicals
Atomic Energy Commission of Canada, Ltd.
Pinawa, Manitoba ROE 1LO
CANADA

Library
Department of Meteorology
University of Stockholm
Arrhenius Laboratory
S-106 91 Stockholm
SWEDEN

A. M. Marko, Director
Atomic Energy Commission of Canada, Ltd.
Biology and Health Physics Division
Chalk River Nuclear Laboratories
P.O. Box 62
Chalk River, Ontario KOJ IJO
CANADA

K. Morita
Librarian
National Institute of Radiological Sciences
9-1, 4-Chome, Anagawa
Chiba-shi, Chiba 260
JAPAN

J. C. Nénot, Deputy Director
Département de Protection
Centre d' Etudes Nucléaires
BP No. 6
F-92260 Fontenay-aux-Roses
FRANCE

J. P. Oliver
ENEA (OECD) Health and Safety Office
38, Blvd. Suchet
Paris
FRANCE

N. Parmentier
Départment de Protection
Centre d'Etudes Nucléaires
BP No. 6
F-92260 Fontenay-aux-Roses
FRANCE

No. of Copies

L. Prahm, Director
Danish Meteorological Institute
Lyngbyvej 100
DK-2100 Copenhagen East
DENMARK

V. Prodi
Department of Physics
University of Bologna
Via Irnerio 46
I-40126 Bologna
ITALY

H. Rodhe
Meteorological Institute
Stockholm University
S-106 91 Stockholm
SWEDEN

P. J. A. Rombout
Inhalation of Toxicology Department
National Institute of Public Health and Environmental Hygiene
P.O. Box 1, 3720 BA Bilthoven
THE NETHERLANDS

M. Roy
Institut de Protection et de Sureté Nucléaire
Department de Protection Sanitaire
Service d'Etudes Apliquées de Protection Sanitaire
BP No. 6
F-92260 Fontenay-aux-Roses
FRANCE

M. Rzekiecki
Commissariat à l'Energie Atmoique
Centre d'Etudes Nucléaires de Cadarache
BP No. 13-St. Paul
Les Durance
FRANCE

G. Schnatz
Battelle-Europe eV
Am Römerhof 35
P.O. box 900160
D-6000 Frankfurt a.M.
FEDERAL REPUBLIC OF GERMANY

No. of Copies

W. Seiler, Director
Fraunhofer Institute for Atmospheric Environmental Research
Kreuzeckbahnstr. 19
D-8100 Garmisch-Partenkirchen
FEDERAL REPUBLIC OF GERMANY

G. Silini
Secretary, UNSCEAR
Vienna International Center
P.O. Box 500
A-1400 Vienna
AUSTRIA

R. Skogstrom, Chief Librarian
Meteorological Institute
University of Stockholm
Arrhenius Laboratory
S-106 91 Stockholm
SWEDEN

J. Slanina
ECN
3 Westerduinweg
NL-1755 ZG Petten
THE NETHERLANDS

H. Smith, Head
Biology Department
National Radiological Protection Board
Chilton, Didcot
Oxon OX11 ORQ
ENGLAND

R. Söderlund
Air Pollution Laboratory
National Environmental Protection Board
P.O. Box 1302
S-171 25 Solna
SWEDEN

J. W. Stather
National Radiological Protection Board
Building 383
Harwell, Didcot
Oxon OX11 ORQ
ENGLAND

No. of Copies

M. J. Suess
Regional Officer for Environmental Hazards
World Health Organization
8, Scherfigsvej
DK-2100 Copenhagen
DENMARK

Sun Shi-quan, Head
Radiation-Medicine Department
North China Institute of Radiation Protection
Tai-yuan, Shan-xi
THE PEOPLE'S REPUBLIC OF CHINA

J. W. Thiessen
Radiation Effects Research Foundation
5-2 Hijiyama Park
Minami - Ward
Hiroshima 732
JAPAN

M. Thorne
International Commission on Radiological Protection
Clifton Avenue
Sutton, Surrey
ENGLAND

United Nations Scientific Committee on the Effects of Atomic Radiation
Vienna International Center
P.O. Box 500
A-1400 Vienna
AUSTRIA

R. Van Aalst
Laboratory for Air Research
RIVM
P.O. Box 1
NL-3720 BA Bilthoven
THE NETHERLANDS

D. Van As
Private Bag X256
Pretoria 0001
Atomic Energy Board
REPUBLIC OF SOUTH AFRICA

No. of Copies

Vienna International Centre Library
Gifts and Exchange
P.O. Box 100
A-1400 Vienna
AUSTRIA

Wang Renzhi
Institute of Radiation Medicine
11# Tai Ping Road
Beijing
THE PEOPLE'S REPUBLIC OF CHINA

Wang Ruifa, Associate Director
Laboratory of Industrial Hygiene
Ministry of Public Health
2 Xinkang Street
Deshangmanwai, Beijing
THE PEOPLE'S REPUBLIC OF CHINA

Wang Yibing
North China Institute of Radiation Protection
P.O. Box 120
Tai-yuan, Shan-xi
THE PEOPLE'S REPUBLIC OF CHINA

Wei Luxin
Laboratory of Industrial Hygiene
Ministry of Public Health
2 Xinkang Street
Deshangmanwai, Beijing
THE PEOPLE'S REPUBLIC OF CHINA

B. C. Winkler
P.O. Box 4587
Pretoria 0001
REPUBLIC OF SOUTH AFRICA

Wu De-Chang
Institute of Radiation Medicine
11# Tai Ping Road
Beijing
THE PEOPLE'S REPUBLIC OF CHINA

Yao Jiaxiang, M.D.
2 Xinkang Street
Deshengmenwai
Beijing 100011
THE PEOPLE'S REPUBLIC OF CHINA

Zhu Zhixian
North China Institute of Radiation Protection
P.O. Box 120
Tai-yuan, Shan-xi
THE PEOPLE'S REPUBLIC OF CHINA

ONSITE

3 DOE Richland Operations Office

D. L. Hoff
J. J. Sutey
M. W. Tiernan

2 Tri-Cities University Center

J. Finnigan
B. Vallet

2 Hanford Environmental Health Foundation

B. D. Breitenstein
L. J. Mass

149 Pacific Northwest Laboratory

O. B. Abbey
K. J. Allwine
R. W. Baalman
D. C. Bader
J. F. Bagley
W. J. Bair (15)
M. Y. Ballinger
W. R. Barchet
N. S. Bloom
C. J. Brandt
K. M. Busness
D. B. Cearlock
E. G. Chapman
T. D. Chikalla
G. A. Crecelius
D. S. Daly
M. T. Dana
J. M. Davidson
W. E. Davis
G. W. Dennis
J. C. Doran
J. G. Droppo
R. C. Easter
C. E. Elderkin (20)
J. W. Falco
R. M. Fleischman
C. S. Glantz
W. A. Glass
J. A. Glissmeyer
D. W. Glover
R. H. Gray
M. J. Graham
R. K. Hadlock
J. M. Hales (5)
R. V. Hannigan
L. C. Harrison
P. C. Hays
G. R. Hilst
D. J. Hoitink
T. W. Horst
J. M. Hubbe
R. A. Keefe
B. J. Kelman
E. W. Kleckner
N. S. Laulainen (5)
G. L. Laws
R. N. Lee
A. C. Leslie
C. G. Lindsey
F. D. Lloyd
D. J. Luecken
J. A. Mahaffey
L. N. McKenney
J. Mishima
J. M. Nielsen
E. L. Owczarski
P. C. Owczarski
J. F. Park
W. T. Pelroy
W. T. Pennell (5)
R. W. Perkins
A. M. Platt
D. C. Powell
J. V. Ramsdell
D. S. Renne
W. D. Richmond
D. R. Roth
G. F. Schiefelbein
L. C. Schmid
B. C. Scott
G. A. Sehmel
D. S. Sharp
E. D. Skyllingstad
W. G. N. Slinn (5)
G. M. Stokes
R. A. Stokes
J. A. Stottlemyre
D. L. Strenge
J. M. Thorp
L. H. Toburen
B. E. Vaughan
L. L. Wendell (5)
C. D. Whiteman
R. E. Wildung
W. R. Wiley
R. K. Woodruff
T. A. Zinn
Life Science Library (2)
Publishing Coordination (2)
Technical Report Files (5)